UNIVERSIDADE FEDERAL DE VIÇOSA

Gênese do solo e estabilidade da matéria orgânica em ambientes periglaciais de Kangerlussuaq, Groenlândia Ocidental

Alex Xavier Pinheiro
Magister Scientiae

VIÇOSA - MINAS GERAIS
2026

ALEX XAVIER PINHEIRO

Gênese do solo e estabilidade da matéria orgânica em ambientes periglaciais de Kangerlussuaq, Groenlândia Ocidental

Dissertação apresentada à Universidade Federal de Viçosa, como parte das exigências do Programa de Pós-Graduação em Solos e Nutrição de Plantas, para obtenção do título de *Magister Scientiae*.

Orientador: Marcio Rocha Francelino

Coorientadores: Carlos E. G. R. Schaefer
Lucas de Carvalho Gomes

VIÇOSA - MINAS GERAIS
2026

Ficha catalográfica elaborada pela Biblioteca Central da Universidade Federal de Viçosa - Campus Viçosa

T
P654g
2026

Pinheiro, Alex Xavier, 1999-
Gênese do solo e estabilidade da matéria orgânica em ambientes periglaciais de Kangerlussuaq, Groenlândia Ocidental / Alex Xavier Pinheiro. – Viçosa, MG, 2026.
1 dissertação eletrônica (114 f.): il. (algumas color.).

Texto em português e inglês.
Orientador: Márcio Rocha Francelino.
Dissertação (mestrado) - Universidade Federal de Viçosa, Departamento de Solos, 2026.
Inclui bibliografia.
DOI: https://doi.org/10.47328/ufvbbt.2026.191
Modo de acesso: World Wide Web.

1. Solos - Groenlândia. 2. Solos - Formação - Ártica, Região. 3. Húmus. 4. Mudanças climáticas. 5. Processos eólicos. 6. Processos periglaciais. I. Francelino, Márcio Rocha, 1966-. II. Universidade Federal de Viçosa. Departamento de Solos. Programa de Pós-Graduação em Solos e Nutrição de Plantas. III. Título.

CDD 22. ed. 631.417

Bibliotecário(a) responsável: Bruna Silva CRB-6/2552

ALEX XAVIER PINHEIRO

Gênese do solo e estabilidade da matéria orgânica em ambientes periglaciais de Kangerlussuaq, Groenlândia Ocidental

Dissertação apresentada à Universidade Federal de Viçosa, como parte das exigências do Programa de Pós-Graduação em Solos e Nutrição de Plantas, para obtenção do título de *Magister Scientiae*.

APROVADA: 27 de fevereiro de 2026.

Assentimento:

_____

Alex Xavier Pinheiro
Autor

_____

Marcio Rocha Francelino
Orientador

Aos meus admiráveis pais Sebastião e Mercês e minha querida irmã, Flávia de Fátima, dedico o presente trabalho.

AGRADECIMENTOS

Aos meus pais e irmã pelo apoio e suporte inegável diante dos meus caminhos e desafios desejados e espontâneos.

Aos grandes amigos e colegas de profissão que permitiram uma trajetória iluminada de conhecimento, desafios compartilhados e leveza em meio às intempéries naturais do processo e da vida.

Ao meu estimado orientador Dr. Márcio Rocha Francelino e prezados coorientadores, Dr. Carlos Ernesto Reynaud Schaefer e Dr. Lucas de Carvalho Gomes, pelo apoio e confiança no desafio ofertado e aceito.

Ao Departamento de Solos e ao Programa de Pós-Graduação de Solos e Nutrição de Plantas – sendo aqui agradecido especialmente aos Professores, pelos ensinamentos diversos, Técnicos, pelo comprometimento e dedicação as suas atividades e ao apoio à ciência brasileira, e a todos os outros Funcionários pela dedicação ao decorrer de suas atividades a fim de manter e melhorar o Departamento de Solos.

Agradecimentos especiais ao Laboratório de Geoprocessamento e Sensoriamento Remoto (LabGeo), onde fiz morada profissional, e ao Terrantar por todas as oportunidades, desafios intelectuais e resiliência demandada.

À Universidade Federal de Viçosa, pela oportunidade de realizar a pós-graduação.

Este trabalho foi realizado com o apoio das seguintes agências de pesquisa brasileiras: Coordenação de Aperfeiçoamento de Pessoal de Nível Superior – Brasil (CAPES) – Código de Financiamento 001, Fundação de Amparo à Pesquisa do Estado de Minas Gerais (FAPEMIG) e Conselho Nacional de Desenvolvimento Científico e Tecnológico (CNPq).

“On maps of the country
We must draw points and lines to show we have been here – and are here today,
here where the foxes run and birds nest and the fish spawn”.
“Nuna assiliorpaat uanngaanniit uunga titarlugu aana killissaa aana ilissi aana uagut
Tuttut uaniipput aaku timmissat aamma aaku aalisakkat”.
(Aqqaluk Lynge)

RESUMO

PINHEIRO, Alex Xavier, M.Sc., Universidade Federal de Viçosa, fevereiro de 2026. **Gênese do solo e estabilidade da matéria orgânica em ambientes periglaciais de Kangerlussuaq, Groenlândia Ocidental**. Orientador: Marcio Rocha Francelino. Coorientadores: Carlos Ernesto Goncalves Reynaud Schaefer e Lucas de Carvalho Gomes.

O Ártico está aquecendo aproximadamente quatro vezes mais rápido que a média global, impulsionando a deglaciação e expondo novas superfícies antes cobertas pelo gelo. Compreender os processos que governam a formação dos solos e a estabilidade da matéria orgânica nessas regiões é essencial para avaliar a vulnerabilidade dos estoques de carbono às mudanças climáticas. A presente dissertação buscou investigar os processos pedogenéticos e os mecanismos de estabilização da matéria orgânica em solos periglaciais de Kangerlussuaq, Groenlândia Ocidental, através de abordagens mineralógicas, geoquímicas, isotópicas e de monitoramento térmico. Nove perfis de solo foram coletados ao longo de um gradiente de distância da Geleira Russell (0 a 33 km), descritos segundo a Base de Referência Mundial para Recursos de Solo e classificados como Regosol, Cryosol, Podzol, Arenosol e Phaeozem, refletindo a elevada pedodiversidade da região. Os perfis foram submetidos a análises de difração de raios-X (DRX) das frações areia, silte e argila, fluorescência de raios-X (FRX), fracionamento físico da matéria orgânica (POM/MAOM), análises isotópicas (^{13}C, ^{1}N), extrações seletivas de óxidos de Fe-Al e monitoramento térmico contínuo de 14 meses a 10, 50 e 130 cm de profundidade. Os resultados demonstraram composição mineralógica uniforme dominada por minerais primários (quartzo, albita, anfibólios) em todas as frações granulométricas, incluindo a fração argila, indicando que esta consiste predominantemente de rocha triturada produzida por moagem mecânica glacial. Os baixos valores do Índice de Alteração Química (CIA, média 49,64) e altos valores do Índice de Variabilidade Composicional (ICV, média 1,24) confirmam estágio inicial de intemperismo químico. Descontinuidades líticas foram identificadas em quatro perfis, acopladas a gradientes invertidos de intemperismo, fornecendo evidência estratigráfica de deposição eólica episódica que atua como retardante pedogenético, reconfigurando continuamente as condições superficiais do solo. O fracionamento físico da matéria orgânica revelou razões C:N elevadas na fração POM (13–91) e mais baixas na fração MAOM (10–26), refletindo diferentes graus de processamento microbiano. Contudo, os baixos valores do índice de estabilidade relativa (n, mediana 1,01), as concentrações limitadas de óxidos de Fe-Al amorfos (Fe: 0,11–2,07 g kg^{1}; Al: 0,03–1,46 g kg^{1}) e a ausência de correlação

significativa entre carbono orgânico e essas fases minerais indicam que a proteção organo-mineral mediada por Fe-Al é restrita, sendo a estabilização física por enterramento o mecanismo dominante. A ocorrência de pH próximo à neutralidade e elevados teores de Ca^{2} trocável sugere adicionalmente que pontes catiônicas mediadas por Ca^{2} podem representar uma via secundária de estabilização onde os óxidos de Fe-Al são escassos. O monitoramento térmico revelou heterogeneidade vertical e temporal pronunciada, com camadas superficiais apresentando amplas variações sazonais e acúmulo substancial de graus-dia de descongelamento (TDD acumulado de até 1.017 degree-days), enquanto camadas subsuperficiais exibiram elevada frequência de dias isotérmicos, estabelecendo as condições de base necessárias para futuras investigações sobre mineralização da MOS. A integração dos resultados confirma um processo de dupla gênese para os solos de Kangerlussuaq, onde o legado de intemperismo físico glacial estabelece uma linha de base mineralógica uniforme e a deposição eólica contemporânea retarda a diferenciação pedogenética, resultando em estoques de carbono potencialmente vulneráveis à mineralização acelerada sob cenários de aquecimento contínuo no Ártico. Evidências de podzolização incipiente em múltiplos perfis, satisfazendo os critérios do qualificador Protospodic, reforçam a necessidade de ferramentas taxonômicas mais sensíveis ao desenvolvimento pedogenético incipiente em paisagens periglaciais em rápida transformação.

Palavras-chave: solos periglaciais; matéria orgânica do solo ; deposição eólica; mudanças climáticas; Ártico

ABSTRACT

PINHEIRO, Alex Xavier, M.Sc., Universidade Federal de Viçosa, February, 2026. **Soil genesis and organic matter stability in periglacial environments of Kangerlussuaq, western Greenland**. Adviser: Marcio Rocha Francelino. Co-advisers: Carlos Ernesto Goncalves Reynaud Schaefer and Lucas de Carvalho Gomes.

The Arctic is warming approximately four times faster than the global average, driving accelerated deglaciation and exposing new terrestrial surfaces. Understanding the processes governing soil formation and organic matter stability in these regions is essential for assessing carbon stock vulnerability to climate change. This dissertation investigated pedogenic processes and organic matter stabilization mechanisms in periglacial soils of Kangerlussuaq, Western Greenland, through mineralogical, geochemical, isotopic, and thermal monitoring approaches. Nine soil profiles were collected along a gradient of distance from Russell Glacier (0 to 33 km), described according to the World Reference Base for Soil Resources, and classified as Regosols, Cryosols, Podzol, Arenosol, and Phaeozem, reflecting the high pedodiversity of the region. Profiles were subjected to X-ray diffraction (XRD) of sand, silt, and clay fractions, X-ray fluorescence (XRF), physical fractionation of soil organic matter (POM/MAOM), isotopic analyses (^{13}C, ^{1}N) of the organic fractions, selective extractions of Fe-Al oxides, and continuous thermal monitoring over 14 months at depths of 10, 50, and 130 cm. Results demonstrated uniform mineralogical composition dominated by primary minerals (quartz, albite, amphiboles) across all particle-size fractions, including the clay fraction, indicating that it consists predominantly of rock flour produced by glacial mechanical grinding. Low Chemical Index of Alteration values (CIA, mean 49.64) and high Index of Compositional Variability values (ICV, mean 1.24) confirm an early stage of chemical weathering. Lithic discontinuities identified in four profiles, coupled with inverted weathering gradients, provide stratigraphic evidence of episodic aeolian deposition acting as a pedogenetic retardant that continuously reconfigures soil surface conditions. Physical fractionation of organic matter revealed high C:N ratios in the POM fraction (13–91) and lower ratios in the MAOM fraction (10–26), reflecting different degrees of microbial processing. However, low relative stability index values (n, median 1.01), limited concentrations of amorphous Fe-Al oxides (Fe: 0.11–2.07 g kg^{1}; Al: 0.03–1.46 g kg^{1}), and the absence of significant correlations between organic carbon and these mineral phases indicate that Fe-Al-mediated organo-mineral protection is restricted, with physical stabilization through burial representing the dominant mechanism. The co-occurrence of near-neutral

pH and elevated exchangeable Ca^2 additionally suggests that Ca^2 mediated cation bridging may represent a secondary stabilization pathway where Fe-Al oxides are scarce. Thermal monitoring revealed pronounced vertical and temporal heterogeneity, with surface layers exhibiting wide seasonal temperature variations and substantial accumulation of thawing degree-days (cumulative TDD up to 1,017 degree-days), while subsurface layers showed high frequency of isothermal days, establishing the baseline conditions necessary for future investigations of SOM mineralization dynamics. Integration of results tests and confirms a dual-genesis framework for Kangerlussuaq soils, in which the legacy of glacial physical weathering establishes a uniform mineralogical baseline and contemporary aeolian deposition retards pedogenic differentiation, resulting in carbon stocks potentially vulnerable to accelerated mineralization under continued Arctic warming scenarios. Evidence of incipient podzolization across multiple profiles, satisfying the criteria of the Protospodic qualifier, reinforces the need for taxonomic tools more sensitive to incipient pedogenetic development in rapidly changing periglacial landscapes.

Keywords: periglacial soils; soil organic matter; aeolian deposition; climate change ; Arctic

SUMÁRIO

1. INTRODUÇÃO GERAL

O Ártico está aquecendo aproximadamente quatro vezes mais rápido que a média global, fenômeno conhecido como amplificação ártica (Rantanen et al., 2022). Esse aquecimento acelerado tem impulsionado mudanças ambientais na região, incluindo o recuo de geleiras, o degelo do permafrost e o aumento da duração das estações de crescimento vegetal. Em Kalaallit Nunaat (Groenlândia), essas mudanças são particularmente pronunciadas pelo manto de gelo groenlandês que tem apresentado perda de massa consistente desde a década de 1990, tornando-se um dos principais contribuintes para a elevação do nível do mar global (Van den Broeke et al., 2017; Chen et al., 2017). Sob condições de aquecimento, projeções indicam que o balanço de massa superficial do manto de gelo de groenlandês poderá tornar-se negativo no futuro próximo, havendo mais descongelamento do que produção de gelo na região (Noël et al., 2021).

A deglaciação contínua e a consequente exposição de superfícies terrestres estão promovendo uma transição gradual em direção a ecossistemas de base terrestre na Groenlândia. Esse processo é evidenciado pelo avanço da agricultura e da criação de ovelhas para o norte (Masson-Delmotte et al., 2012), bem como pela rápida colonização vegetal de áreas recém-expostas (Grimes et al., 2024). Considerando que a Groenlândia deverá tornar-se mais quente e úmida até o final do século XXI (Zhang et al., 2024), o subsequente aumento na exposição de solos e a rápida colonização por vegetação demandam uma compreensão mais aprofundada dos processos pedogenéticos que operam nos diversos sistemas da ilha.

Kangerlussuaq, localizado na Groenlândia Ocidental, representa a maior região livre de gelo da ilha (Anderson & Stedmon, 2007). A região apresenta um histórico climático complexo, marcado por resfriamento ao longo do século XX seguido de aquecimento acelerado nas últimas décadas (Anderson et al., 2017). Essas mudanças têm impulsionado rápidas alterações ao longo da paisagem, incluindo flutuações glaciais (Knight et al., 2007) e transições florísticas caracterizadas pela proliferação de gramíneas e emergência de táxons colonizadores rápidos em resposta ao alongamento das estações quentes (Silva et al., 2025). Tais dinâmicas influenciam fundamentalmente o desenvolvimento dos solos, exigindo monitoramento contínuo dado o papel central do Ártico nos ciclos globais de carbono e clima.

A pedogênese em ambientes periglaciais é governada pela interação entre processos físicos herdados de períodos glaciais e processos contemporâneos de deposição e transformação. Em Kangerlussuaq, a combinação de intenso intemperismo físico, crioclastia e cominuição glacial, com regimes deposicionais fluvioglaciais e eólicos ativos (Sechi et al., 2024; Willemse et al., 2003) cria condições únicas para o desenvolvimento dos solos. A deposição eólica de loess, documentada ao longo de pelo menos 5 ka na região, representa não

apenas uma fonte de material parental, mas um agente pedogenético ativo capaz de soterrar horizontes superficiais e interromper a diferenciação química progressiva. Compreender como esses processos interagem e determinam as trajetórias pedogenéticas é essencial para prever a resposta dos solos árticos às mudanças climáticas em curso e para aprimorar os sistemas de classificação taxonômica aplicados a paisagens em rápida transformação.

Paralelamente à questão da gênese dos solos, a estabilidade da matéria orgânica do solo (MOS) em ambientes árticos representa uma preocupação global significativa. Estima-se que aproximadamente 1672 Pg de carbono orgânico estejam contidos nos solos circumpolares do norte, dos quais cerca de 88% (1466 Pg) encontram-se preservados em camadas e depósitos permanentemente congelados (Tarnocai et al., 2009). Embora esses solos atuem como grandes estoques de carbono devido às baixas temperaturas e limitada atividade biológica, persistem incertezas sobre a estabilidade dessa matéria orgânica sob condições de aquecimento (Alekseev & Abakumov, 2022). A estabilização da MOS pode ocorrer através de diferentes mecanismos, como a agregação física, ligações organo-minerais mediadas por óxidos de Fe e Al amorfos, e inibição bioquímica decorrente das baixas temperaturas (Cotrufo et al., 2013, 2015; Herndon et al., 2017). Contudo, em solos desenvolvidos sobre material parental de intemperismo predominantemente físico, a disponibilidade de fases minerais reativas pode ser restrita, comprometendo a formação de associações organo-minerais estáveis (Kleber et al., 2005). Adicionalmente, em perfis com pH próximo à neutralidade, como os observados em solos sobre substrato glacialmente derivado rico em bases, íons Ca^{2+} podem atuar como ponte entre compostos orgânicos e superfícies minerais, representando uma via secundária de estabilização que complementa ou substitui parcialmente os mecanismos mediados por Fe e Al (Rowley et al., 2018). A importância relativa dessas vias em solos periglaciais jovens permanece insuficientemente compreendida.

Além disso, o regime térmico do solo exerce controle direto sobre os processos microbianos que regulam a decomposição da MOS. Ciclos de congelamento-descongelamento, períodos de descongelamento sazonal e a variação térmica ao longo do perfil podem tanto estimular quanto inibir a atividade microbiana, afetando as taxas de mineralização do carbono (Mikan et al., 2002; Conant et al., 2011). Em solos com proteção mineral limitada, a combinação de exposição térmica sazonal com estabilização organo-mineral insuficiente pode ampliar a vulnerabilidade dos estoques de carbono à perda sob condições climáticas mais quentes. O monitoramento térmico contínuo em múltiplas profundidades representa, portanto, uma ferramenta essencial para caracterizar os regimes de temperatura que atualmente

condicionam os processos pedogenéticos e de decomposição, e para fundamentar projeções futuras sobre a resposta desses sistemas ao aquecimento ártico.

Diante desse contexto, a presente dissertação investiga a pedogênese e a estabilidade da MOS em solos periglaciais de Kangerlussuaq, Groenlândia Ocidental, através de uma abordagem multi-analítica que integra dados mineralógicos, geoquímicos, isotópicos e térmicos. O trabalho está organizado em dois capítulos complementares.

O primeiro capítulo testa e confirma um *framework* de dupla gênese para os solos proglaciais de Kangerlussuaq. A partir de análises de fluorescência de raios-X (FRX), difração de raios-X (DRX) das frações argila, silte e areia, extrações seletivas de óxidos de Fe e Al, e análises estatísticas multivariadas em nove perfis coletados ao longo de um gradiente de distância da Geleira Russell, demonstrou-se que a composição mineralógica é governada pelo legado de cominuição glacial, enquanto a evolução morfológica e a dinâmica do carbono são controladas pela deposição eólica contemporânea. A deposição eólica atua como principal agente pedogenético retardante ao introduzir material minimamente intemperizado que interrompe a continuidade vertical dos gradientes pedogenéticos e soterra horizontes orgânicos. Os resultados fornecem ainda evidência de podzolização incipiente em múltiplos perfis, manifestada pelo acúmulo subsuperficial de Fe, Al e carbono orgânico. Embora os horizontes espódicos diagnósticos da WRB não estejam presentes, os perfis analisados satisfazem os critérios do qualificador *Protospodic*, cuja extensão formal como subqualificador de *Regosols* é proposta como ferramenta taxonômica necessária para capturar o desenvolvimento pedogenético incipiente em paisagens periglaciais em rápida transformação.

O segundo capítulo examina as consequências dessa gênese particular para a estabilidade da MOS por meio do fracionamento físico em fração particulada (POM) e fração associada a minerais (MAOM), da caracterização isotópica ($\delta^{13}C$, $\delta^{15}N$) de ambas as frações para estimativa da estabilidade relativa da MOS, e da quantificação de óxidos de Fe e Al amorfos e cristalinos por extrações seletivas para avaliação dos mecanismos de proteção mineral. Adicionalmente, apresentam-se os resultados de um sistema de monitoramento térmico contínuo instalado em três perfis a profundidades de 10, 50 e 130 cm ao longo de 14 meses, com o objetivo de caracterizar a heterogeneidade vertical e sazonal do regime térmico e estabelecer as condições de base necessárias para futuras investigações sobre a relação entre temperatura e mineralização da MOS nessa paisagem.

Dessa forma, esta dissertação contribui para a compreensão dos processos que governam a formação e a vulnerabilidade dos solos em ambientes periglaciais, fornecendo

subsídios para avaliar a resposta desses sistemas às mudanças climáticas projetadas para o Ártico. Os resultados obtidos têm implicações para a classificação taxonômica de solos em regiões de deglaciação acelerada, para a compreensão dos mecanismos de estabilização do carbono em solos jovens sobre substrato glacial, e para o delineamento de estratégias de monitoramento em ecossistemas árticos vulneráveis.

REFERÊNCIAS GERAIS

Alekseev, I. and Abakumov, E. (2021). Soil organic carbon stocks and stability of organic matter in permafrost-affected soils of Yamal region, Russian Arctic. *Geoderma Regional*, p.e00454. https://doi.org/10.1016/j.geodrs.2021.e00454.

Anderson, N.J., Stedmon, C.A. (2007). The effect of evapoconcentration on dissolved organic carbon concentration and quality in lakes of SW Greenland. *Freshwater Biology,* 52(2), 280–289. https://doi.org/10.1111/j.1365-2427.2006.01688.x.

Anderson, N.J., Saros, J.E., Bullard, J.E., Cahoon, S.M.P., McGowan, S., Bagshaw, E.A., Barry, C.D., Bindler, R., Burpee, B.T., Carrivick, J.L., Fowler, R.A., Fox, A.D., Fritz, S.C., Giles, M.E., Hamerlik, L., Ingeman-Nielsen, T., Law, A.C., Mernild, S.H., Northington, R.M. and Osburn, C.L. (2017). The Arctic in the Twenty-First Century: Changing Biogeochemical Linkages across a Paraglacial Landscape of Greenland. *BioScience*, 67(2), 118–133. https://doi.org/10.1093/biosci/biw158.

Chen, X., Zhang, X., Church, J.A., Watson, C.S., King, M.A., Monselesan, D., Legresy, B. and Harig, C. (2017). The increasing rate of global mean sea-level rise during 1993–2014. *Nature Climate Change*, 7(7), 492–495. https://doi.org/10.1038/nclimate3325.

Conant, R.T., Ryan, M.G., Ågren, G.I., Birge, H.E., Davidson, E.A., Eliasson, P.E., Evans, S.E., Frey, S.D., Giardina, C.P., Hopkins, F.M., Hyvönen, R., Kirschbaum, M.U.F., Lavallee, J.M., Leifeld, J., Parton, W.J., Megan Steinweg, J., Wallenstein, M.D., Martin Wetterstedt, J.Å. and Bradford, M.A. (2011). Temperature and soil organic matter decomposition rates - synthesis of current knowledge and a way forward. *Global Change Biology*, 17(11), 3392–3404. https://doi.org/10.1111/j.1365-2486.2011.02496.x.

Cotrufo, M.F., Wallenstein, M.D., Boot, C.M., Denef, K. and Paul, E. (2013). The Microbial Efficiency-Matrix Stabilization (MEMS) framework integrates plant litter decomposition with soil organic matter stabilization: do labile plant inputs form stable soil organic matter? *Global Change Biology*, 19(4), 988–995. https://doi.org/10.1111/gcb.12113.

Cotrufo, M.F., Soong, J.L., Horton, A.J., Campbell, E.E., Haddix, Michelle L., Wall, D.H. and Parton, W.J. (2015). Formation of soil organic matter via biochemical and physical pathways of litter mass loss. *Nature Geoscience*, 8(10), 776–779. https://doi.org/10.1038/ngeo2520.

Grimes, M., Carrivick, J.L., Smith, M.W. and Comber, A.J. (2024). Land cover changes across Greenland dominated by a doubling of vegetation in three decades. *Scientific Reports*, 14(1), p.3120. https://doi.org/10.1038/s41598-024-52124-1.

Herndon, E., Amineh AlBashaireh, Singer, D.J., Taniya Roy Chowdhury, Gu, B. and Graham, D.Y. (2017). Influence of iron redox cycling on organo-mineral associations in Arctic tundra soil. *Geochimica et Cosmochimica Acta*, 207, 210–231. https://doi.org/10.1016/j.gca.2017.02.034.

IUSS Working Group WRB. (2022). World Reference Base for Soil Resources. International classification system for naming soils and creating legends for soil maps. 4th edition. International Union of Soil Sciences (IUSS), Vienna.

Kleber, M., Mikutta, R., Torn, M.S. and Jahn, R. (2005). Poorly crystalline mineral phases protect organic matter in acid subsoil horizons. *European Journal of Soil Science*, 0(0), p.050912034650054. https://doi.org/10.1111/j.1365-2389.2005.00706.x.

Knight, P.G., Jennings, C.E., Waller, R.I. and Robinson, Z.P. (2007). Changes in ice-margin processes and sediment routing during ice-sheet advance across a marginal moraine. *Geografiska annaler. Series A, Physical geography/Geografiska annaler. Series A. Physical geography*, 89(3), 203–215. https://doi.org/10.1111/j.1468-0459.2007.00319.x.

Masson-Delmotte, V., Swingedouw, D., Landais, A., Seidenkrantz, M.-S., Gauthier, E., Bichet, V., Massa, C., Perren, B., Jomelli, V., Adalgeirsdottir, G., Hesselbjerg Christensen, J., Arneborg, J., Bhatt, U., Walker, D.A., Elberling, B., Gillet-Chaulet, F., Ritz, C., Gallée, H., van den Broeke, M. and Fettweis, X. (2012). Greenland climate change: from the past to the future. *Wiley Interdisciplinary Reviews: Climate Change*, 3(5), 427–449. https://doi.org/10.1002/wcc.186.

Mikan, C.J., Schimel, J.P. and Doyle, A.P. (2002). Temperature controls of microbial respiration in arctic tundra soils above and below freezing. *Soil Biology and Biochemistry*, 34(11), 1785–1795. https://doi.org/10.1016/s0038-0717(02)00168-2.

Noël, B., van Kampenhout, L., Lenaerts, J.T.M., van de Berg, W.J. and van den Broeke, M.R. (2021). A 21st Century Warming Threshold for Sustained Greenland Ice Sheet Mass Loss. *Geophysical Research Letters*, 48(5). https://doi.org/10.1029/2020gl090471.

Rantanen, M., Karpechko, A.Y., Lipponen, A., Nordling, K., Hyvärinen, O., Ruosteenoja, K., Vihma, T., Laaksonen, A. (2022). The Arctic has warmed nearly four times faster than the globe since 1979. *Commun Earth Environ*, *3*,1–10. https://doi.org/10.1038/s43247-022-00498-3

Rowley, M.C., Grand, S. and Verrecchia, É.P. (2017). Calcium-mediated stabilisation of soil organic carbon. *Biogeochemistry*, 137(1-2), pp.27–49. doi:https://doi.org/10.1007/s10533-017-0410-1.

Sechi, D., Stevens, T., Hällberg, P., Smittenberg, R.H., Molnár, M., Kertész, G.T., Buylaert, J.P., Schneider, R., Edward, C., Rasmussen, K.R., Knudsen, N.A.T., Andreucci, S. and Pascucci, V. (2024). High resolution luminescence and radiocarbon dating of Holocene Aeolian silt (loess) in west Greenland. *Quaternary Geochronology*, 84, p.101579. https://doi.org/10.1016/j.quageo.2024.101579.

Silva, T., Whitley, B.S., Biersma, E.M., Abermann, J., Raundrup, K., de Vere, N., Høye, T.T., Haring, V. and Schöner, W. (2025). Bio-climatic factors drive spectral vegetation changes in Greenland. *Biogeosciences*, 22(17), 4601–4626. https://doi.org/10.5194/bg-22-4601-2025.

Tarnocai, C., Canadell, J.G., Schuur, E.A.G., Kuhry, P., Mazhitova, G. and Zimov, S. (2009). Soil organic carbon pools in the northern circumpolar permafrost region. *Global Biogeochemical Cycles*, 23(2), p.n/a-n/a. https://doi.org/10.1029/2008gb003327.

Ten Brink, N.W. and Weidick, A. (1974). Greenland Ice Sheet History Since the Last Glaciation. *Quaternary Research*, 4(4), 429–440. https://doi.org/10.1016/0033-5894(74)90038-6.

van den Broeke, M., Box, J., Fettweis, X., Hanna, E., Noël, B., Tedesco, M., van As, D., van de Berg, W.J. and van Kampenhout, L. (2017). Greenland Ice Sheet Surface Mass Loss: Recent Developments in Observation and Modeling. *Current Climate Change Reports*, 3(4), 345–356. https://doi.org/10.1007/s40641-017-0084-8.

Willemse, N.W., Koster, E.A., Hoogakker, B. and van Tatenhove, F.G.M. (2003). A continuous record of Holocene eolian activity in West Greenland. *Quaternary Research*, 59(3), 322–334. https://doi.org/10.1016/s0033-5894(03)00037-1.

Zhang, Q., Huai, B., Ding, M., Sun, W., Liu, W., Yan, J., Zhao, S., Wang, Y., Wang, Y., Wang, L., Che, J., Dou, J. and Kang, L. (2024). Projections of Greenland climate change from CMIP5 and CMIP6. *Global and Planetary Change*, 232, p.104340. https://doi.org/10.1016/j.gloplacha.2023.104340.

2. CAPÍTULO 1: Dual-genesis framework for proglacial soils: Physical weathering legacy vs. contemporary aeolian deposition in Kangerlussuaq, western Greenland

Abstract: Rapid deglaciation in the Arctic is exposing vast terrestrial surfaces, yet the interplay between glacial processes and contemporary soil dynamics remains insufficiently understood in recently deglaciated terrains. This study proposes a dual-genesis framework for periglacial soils in Kangerlussuaq, western Greenland, in which a physical weathering legacy and a contemporary aeolian depositional regime interact to control pedogenetic trajectories. Nine soil profiles, classified as Regosols, Cryosols, Podzol, Arenosol, and Phaeozem, were collected along a gradient from the Russell Glacier. Bulk geochemistry (XRF), XRD of sand, silt, and clay fractions, and selective extractions of Fe and Al oxides were investigated. Dominance of albite and quartz across all particle-size fractions indicates a uniform mineralogical baseline, with the clay fraction consisting primarily of physically ground rock flour rather than pedogenic secondary phyllosilicates. Low Chemical Index of Alteration (CIA) values and high Index of Compositional Variability (ICV) confirm an immature weathering stage. Lithic discontinuities identified in four profiles, together with elevated subsurface C:N ratios consistent with burial and cryogenic preservation of relatively undecomposed organic matter, provide stratigraphic evidence of recurring aeolian depositional events. Our findings demonstrate that contemporary aeolian deposition acts as a primary pedogenetic retardant, disrupting the vertical continuity of pedogenic gradients, overriding in situ chemical weathering, and physically protecting organic matter through burial into cryic thermal regimes.

1. Introduction

Kalaallit Nunaat (Greenland) retains approximately 80% of its landmass under glaciers, ice caps, and the Greenland Ice Sheet (GrIS) (Masson-Delmotte et al., 2012). Currently, the GrIS is a primary contributor to global sea-level rise, exhibiting consistent mass loss since the 1990s (Van den Broeke et al., 2017; Chen et al., 2017). Under sustained warming, projections suggest the surface mass balance may become negative in the near future (Noël et al., 2021). This persistent deglaciation and the resulting exposure of terrestrial surfaces are driving a shift toward terrestrial-based ecosystems, evidenced by the northward advance of agriculture and sheep pastoralism (Masson-Delmotte et al., 2012). Given that, Greenland is expected to become warmer and wetter by the end of the 21st century (Zhang et al., 2024), increased soil exposure and vegetation expansion (Grimes et al., 2024) will likely alter soil development. This shift indicates a need for a broader pedological perspective to understand the resulting trajectories in these systems.

Kangerlussuaq, located in western Greenland at the head of a fjord near the GrIS, is the largest ice-free region in Greenland (Anderson & Stedmon, 2007). This area is of significant scientific interest due to its pronounced cooling during the 20th century and its current accelerated warming, leading to rapid climatic and geomorphic changes (Anderson et al., 2017). Notable alterations include glacier advance episodes from 1964 to 2002 (Knight et al., 2007), jökulhlaup cycles (Russell et al., 2011), and vegetation increments over the last years (Grimes et al., 2024; Silva et al., 2025). These dynamics fundamentally influence soil development, demanding continuous monitoring as the Arctic remains the fastest-warming region on Earth (Bruhwiler et al., 2021).

Pedogenesis is defined by the interaction of climate, organisms, topography, time, and parent material (Dokuchaev, 1886). These factors are fundamental to the differentiation of diagnostic horizons and taxonomic classification in different soil systems (Bockheim et al., 2014). In highly active and sensitive landscapes like Kangerlussuaq, deciphering these processes is essential for tracking soil evolution. While advancing flora may stimulate microbiological diversity and organic matter accumulation, the pedogenic signal is simultaneously constructed by intense fluvioglacial and aeolian depositional regimes (Sechi et al., 2024).

Considering the rapid environmental shifts in Kangerlussuaq, the degree to which relict physical processes and contemporary sediment dynamics dictate soil developmental trajectories

remains insufficiently quantified. This research seeks to bridge this gap by evaluating the pedogenetic evolution of periglacial soils through a multi-analytical approach. We propose a dual-genesis framework to be tested against mineralogical and geochemical evidence: first, that a relict phase of intense physical weathering, cryoclasm, and glacial comminution, established a uniform mineralogical baseline across soil fractions; and second, that contemporary aeolian deposition of loess acts as a primary pedogenetic retardant.

2. Material and methods

2.1. Study Area

The Kangerlussuaq region is in the western part of Greenland within the Nagssugtoqidian orogenic belt, which comprises Archean Eon gneiss reworked during the Proterozoic (Kalsbeek et al., 1987). The climate is classified as Polar Tundra (ET), characterized by dry, cold conditions with average summer temperatures of 0–10°C (Beck et al., 2018). The dominant vegetation is tundra, reflecting the region's low-temperature and short growing season. The Proterozoic metamorphism has left a legacy of eroded uplands, contributing to the deep fjords and glacial valleys that define the modern landscape.

At the onset of Holocene, the Kangerlussuaq region was entirely ice-covered. Gradual ice retreat occurred throughout this period due to warming during the early Holocene, when mean temperatures in central Greenland were approximately 1°C higher than today (Vinther et al., 2009). This progressive warming, combined with reduced snow accumulation due to regional aridity, facilitated the formation of multiple moraine systems, including the Sarfartôq-Advedtleq moraines (dated to 8,896–9,727 yr BP) and the Ørkendalen moraines (6,406–7,028 yr BP) (Ten Brink & Weidick, 1974).

Regional glacier recession culminated around 4,000 yr BP, followed by a later advance strongly influenced by the Little Ice Age (0.7–0.1 kyr BP) (Weidick, 1993; Foreman et al., 2007). Sedimentological records indicate repeated geomorphic changes, including ice-margin retreat (forming the earliest regional moraines), marine transgression-regression cycles (depositing fluvioglacial sediments), and recent neoglacial ice advances (Storms et al., 2012).

2.2. Sampling and description of soil profiles

Fieldwork was conducted during the summers of 2024 and 2025. Nine representative soil profiles were selected across the region (Figure 1) based on elevation (Figure 2), distance

from the glacier margin, parent material, and accessibility. Each profile was described following the guidelines of the World Reference Base for Soil Resources (IUSS, 2022) and collected following international soil sampling protocols (Schoeneberger et al., 2012). Carbonate presence was assessed in the samples using a 10% HCl "fizz test". Bulk samples were air-dried, disaggregated, and sieved through a 2mm mesh to obtain the air-dried fine earth fraction for subsequent analysis.

2.3. Bulk Soil Analysis

After air-drying, subsamples of each horizon were collected to determine the total organic carbon in soil using Walkley-Black method (Walkley and Black, 1934) and then multiplied by a correction factor of 1.3 due to the incomplete recovery of total organic carbon (IUSS, 2022). Total nitrogen content was determined through Kjeldahl method, considering sulfuric acid digestion followed by titration. Soil pH was measured in a 1:2.5 soil-to-deionized-water suspension and in a 1 mol.L^{-1} KCl solution. Al^{3+} was extracted with KCl (1 mol.L^{-1}) and determined volumetrically with a NaOH (0.025 mol.L^{-1}) solution. Particle-size distribution was analyzed following dispersion with 0.1 mol L^{-1} $Na_6[(PO_3)_6]$ (sodium hexametaphosphate) under slow agitation (50 rpm) for 16 hours using a Wagner-type shaker. Coarse sand (2.0–0.2 mm) and fine sand (0.2–0.053 mm) fractions were separated by sieving, while clay content was determined by the pipette method, and silt content was calculated by the difference between the total soil mass and the sum of sand and clay fractions (Embrapa, 2017). Iron and aluminum oxides were quantified by two selective extractions in triplicates for each analysis: (I) amorphous and poorly crystalline phases (Fe_{ox} and Al_{ox}) were extracted using 0.2 mol L^{-1} acid ammonium oxalate at pH 3.0 (McKeague and Day, 1966), and (II) crystalline phases (Fe_{DCB} and Al_{DCB}) were extracted using the dithionite–citrate–bicarbonate (DCB) method (Mehra & Jackson, 1960). The extracted Fe and Al concentrations were determined by atomic absorption spectrometry.

Additionally, due to the low clay content, bulk soil samples were analyzed using X-ray fluorescence (XRF). The material was macerated to at least 150 mesh and then fused with lithium tetraborate to produce pastilles. Elemental analysis was quantified by an X-ray fluorescence spectrometer. Chemical index of alteration (CIA) (eq. 1) and Index of Compositional Variability (ICV) (eq. 2) were measured to quantify geochemical weathering. To achieve the CIA, each oxide in the formula was converted to moles. Furthermore, the CAO* was corrected for carbonate and apatite content, as widely recommended (McLennan, 1993).

To a conservative value, the rule of CaO content is less than the Na_2O content, CaO* will be used; if the CaO content is greater than the Na_2O content, the CaO* content is considered equal to the Na_2O content (Yang et al., 2023). Complementary, TiO_2:ZrO_2 and Al_2O_3:SiO_2 per clay were calculated along the profiles.

$$CIA = \left(\frac{Al2O3}{Al2O3 + K2O + Na2O + CaO*}\right) x\ 100 \qquad \textit{Equation 1.}$$

$$ICV = \left(\frac{Fe2O3 + K2O + Na2O + CaO + MgO + MnO + TiO2}{Al2O3}\right) \textit{ Equation 2.}$$

2.4. Mineralogical analysis

Minerals in clay, silt, and sand fractions were identified in distinct horizons from each profile. Particle-size fractionation followed the protocol described by Urely & Drees (2008). The sand fraction was sieved and wet, while the clay and silt were separated through repeated siphoning of the dispersed material, every 24 hours, and the upper 20 cm were extracted. Removal of organic matter through sodium hypochlorite method (Urely & Drees, 2008) was realized before the X-ray diffraction (XRD) analysis and then dried. Mineralogical composition was determined by XRD using Co-Kα radiation at 0.02 °2θ s^{-1} in the range of 3–70 °2θ for the sand fraction and silt using the random powder mount method (Urely & Drees, 2008). The clay fraction was analyzed using the Glass Slide Mounts method (Urely & Drees, 2008). For this purpose, the clay minerals were studied just in their natural state. All the samples analyzed have their peaks confirmed through the use of X'Pert HighScore Plus and bibliography from Chen (1977), and Chicagov et al. (2001).

2.5. Morphometric analysis

Topographic variables (altitude, slope, aspect) were derived from a digital elevation model of Arctic ArcticDEM with 2 m spatial resolution generated by applying stereo auto-correlation techniques to overlapping pairs of high-resolution optical satellite images (Porter et al., 2023). Slope and aspect were calculated using SAGA GIS in R v4.1.3 (R Studio Team, 2022). Northness and eastness were computed as cosine and sine transformations of aspect, respectively, to obtain continuous variables suitable for correlation analysis (Roberts, 1986).

2.6. Statistical procedures

All data collected were subjected to statistical analysis using R v4.1.3 (R Studio Team, 2022). Non-parametric statistical tests were applied to evaluate relationships among soil properties and spatial parameters. Spearman's rank correlation coefficients (ρ_s) were used to assess associations among chemical, morphometric, and physical variables, as these data showed non-linear relationships and non-normal distributions. In addition, a Principal Component Analysis (PCA) was performed to identify the main gradients controlling soil geochemical composition, organic carbon, and landscape patterns. PCA loadings and scores were examined to interpret the influence of environmental variables. PCA was performed using individual soil samples (n = 33) as observations and soil properties (n = 28) as variables. Although the number of observations is only slightly higher than the number of variables, PCA remains an exploratory tool for identifying dominant geochemical and pedogenetic gradients.

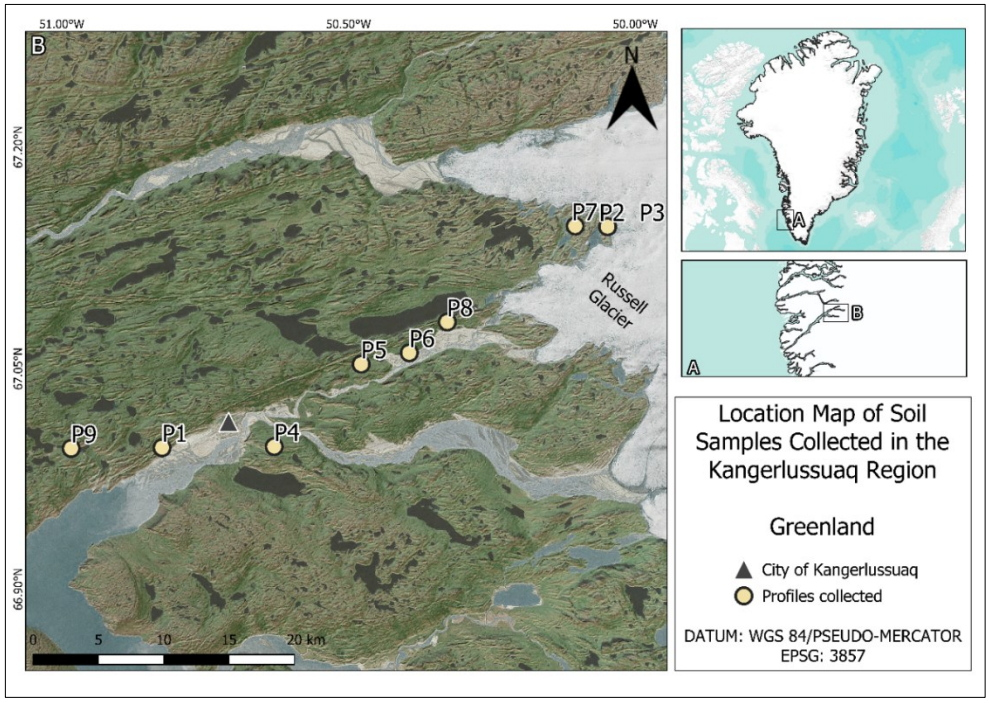

Figure 1: Map of profiles collected in the region.

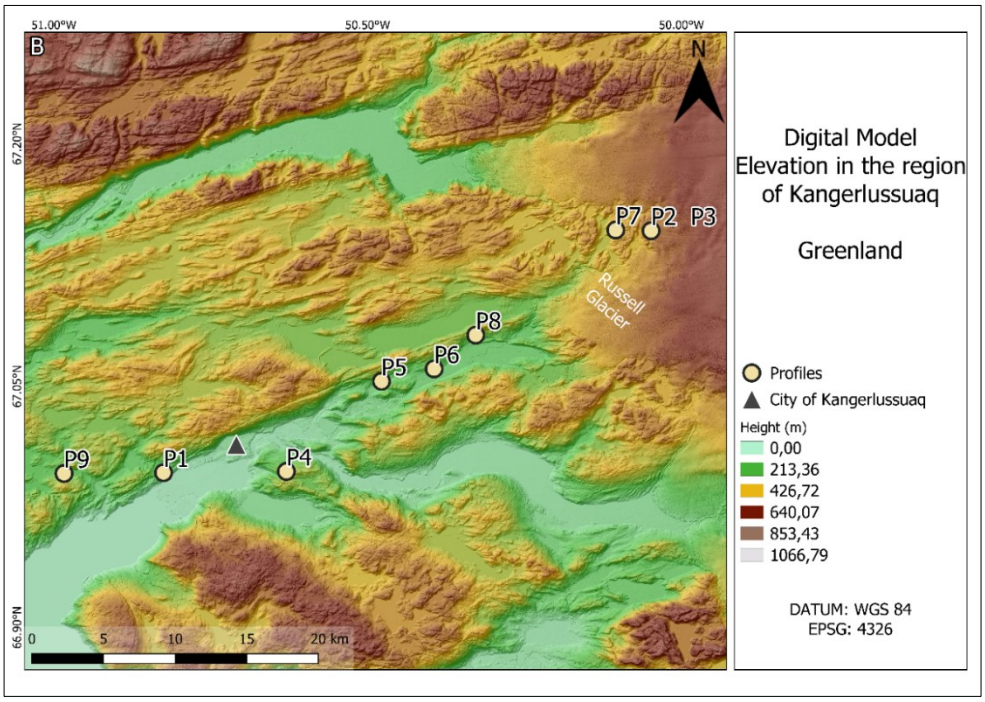

Figure 2: Elevation map across profiles collected.

3. Results

3.1. Topographic and Environmental Setting

The regional topography exhibits high complexity, with slope gradients ranging from 0º to 87.03º (Figure 3). The specific sampling sites were situated on stable landforms with slope gradients between 4.24º and 12.24º (7.55% to 25.39%), classified as gently sloping to moderately steep (FAO, 2006). Aspect varied across the study area: profiles P1, P2, and P5 were located on southeast-facing slopes; P4 and P7 occupied northwest-facing positions; and P6 and P9 were situated on south- and north-facing slopes, respectively (Figure 4). The samples collected were represented of three lithic classification of the region: profiles P1, P2, P3, P4, P7, and P8 were sampled from areas underlain by orthogneiss, while P5 was collected from undifferentiated Quaternary cover and P6 from a glaciofluvial deposit (Figure 5).

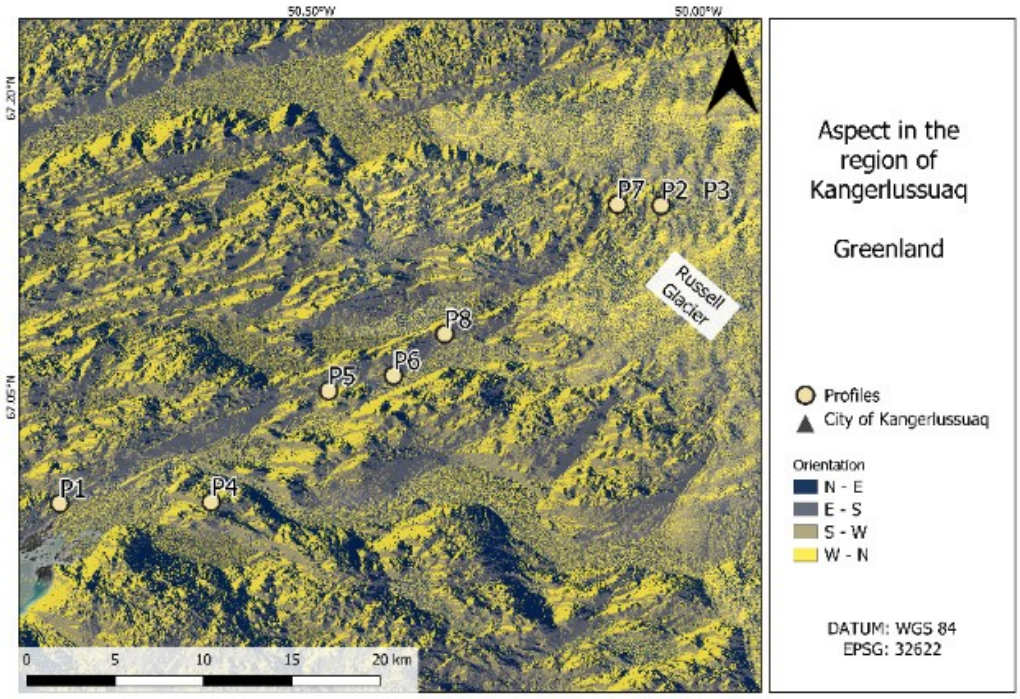

Figure 3: Regional aspect of Kangerlussuaq region.

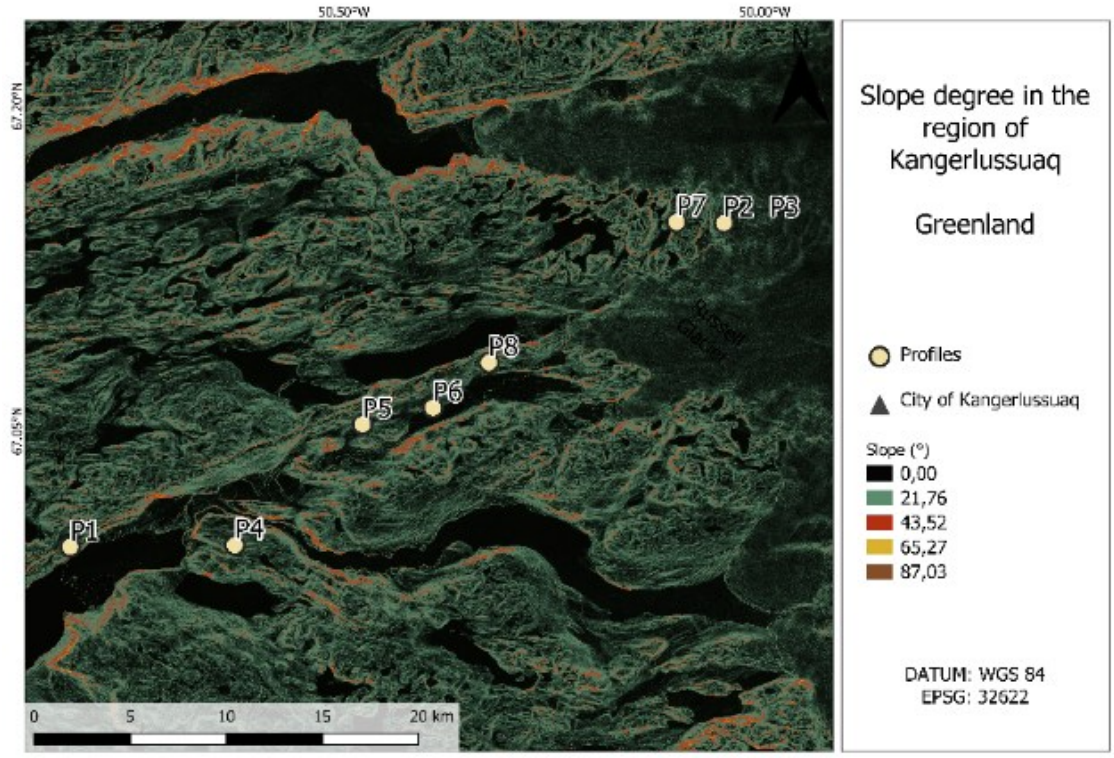

Figure 4: Regional slope of Kangerlussuaq region.

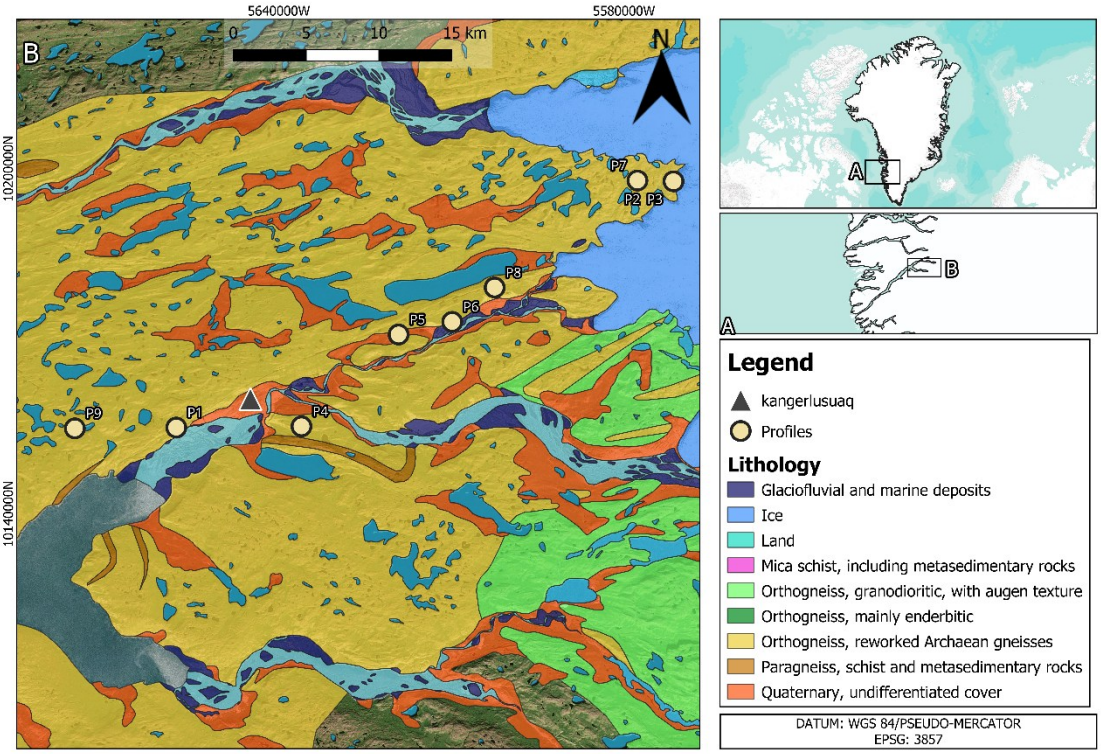

Figure 5: Regional lithology.

7

3.2. Soil Morphology and properties identified.

The soils of the Kangerlussuaq region were sampled along a proglacial-periglacial transect, extending from the proximal glacier margin to the distal fjord-sea interface. Altitude varied between 112 and 513 meters above sea level (a.s.l) (Table S1). Variations of the coarse sand/fine sand ratio indicated lithic discontinuities in the P1, P2 and P6, plus P7 within an organic horizon buried which were also validated along the fieldwork. These profiles are found at different distances from glaciers and at different altitudes.

Profile P1, situated 29.07 km from Russell Glacier, 112.68 a.s.l, slope of 18.84%, was classified as a Hypereutric Leptic Regosol (Siltic, Gelic, Humic, Raptic, Protospodic). It exhibits illuvial accumulation processes, along 15 – 25 centimeters, with geochemical signatures resembling protospodic material, though it lacks the diagnostic horizon development required for a Podzol. Specifically, while the accumulation of Fe and Al oxides suggests incipient podzolization (Table S2), the profile maintains a near-neutral pH (7.32) and does not meet the standard WRB color criteria for spodic horizons (Table S1). Profiles P2 and P3, less than 1 km from the glacier, were classified as Hypereutric Leptic Regosol (Loamic, Protospodic, Humic, Raptic), 523 a.s.l, slope of 22.01, while P4, 19.7 km from the glacier, 270 a.s.l, slope of 25.39%, was classified as Mollic Reductaquic Turbic Cryosol (Pantoloamic, Hypereutric, Dorsic, Humic). Profile P5, 11 km from glacier, within 124 a.s.l, slope of 7.55%, was classified as Entic Carbic Podzol (Siltic, Epic, Eutric, Gelic). P6, 7 km from the glacier,

125 a.s.l, slope of 22.73%, was designated as Eutric Aeolic Arenosol (Areninovic, Claric) over Dystric Regosol (Siltic, Humic, Panpaic), highlighting the buried horizon. P7, within 0.97 km from the glacier, 350 a.s.l, slope of 24.31%, was classified as Cambic Someric Phaeozem (Loamic, Humic, Gelic) over Eutric Regosol (Histic, Gelic, Humic), containing a buried organic-rich horizon (Hb) in 35 to 45 centimeters. Profile P8, having 3.81 km distance from glacier, 211 a.s.l, slope of 12.69%, was identified as a Histic Turbic Cryosol (Siltic, Folic, Humic, Turbic, Protospodic), which also has incipient podzolization, along 50 – 60 centimeters, process identified which did not meeting the criteria establish by IUSS (2022) (Table S1). Profile P9, having 33.37 km distance from glacier, 203 a.s.l, slope of 13.61%, was identified as a Protic Histic Turbic Cryosol (Loamic, Hypereutric, Endic, Humic, Limnic, Raptic, Aeolic). Within this group, soil thickness varied between 35 and 80 cm, with texture serving as a primary diagnostic criterion for differentiation, especially sand fractions.

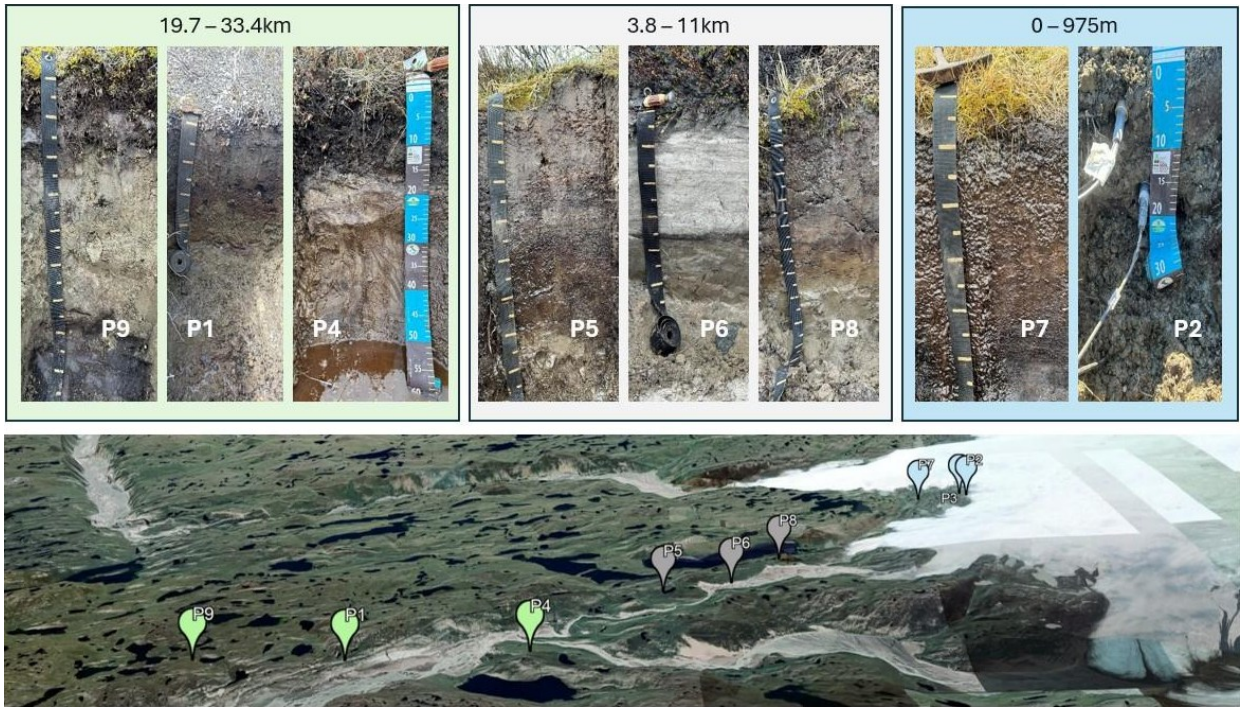

Figure 6: Soil profiles grouped by distance from the glacier.

3.3. Physicochemical attributes

Soil pH_{H2O} varies from acidic to near-neutral (Table S2), especially in the deeper horizons of profiles. The pH varied between 7.58, in the P1 2C horizon, and 4.59 in the P9 O horizon, with a median of 5.9. The base saturation in the profiles collected ranged from 34.9%, found in P9 in the O horizon, and the highest value, 98%, found on P1 2C horizon, and has a median of

70.6%. The organic carbon content determined by the Walkley-Black method varied between 0.09%, in P6 at A horizon, and 28.84%, in P9 at O horizon, with a median of 6.05. The total nitrogen ranged between 0.004% and 0.814%, with a median of 0.189%. The C/N ratios ranged between 4.02 and 130.96, with a median of 32.04. In some profiles it was observed that accumulation of total organic carbon in subsurface layers and some decreased C:N ratios along the subsurface (Figure 7).

The textural classes varied into Silt Loam, Loam, Sandy Loam, and Silt, serving as a decisive factor in the taxonomic differentiation of the profiles. A high Silt/Clay ratio was observed throughout the study area, ranging from 2.11 to 9.26 (median 3.82), the Sand/Clay ratio ranged between 0.33 to 28.66 (median 3.95), and the Sand/Silt ratio ranged between 0.11 to 11 (median of 0.92), these values show predominance of Silt fraction over Clay and Sand fractions (Table S2).

The Fe_{ox} concentrations ranged from 0.109 to 2.067 $g.kg^{-1}$ (mean 0.612 $g.kg^{-1}$) while Fe_{DCB} ranged from 0.240 to 2.284 $g.kg^{-1}$ (mean of 1.269 $g.kg^{-1}$). For aluminum, Al_{ox} varied between 0.033 and 1.455 $g.kg^{-1}$ (mean of 0.387 $g.kg^{-1}$) and Al_{DCB} between 0.045 and 1.201 $g.kg^{-1}$ (mean of 0.384 $g.kg^{-1}$). The ratio Fe_{OX}/Fe_{DCB} ranged between 0.165 and 1.218, with a mean of 0.551, reflecting a dominance of amorphous iron phases (Figure 8). Al_{OX}/Al_{DCB} ratio ranged from 0.212 to 4.302, with a median of 1.269. Values of $Fe_{OX}/FE_{DCB} > 1$ are not common, but are relatable in the literature (Vodyanitskiia et al., 2007; Schwertmann, 1988; Schwertmann et al., 1986).

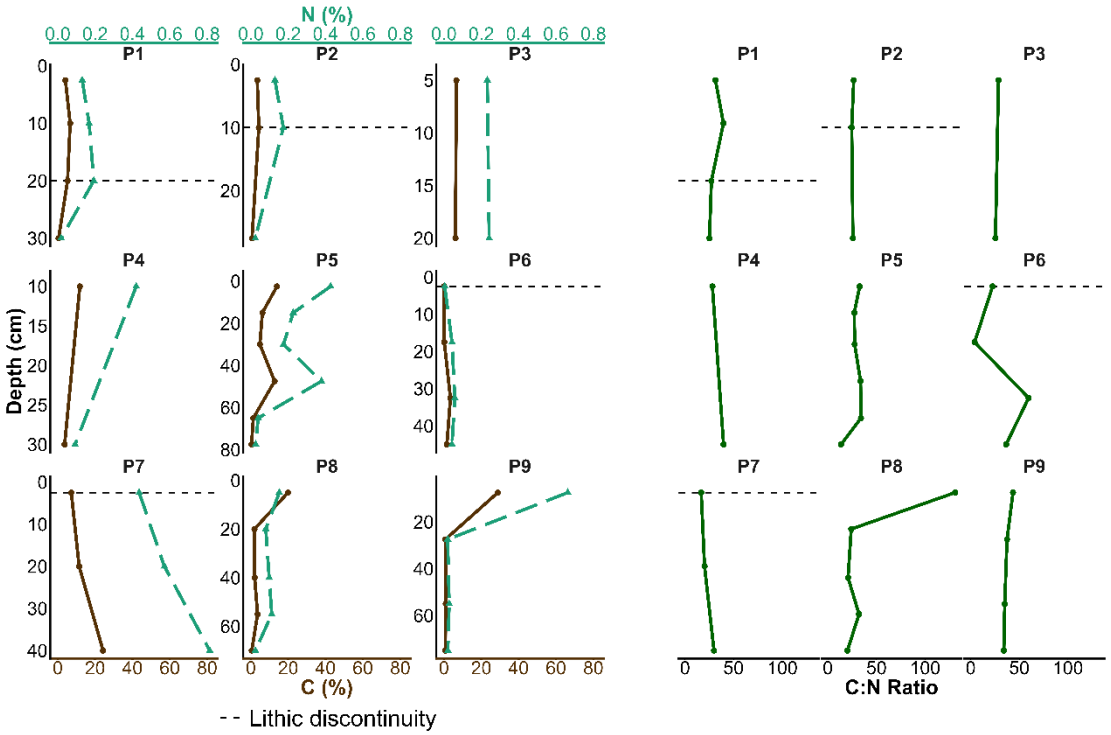

Figure 7: C:N ratio and content in the soil profiles.

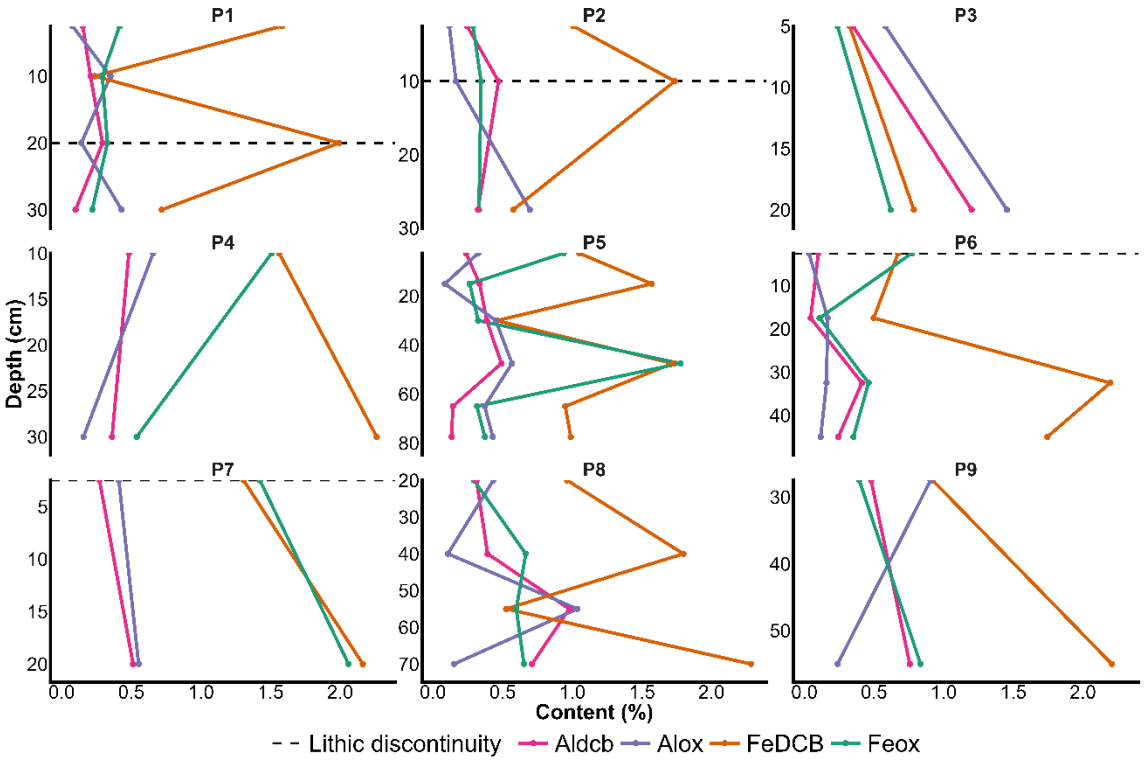

Figure 8: Fe and Al extraction from Oxalate and Dithionite-Citrate-Bicarbonate.

3.4. Bulk Geochemistry and Weathering Index

The main contents found in the soils were SiO_2, Al_2O3, Fe_2O3, CaO, Na_2O, K_2O, and MgO, respectively (Table S3). SiO_2 ranged from 47.7 to 75.9% with a median of 64.3%, where the lowest value was found in P9, horizon C3, and the highest in P6, horizon C1 (Table S3). The CIA ranged from 47.73, in P8 horizon C, to 51.36, P5 horizon C2, with a mean of 49.64 (Figure 9). The values reached are lower than the proposed values characterized by weak weathering, which are between 50 and 60 (Fedo et al., 1995). The ICV values varied between 0.94, P6 horizon C1, and 1.54, P5 horizon C2, with a mean of 1.24, being predominantly classified as immature soils since most values are higher than 1 (Cox et al., 1995). Furthermore, as observed in ACNK ternary diagram, all samples collected are in the Feldspar joint, which is exactly the value of 50 from the CIA, and nearest of the plagioclase material (Figure 10). This value corresponds, as expected, of samples being derived from felsic material, being the major local composition (Kalsbeek et al., 1987). Ti:Zr ranged between 7.37 – 22.5 (Figure 9) and Si:Al 4.28 – 5.88 (Figure 11).

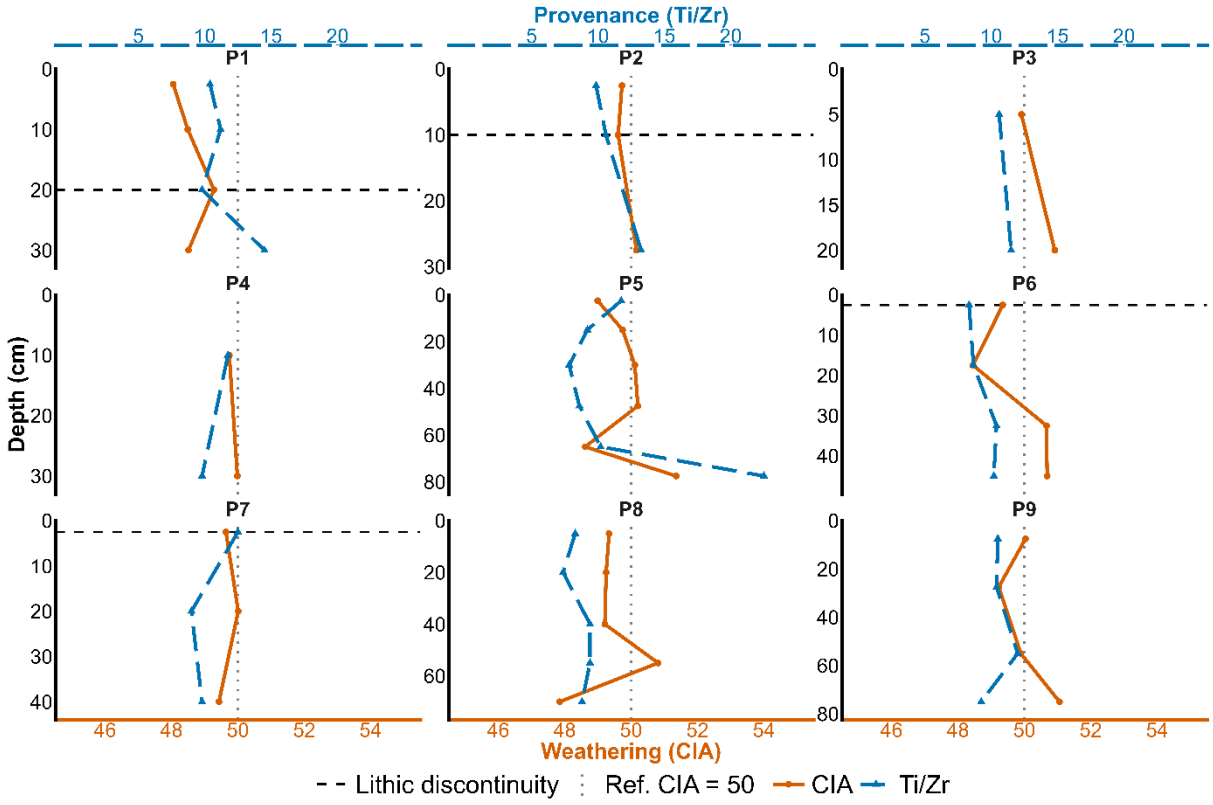

Figure 9: CIA and Ti/Zr ratio along the soil profiles collected.

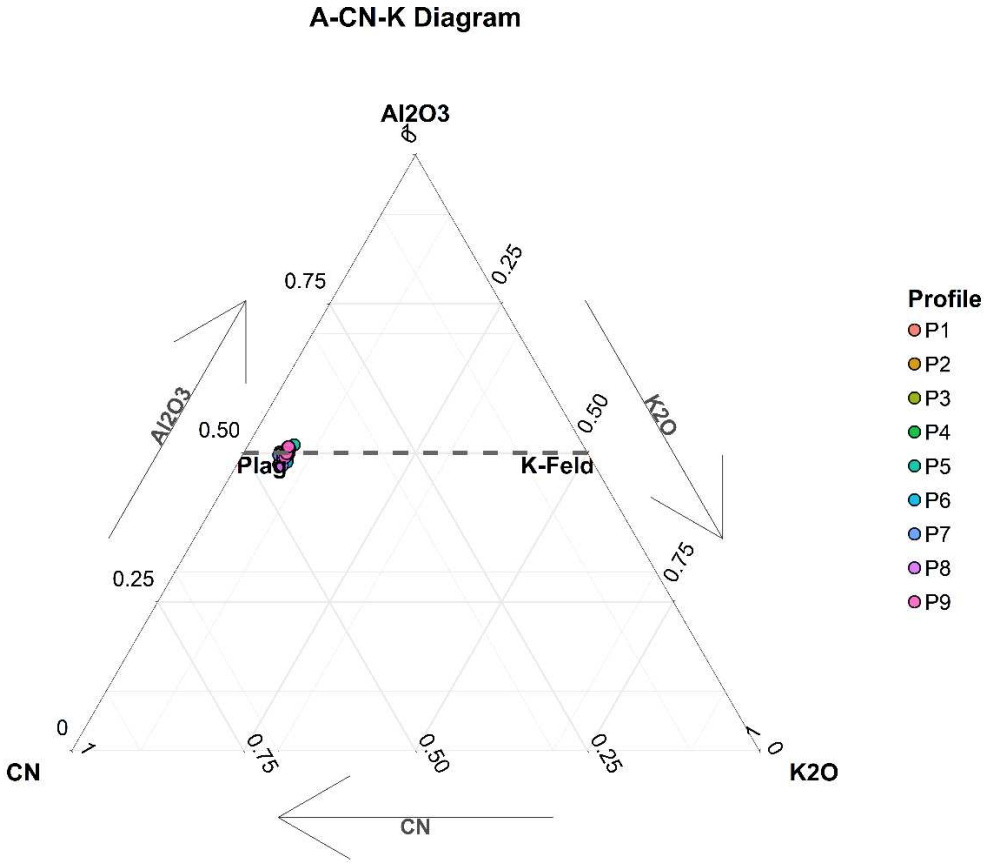

Figure 10: ACNK ternary diagram.

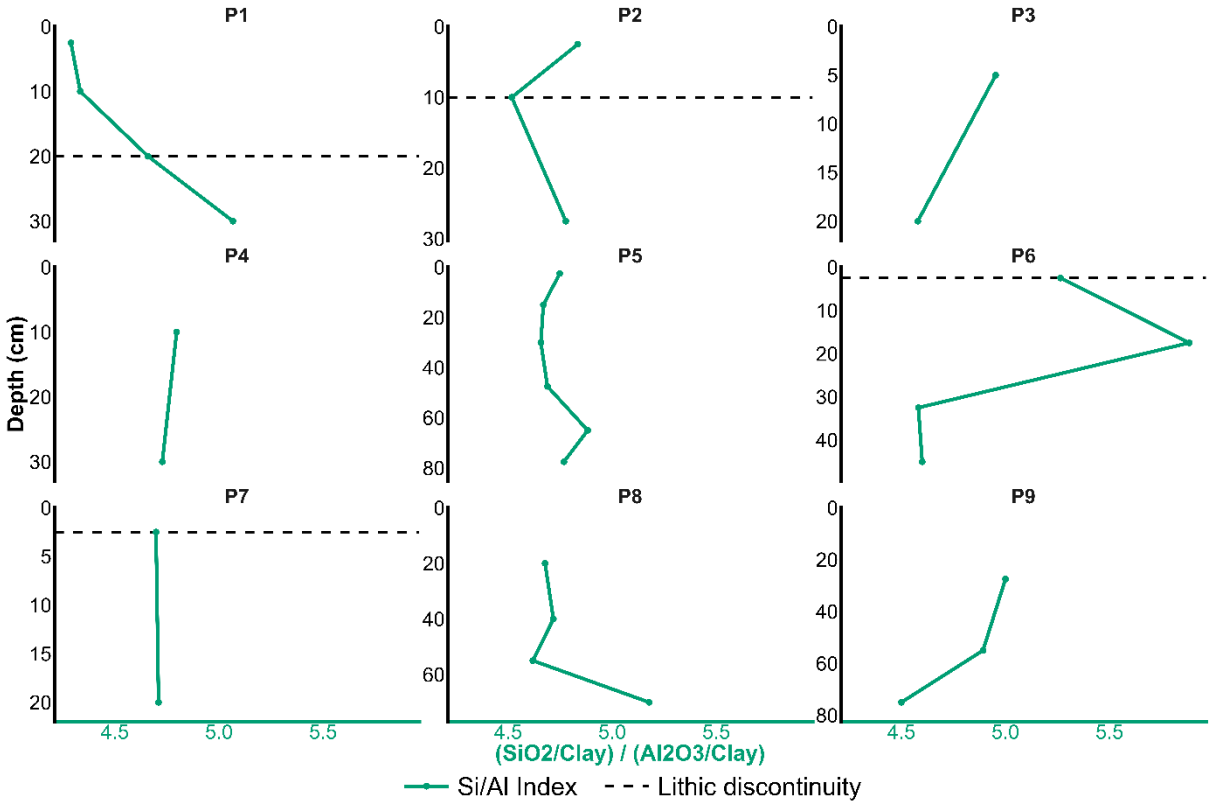

Figure 11: Si:Al ratio.

3.5. X-ray diffraction

Representative samples from surface and subsurface horizons were selected for XRD analysis across sand, silt, and clay fractions. As no secondary phyllosilicates were detected in the natural clay fraction, further chemical or thermal treatments were not required. Quartz (Q) and albite (A) were ubiquitous in all analyzed samples. In surface layers, such as the AE horizon of P2 (Figure 12), phyllosilicates consistent with primary micas (M) were identified exclusively in the clay fraction, whereas feldspars and amphiboles were present across all size fractions. In this same horizon, minerals of the serpentine group (S) were detected in the silt and sand fractions. Similarly, deeper layers, as P6 2C2 and P9 C2, (Figures 13 and 14) were found amphiboles, quartz, and albite. Minor variations were restricted to the sand fraction, including peaks of serpentine (S) in P9 (C2) and orthoclase (Ort) in P6 (2C).

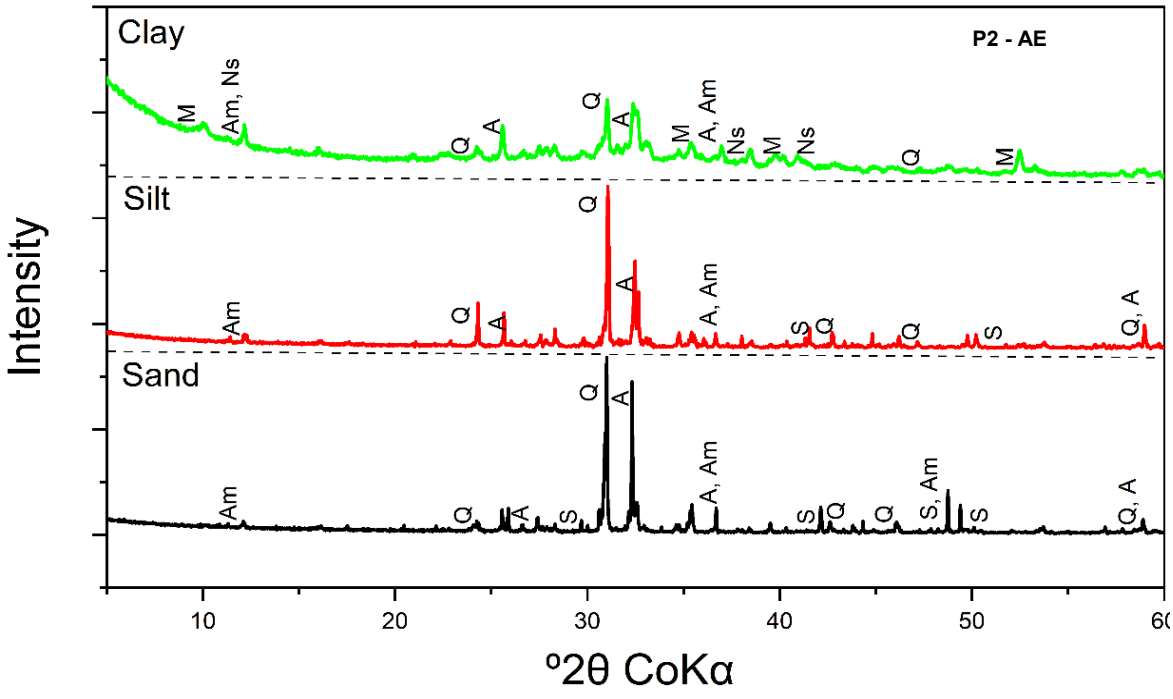

Figure 12: XRD from P2, horizon AE. Where M – Mica, Am – Amphibole, Q – Quartz, Ns – Nesosilicate.

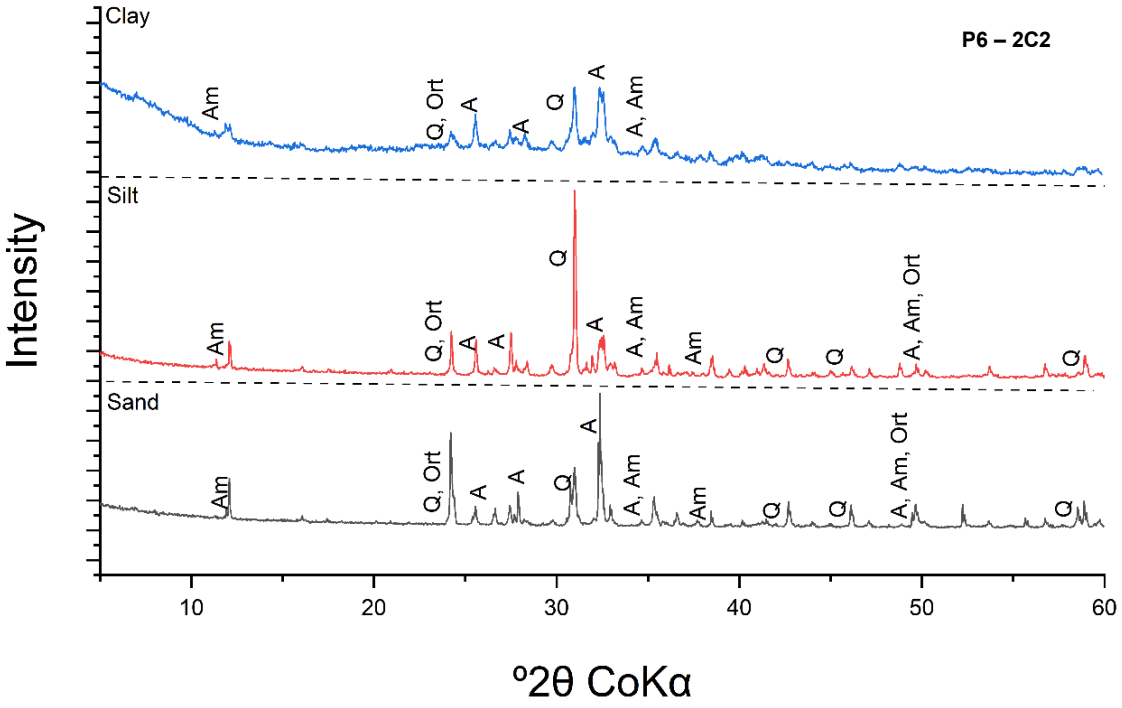

Figure 13: XRD from P6, horizon 2C. Where A – Albite, Am – Amphibole, Q – Quartz, Ort – Orthoclase.

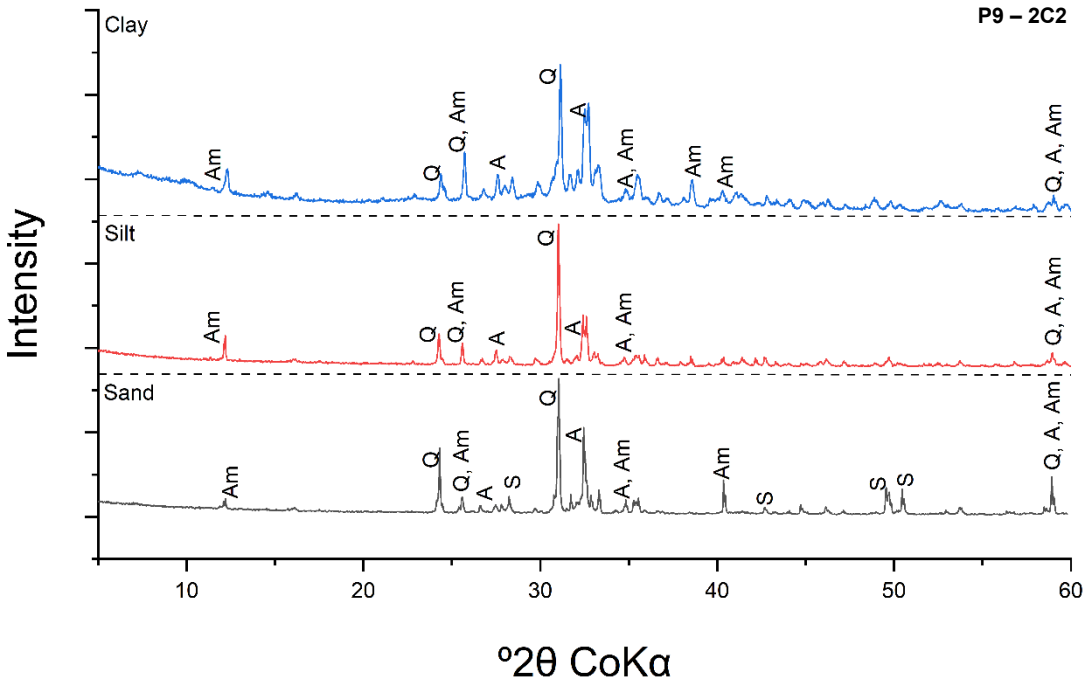

Figure 14: XRD from P9, horizon C2. Where Q – Quartz, Am – Amphibole, A – Albite, S – Serpentinite.

3.6. Statistical Analysis.

The first three principal components explained 26.4%, 15.8%, and 13.4% of the total variance, respectively, accounting for 57.6% of the cumulative variance. Therefore, PC1, PC2, and PC3 were selected for interpretation and discussion (Figure 15).

The first component (PC1) has a great alignment with the contents of SiO2, CaO, MgO, Clay, organic carbon, sand and silt. PC1 demonstrate an antagonism between the coarse fraction, Sand and SiO_2, divalent oxides, clay and organic matter. The close alignment of MgO, CaO, organic carbon, and P_2O_5 with clay and silt fractions suggests that these nutrients and organic matter are preferentially hosted within the finer soil matrix.

The second component (PC2) is primarily composed of extractable phases, specifically Fe_{DCB}, Fe_{OX} and Al_{OX}, representing the pedogenic oxide pool. The third component (PC3) captures the influence of topographic and environmental variables on soil properties. The main loadings include TiO_2, Fe_2O_3, MnO, N and Altitude (Figure S1). Notably the slope is in the opposite direction of TiO_2, Fe_2O_3, MnO, Sand, K_2O, while showing a positive relationship with the clay fraction.

The relation between PC2 and PC3 variables demonstrates an interesting contribution where the morphometrical components determine some physicochemical components (Figure S1). For instance, the presence of eastness aligned with the sand fraction, which is also in the opposite direction of Silt and Na_2O, reflects a distinct spatial distribution of sediments potentially linked to regional aeolian dynamics. Furthermore, the observed divergence between slope and carbon accumulation indicates that more stable, low-gradient landforms favor the preservation of organic matter.

Spearman's rank correlation analysis was performed to complement the PCA and evaluate relationships among soil physicochemical and geochemical variables (Figure S2). Sand content was negatively correlated with CaO, MgO, AlO_3, and carbon, but positively correlated with SiO_2 ($p = 0.67$), reflecting the dominance of quartz in the coarse fraction. In contrast, silt and clay fractions showed positive correlations with major oxides and C, and negative correlations with SiO_2, indicating the preferential association of nutrients and organic matter with finer particle sizes. The strong positive correlations between clay content and C ($p = 0.93$) and nitrogen ($p = 0.80$) highlight the role of fine fractions in stabilizing organic matter. Furthermore, the positive correlation between the silt fraction and the C/N ratio ($p = 0.56$) supports the role

of aeolian deposition in burying relatively fresh, less-decomposed organic matter. Finally, positive correlations among CaO, MgO, and Fe_2O_3 suggest the co-occurrence of these elements in primary silicate minerals, consistent with mineralogical inheritance and limited chemical weathering.

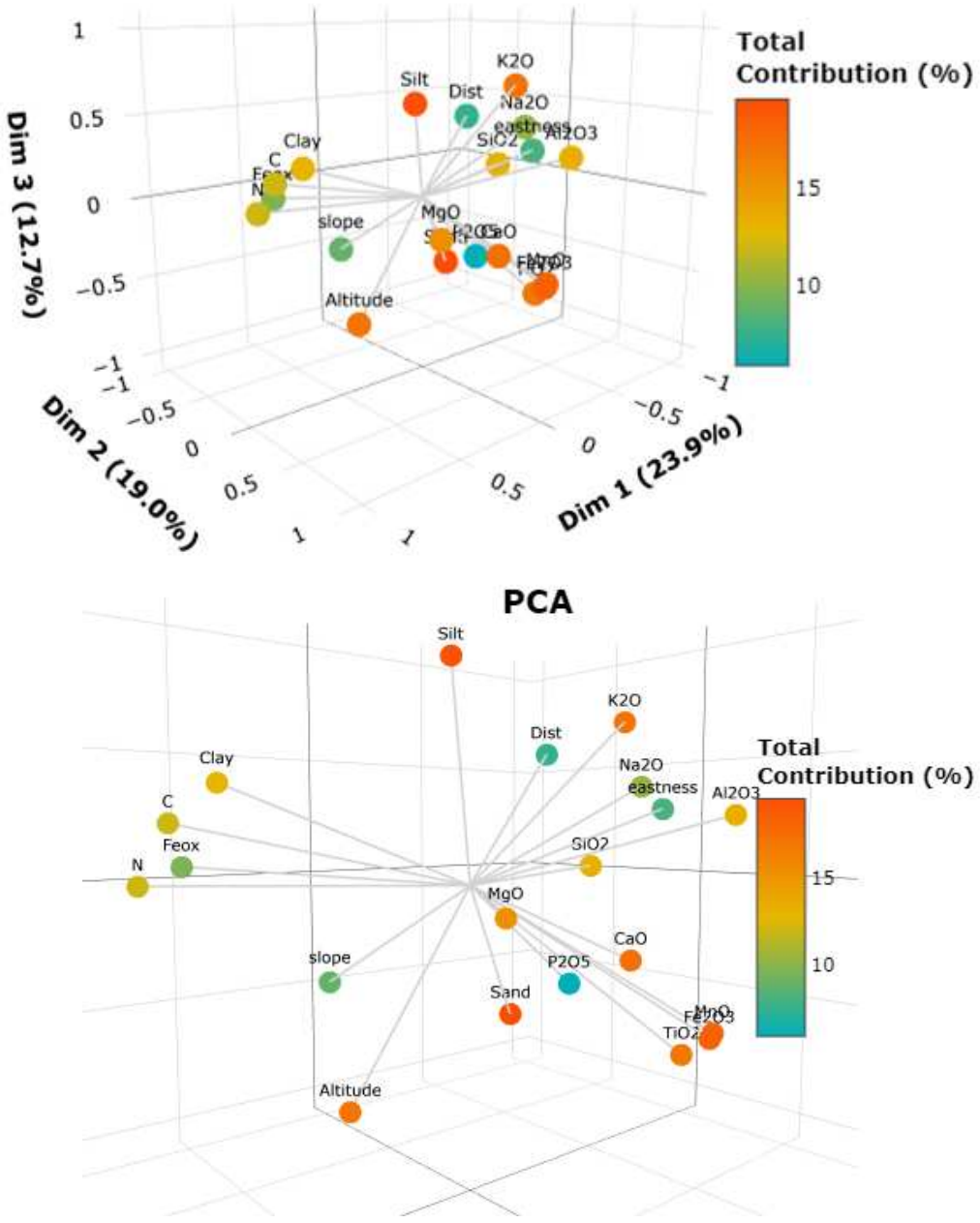

Figure 15: PCA analysis.

4. Discussion

4.1. Glacial legacy: Physical weathering dominates parent material.

Integrated geochemical, mineralogical, and textural data indicate that physical weathering processes exert dominant control on soil parent material in the Kangerlussuaq region. Across all profiles, Chemical Index of Alteration (CIA) values consistently fall within the lower range associated with weak chemical development (Fedo et al., 1995) and are notably lower than those reported for other High Arctic environments, including Svalbard (Yang et al., 2023; Wojcik, 2013) and western Siberia (Moskovchenko & Romanenko, 2022). Furthermore, these values show no increase with depth, indicating limited base cation depletion and an absence of progressive in situ chemical weathering (Table S3). This interpretation is further supported by the ACNK diagram (Figure 8), which shows that samples cluster near the plagioclase vertex. Such a distribution reflects minimal feldspar hydrolysis and suggests that kinetic conditions for silicate alteration are strongly inhibited under prevailing regional climatic conditions.

Soils are overwhelmingly composed of silt- and sand-sized particles, with median silt/clay and sand/clay ratios of 3.82 and 3.95, respectively (Table S2). This granulometric signature is consistent with sediment production through glacial comminution and physical weathering (Wright, 2007; Melke & Chodorowski, 2006). Furthermore, the prevalence of sand and silt coupled with high base saturation and low pedogenic oxide concentrations, reflects a weathering regime where chemical transformation is strictly limited. These findings align with other polar studies (Thomas et al., 2023), where soil development is governed by physical processes, such as cryoclasty and glacial comminution, rather than advanced chemical alteration (Hall et al., 2002).

Aeolian reworking represents one of the main sources of fine material; however, the overall homogeneity of particle-size distributions suggests that sediment supply and physical inheritance outweigh pedogenic particle translocation as illuviation of particles, oxides, and organic matter through water saturation or cryoturbation. In polar regions, such granulometric distributions are commonly explained by the “glacial–aeolian” hypothesis, which posits that the Quaternary is a silt-rich period due to intense tectonic and glacial activity (Assalay et al., 1998; Wright, 2007). Regional stratigraphic studies further indicate that the Kangerlussuaq area experienced at least two distinct phases of loess deposition over the last 5 ka (Willemse et al., 2003; Sechi et al., 2024).

Mineralogical evidence provides the most direct constraint on chemical weathering intensity, considering that lithogenic minerals tend to demonstrate low resistance to chemical and physical weathering. XRD patterns of untreated clay fractions are dominated by primary silicates, and no clear diagnostic peaks of secondary phyllosilicates were detected. However, low-abundance or poorly crystalline secondary phases cannot be excluded. The minerals include quartz, albite, and amphiboles, which closely match the mineralogical composition of local morainic deposits (Auqué et al., 2019). The persistence of primary silicates in the finest fraction indicates that clay-sized particles were largely generated by mechanical grinding rather than by the formation of secondary phyllosilicates. This interpretation is further supported by Spearman's rank correlations, which show associations between CaO and MgO with the silt and clay fractions and between P_2O_5 and the clay fraction (Figure S1), while SiO_2 correlates positively with the sand fraction, consistent with a physically derived mineral assemblage across all size classes.

Taken together, these results indicate that soils in the Kangerlussuaq area largely retain the mineralogical and geochemical signature of glacially derived parent material, as sediments from the glacier and the formation of tillites, with chemical weathering playing a subordinate role in soil development. However, chemical weathering is observed, as evidenced by elevated Fe_{OX}/Fe_{DCB} ratios with some horizons > 1, which may be enriched in Fe-organic complexes. These values are associated with higher quantities of Fe (II) that can be influenced due to organic matter and climate, which may catalyze the potential of oxalate ammonium extraction (Schwertmann et al., 1986). Furthermore, these values may be linked with higher contents non-crystalline, short-range-order (SRO) minerals, ferrihydrite for example, or be an artefact from mineralogy, especially in presence, even in trace amounts, of magnetite (Siqueira et al., 2021; Walker, 1983), siderite or pyrite (Vodyanitskiia et al., 2007). These secondary phases do not meet the diagnostic horizon thresholds due to restrictive climatic conditions and episodic burial by fresh parent material. Pedogenic processes therefore operate within a physically inherited substrate that remains only weakly altered, providing the baseline upon which subsequent sedimentary inputs and episodic soil-forming processes act.

4.2. Dynamic between aeolian burial and pedogenic processes along the profiles

Lithic discontinuities identified across the studied profiles indicate that aeolian deposition has been an influential process in the Kangerlussuaq region. Four of the nine profiles (P1, P2, P6, and P7) exhibit abrupt textural shifts between adjacent horizons that meet the IUSS (2022)

criteria for lithic discontinuities. In Profile P1, the discontinuities occur primarily at the transition from a Bhs to 2C horizon, suggesting that the entire overlaying pedon is composed of allochthonous material distinct granulometric from the underlying parent substrate. In contrast, profiles P2, P6 and P7 display discontinuities within surface and upper subsurface horizons, reflecting a more heterogeneous stratigraphy shaped by the repeated sediment inputs and partial soil development.

Although no site-specific chronology is available, the vertical distribution of these discontinuities is broadly consistent with episodic aeolian activity documented in regional stratigraphic records (Sechi et al., 2024). In this context, deeper discontinuities may tentatively correspond to earlier phases of enhanced aeolian deposition, whereas shallow or surface discontinuities likely reflect more recent sediment inputs. These interpretations remain hypothetical and should be considered cautiously, particularly given the potential for sediment reworking and redistribution under high-energy aeolian conditions (Sechi et al., 2024).

In addition to depositional features, several profiles exhibit irregular or wavy horizon boundaries (Figure 16), being an indicative of cryoturbation (IUSS, 2022). This process occurs within the active layer, where differential frost heave and cryostatic pressure during annual freeze-thaw cycles lead to the mechanical mixing of soil materials. As the soil freezes, the formation of ice lenses creates uneven pressure that displaces soil particles and distorts originally horizontal layers into the wavy or convoluted structures observed.

Figure 16: Soil profiles with irregular and/or wavy horizons (P7, P9) and buried horizon (P7, P6 and P9). Black circles indicating buried horizons and blue circles indicating irregular and/or wavy horizons.

On the other hand, the buried horizons are characterized by smooth boundaries, typical of depositional interfaces (IUSS, 2022) and observed among the burial horizons identified. The coexistence of cryoturbation structures and lithic discontinuities highlights the simultaneous operation of vertical mixing and stratigraphic preservation within soil profiles, underscoring the complexity of soil formation processes in permafrost-affected environments.

Despite the dominance of physical weathering, morphological and geochemical evidence indicate the onset of incipient chemical weathering and vertical translocation processes. Profiles P1, P2, and P8 display organic-depleted eluvial horizons overlying subsurface layers enriched in organic carbon and oxalate-extractable Fe and Al (Figure 7). These accumulations suggest limited eluviation-illuviation processes driven by seasonal permafrost thaw, which can mobilize organic acids and organo-mineral complexes (Sheinkman et al., 2025). However, fully developed spodic horizons sensu IUSS (2022) are absent, as soil pH remains near-neutral, indicating chemical conditions that constrain metal mobilization and inhibit progression toward classical Podzol development. The incipient nature of these processes is nevertheless taxonomically significant. The Protospodic qualifier, which identifies initial illuviation conditions through an Al_{ox} value ≥ 1.5 times that of the lowest Al_{ox} value in all overlying mineral layers (IUSS, 2022), is currently not recognized as a subqualifier for Regosols within the WRB framework. However, the profiles analyzed here meet this criterion and would be more accurately characterized as Protospodic Regosols. Incorporating this qualifier would better reflect the subtle but active pedogenetic development occurring between burial events and would provide a taxonomic tool better suited to rapidly warming Arctic landscapes, where permafrost deepening may progressively favor podzolization pathways that differ from those documented by Jakobsen (1989).

Furthermore, geochemical indices, in P9 and P6, reflect the influence of aeolian rejuvenation on pedogenic gradients. CIA values tend to increase in subsurface horizons near lithic discontinuities rather than decreasing systematically with depth (Figure 8), as would be expected under uninterrupted soil development (Jobbágy et al., 2001). These inverted or irregular weathering patterns are consistent with stratigraphic evidence of repeated aeolian inputs, each introducing minimally weathered material that disrupts the vertical continuity of pedogenic gradients rather than allowing progressive chemical differentiation with depth.

Elemental ratios, such as Ti/Zr, are frequently utilized to distinguish parent material contrasts. In these profiles, Ti/Zr ratios exhibit modest vertical variability, with abrupt shifts

occurring primarily across lithic discontinuities. While these patterns may reflect distinct compositional units, their interpretation is constrained by the potential for elemental redistribution within light mineral fractions under high-energy aeolian conditions (Smeck & Wilding, 1980; Drees & Wilding, 1978). Consequently, Ti/Zr ratios, considering the landscape analyzed, serve as supportive rather than definitive indicators of lithological changes through depositional boundaries or not. Complementarily, Si/Al ratios show a marked decrease immediately below lithic discontinuity. This trend reflects an enrichment of Al_2O_3 with depth, contrasting with the SiO_2 rich signatures of the superficial aeolian layers, which are dominated by quartz-rich sand and silt. The enrichment of Al_2O_3 with depth reinforces the idea of illuviation process along the profile and its enrichment through sub-layers.

Together, these observations indicate that soil development in the Kangerlussuaq region follows a polygenic and non-linear trajectory. Seasonal freeze-thaw cycles enable limited pedogenic processes, including incipient eluviation-illuviation, while stratigraphic evidence points to aeolian deposition as the dominant retarding and rejuvenating mechanism. Rather than reflecting progressive chemical maturation, these profiles preserve a record of alternating depositional events and cryogenic reworking, in which aeolian input introduces a minimally weathered mineral substrate that overrides the pedogenic signal accumulated during the preceding interlude. This trajectory is consistent with regional aeolian chronologies (Sechi et al., 2024; Willemse et al., 2003) and explains why geochemical immaturity persists across profiles regardless of their position along the glacial distance gradient

4.3. Topographic and glacial controls on pedogenetic development

The spatial distribution of geochemical and textural properties across the profiles collected indicates a relatively homogeneous physical and geochemical substrate at the regional scale. This is supported by the non-significant Spearman correlation between grain-size fractions and topographic variables such as altitude and distance from glacier. This suggests that the historical aeolian pulses provided consistent material across the region (Sechi et al., 2024), effectively masking the chronological age of the underlying moraines through continuous surface rejuvenation, as evidenced by the uniform ICV and CIA values (Table S3), including near-surface horizons with particularly low CIA.

Despite this regional homogeneity, local topography exerts a distinct filtering effect on mineral and elemental distributions. The PCA reveals an inverse relationship between altitude and elements such as K_2O, Al_2O_3, Fe_{DCB}, and northness (Figure 10). These patterns may suggest

that slope position and aspect modulate soil geochemistry primarily by influencing microclimatic conditions rather than through differences in parent material. North-facing slopes are associated with higher contents of organic carbon, Fe_{DCB}, and total nitrogen, which is consistent with regional studies that have observed deeper organic layers and greater carbon storage under reduced solar radiation, prolonged snow cover, and enhanced moisture retention on north-facing slopes (Henkner et al., 2016; van Soest et al., 2025). These conditions favor organic matter accumulation and contribute to localized geochemical differentiation, even within an otherwise homogeneous aeolian substrate. Furthermore, elemental distribution also reflects the interaction between aeolian transport processes and topography. The significant positive correlation between K_2O content and distance from the glacier, together with the inverse relationship with altitude, may indicate preferential redistribution of K-bearing minerals across the landscape. Since K_2O shows no significant correlation with silt or sand fractions, these trends are unlikely to reflect grain-size effects alone. Instead, they suggest aerodynamic sorting of K-rich primary minerals, such as micas, which are selectively removed from exposed, high-altitude positions and redeposited in lower-lying, more distal areas. This interpretation is consistent with documented aeolian sorting of phyllosilicates in Arctic and other environments (Eden et al., 1999; Muhs, 2018) and is supported by the positive association between silt content and Al_2O_3.

Overall, these results indicate that while aeolian deposition establishes a regionally uniform parent material, local topography and glacial proximity act as filters that modulate elemental distributions and pedogenic expression at the site scale. Rather than driving fundamentally different soil-forming pathways, topographic controls influence the intensity and spatial variability of weak pedogenic processes superimposed on a physically inherited substrate.

4.4. Effects of dual genesis on organic soil matter.

The interaction between aeolian burial and pedogenic processes, as recorded in the stratigraphic evidence across profiles, creates a dual framework that influences the stabilization and fate of SOM. A primary consequence of this framework is the vertical translocation of organic-rich horizons, visually confirmed by the accumulation of organic carbon in subsurface layers (Figure 6). Where aeolian deposition has buried former surface horizons, SOM is effectively moved to depth, where mineralization is slow due to reduced microbial diversity (Blaud et al., 2015). Examples are observed in P6 with 0.17% of a C1 overlying a 2Ab buried

layer with 3.45% at 30 – 35 cm depth and the 2C2 within 1.57%, and P7 within a B horizon accumulating 11.46% of C overlying a Hb with 24.26% of C.

The C:N ratios observed in these profiles generally exceed the standard humus values of 10 to 12 (Kirby et al., 2011). While surface horizons naturally exhibit higher ratios, these values fluctuate along the deep horizons (Figure 7). In P6, characterized by lithic discontinuity, the values of carbon content and C:N ratios increase near the burial contact. This suggests that rapid aeolian deposition preserves relatively fresh organic material by shielding it from decomposition. This preservation likely occurred because of restrictive abiotic conditions at depth, including lower summer temperatures, higher moisture content, and prolonged frozen states (Kaiser et al., 2007).

In addition, our data allows us to distinguish between chemical and physical stabilization mechanisms. In polar regions, amorphous iron and aluminum oxides commonly play a role in chemically binding SOM through organo-mineral associations (Wang et al., 2023). However, in the Kangerlussuaq soils, we found no significant correlation between organic carbon and oxalate-extractable oxides, suggesting that Fe-Al oxide-mediated stabilization contributes modestly to SOM retention in these profiles. This is consistent with the low concentrations of poorly crystalline phases identified across all profiles, reflecting the limited degree of chemical weathering in this landscape. Physical burial into cryic thermal regimes, combined with the low specific surface area of primary silt-sized minerals, therefore appears to be the dominant stabilization pathway. Localized organo-mineral interactions cannot be excluded, particularly where incipient illuviation has redistributed organic components downward, but their contribution to long-term carbon persistence warrants further investigation.

Furthermore, clay and silt fractions showed a positive correlation with organic carbon content, whereas the sand fractions showed a strong negative correlation. This underscores the capacity of fine-textured particles to preserve limited contents of carbon and nitrogen through surface-area interactions (Hassink, 1997). Previous studies highlighted the importance of the clay fraction, specifically swelling clay minerals, in permafrost and SOM stability in the Arctic (Gentsch et al., 2007; Szymanski et al., 2022).

In contrast, certain profiles with proto-illuvial accumulations show lower C:N values in deeper horizons. While cryoturbation and podzolization are known to bury organic matter in Arctic regions (Wang et al., 2023; Wild et al., 2013), the lower C:N ratios in the active layer

may indicate pools of labile, fast-cycling carbon that are quickly mineralized or flushed after the seasonal thaw (Moni et al., 2015). Although these labile fractions represent a minor portion of the total carbon stock, they may work as a primary indicator of shifting carbon dynamics within the deep subsurface.

The burial of A or H horizons initiates a restart of topsoil formation, and where burial events are separated by sufficient intervals, revegetation and pedogenic processes resume on the fresh mineral substrate. Each aeolian depositional event therefore acts as a pedogenic reset, creating a cumulative vertical architecture of organic matter in which recently fixed carbon occupies the current topsoil while progressively older pools are physically protected at depth through burial and cryogenic preservation. This mechanism explains why these soils can maintain substantial organic carbon stocks despite weak chemical stabilization, and why that carbon may be particularly vulnerable to loss if the thermal and depositional conditions that currently maintain it are altered under continued Arctic warming.

5. Conclusions

From the data collected in this study, we confirm a dual-genesis framework for the proglacial soils of Kangerlussuaq, in which mineralogical composition is governed by relict glacial comminution, while morphological evolution and carbon dynamics are controlled by contemporary aeolian deposition. Our findings demonstrate that aeolian deposition is not merely a passive parent material but an active pedogenetic agent that interrupts soil development by burying stable surfaces and disrupting the vertical continuity of pedogenic gradients. This establishes a polygenic and non-linear trajectory that explains why these soils exhibit geochemical immaturity despite prolonged exposure, as stratigraphic evidence of aeolian burial indicates repeated introduction of minimally weathered minerals that override progressive chemical differentiation.

Three key findings support this interpretation. First, primary silicate minerals (quartz, albite, and amphiboles) dominate all particle-size fractions, indicating that the clay-sized fraction consists predominantly of physically derived rock flour rather than pedogenic secondary phyllosilicates. Second, lithic discontinuities observed in four soil profiles, together with inverted weathering gradients and higher CIA values below burial contacts, provide stratigraphic evidence of recurring depositional and burial events. Third, elevated subsurface C:N ratios indicate that physical burial into cryic thermal regimes, rather than organo-mineral

stabilization involving Fe and Al phases, represents the dominant mechanism of organic carbon preservation.

Reflecting this non-linear development, we suggest that while "Protospodic" is not currently a recognized subqualifier for Regosols in the IUSS (2022) framework, its application is essential for accurately characterizing the incipient podzolization occurring in these profiles, and may prove particularly valuable for classifying soils in rapidly changing periglacial environments where incipient pedogenetic signals are easily obscured by depositional disturbance. Adopting this qualifier would better acknowledge the active pedogenetic development identified in these landscapes and the subtle translocation of organo-mineral complexes between burial events.

Future integration of absolute dating techniques, including optically stimulated luminescence (OSL) and radiocarbon analysis, is essential to constrain burial frequency and carbon accumulation rates, thereby improving predictions of long-term carbon stability under projected Arctic warming.

References

Anderson, N.J., Saros, J.E., Bullard, J.E., Cahoon, S.M.P., McGowan, S., Bagshaw, E.A., Barry, C.D., Bindler, R., Burpee, B.T., Carrivick, J.L., Fowler, R.A., Fox, A.D., Fritz, S.C., Giles, M.E., Hamerlik, L., Ingeman-Nielsen, T., Law, A.C., Mernild, S.H., Northington, R.M. and Osburn, C.L. (2017). The Arctic in the Twenty-First Century: Changing Biogeochemical Linkages across a Paraglacial Landscape of Greenland. *BioScience*, 67(2), 118–133. https://doi.org/10.1093/biosci/biw158.

Anderson, N.J., Stedmon, C.A. (2007). The effect of evapoconcentration on dissolved organic carbon concentration and quality in lakes of SW Greenland. *Freshwater Biology,* 52(2), 280–289. https://doi.org/10.1111/j.1365-2427.2006.01688.x.

Assallay, A. (1998). Silt: 2–62 μm, 9–4φ. *Earth-Science Reviews*, 45(1-2), 61–88. https://doi.org/10.1016/s0012-8252(98)00035-x.

Auqué, L.F., I. Puigdomenech, E.-L. Tullborg, Gimeno, M.J., K. Grodzinsky and Hogmalm, K.J. 2019. Chemical weathering in a moraine at the ice sheet margin at Kangerlussuaq, western Greenland. Arctic Antarctic and Alpine Research, 51(1), 440–459. https://doi.org/10.1080/15230430.2019.1660125.

Beck, H.E., Zimmermann, N.E., McVicar, T.R., Vergopolan, N., Berg, A. and Wood, E.F. (2018). Present and Future Köppen-Geiger Climate Classification Maps at 1-km Resolution. *Scientific Data*, 5(5), p.180214. https://doi.org/10.1038/sdata.2018.214.

Blaud, A., Lerch, T.Z., Phoenix, G.K. and Osborn, A.M. (2015). Arctic soil microbial diversity in a changing world. *Research in Microbiology*, 166(10), 796–813. https://doi.org/10.1016/j.resmic.2015.07.013.

Bockheim, J.G., Gennadiyev, A.N., Hartemink, A.E. and Brevik, E.C. 2014. Soil-forming factors and Soil Taxonomy. *Geoderma*, 226-227, 231–237. https://doi.org/10.1016/j.geoderma.2014.02.016.

Bócoli, F.A., Silva, S.H.G., Avanzi, J.C., Silva, B.M., Faria, V.L. de, Totti, M.C.V., Inda, A.V., Frosi, G., Lima, S. de S.F., Uezu, A., Carneiro, M.A.C., Ottoni, M.V. and Curi, N. 2024. Paleosol marked by contrasting formation processes: A pilot study using digital morphometrics

in Southeastern Brazil. *CATENA*, 234, p.107550. https://doi.org/10.1016/j.catena.2023.107550.

Bullard, J.E., Prater, C., Baddock, M.C. and Anderson, N.J. (2023). Diurnal and seasonal source-proximal dust concentrations in complex terrain, West Greenland. *Earth Surface Processes and Landforms*, 48(14), 2808–2827. https://doi.org/10.1002/esp.5661.

Bruhwiler, L., Parmentier, F.-J.W., Crill, P., Leonard, M. and Palmer, P.I. (2021). The Arctic Carbon Cycle and Its Response to Changing Climate. *Current Climate Change Reports*, 7(1), 14–34. https://doi.org/10.1007/s40641-020-00169-5.

Chen, X., Zhang, X., Church, J.A., Watson, C.S., King, M.A., Monselesan, D., Legresy, B. and Harig, C. (2017). The increasing rate of global mean sea-level rise during 1993–2014. *Nature Climate Change*, 7(7), 492–495. https://doi.org/10.1038/nclimate3325.

Chen, P., (1977), Table of key lines in X-ray powder diffraction patterns of minerals in clays and associated rocks: Indiana Geological Survey Occasional Paper 21, 67 p.

Chichagov, A.V., Varlamov, D.A., Dilanyan, R.A., Dokina, T.N., Drozhzhina, N.A., Samokhvalova, O.L. and Ushakovskaya, T.V. (2001). MINCRYST: A crystallographic database for minerals, local and network (WWW) versions. *Crystallography Reports*, 46(5), pp.876–879. doi:https://doi.org/10.1134/1.1405882.

Cox, R.B., Lowe, D.R. and Cullers, R.L. (1995). The influence of sediment recycling and basement composition on evolution of mudrock chemistry in the southwestern United States. *Geochimica et Cosmochimica Acta*, 59(14), 2919–2940. https://doi.org/10.1016/0016-7037(95)00185-9.

Drees, L.R. and Wilding, L.P. (1978). Elemental Distribution in the Light Mineral Isolate of Soil Separates. *Soil Science Society of America Journal*, 42(6), 976–978. https://doi.org/10.2136/sssaj1978.03615995004200060031x.

Eden, D.N., Qizhong, W., Hunt, J.L. and Whitton, J.S. (1994). Mineralogical and geochemical trends across the Loess Plateau, North China. *CATENA*, 21(1), 73–90. https://doi.org/10.1016/0341-8162(94)90032-9.

Fedo, C.M., Wayne Nesbitt, H. and Young, G.M. (1995). Unraveling the effects of potassium metasomatism in sedimentary rocks and paleosols, with implications for paleoweathering conditions and provenance. *Geology*, 23(10), p.921. https://doi.org/10.1130/0091-7613(1995)023%3C0921:uteopm%3E2.3.co;2.

Gentsch, N., Mikutta, R., Ricardo José Alves, Barta, J., Petr Čapek, Antje Gittel, Gustaf Hugelius, Kuhry, P., Nikolay Lashchinskiy, Juri Palmtag, Richter, A., Šantrůčková, H., Jörg Schnecker, Shibistova, O., Urich, T., Wild, B. and Guggenberger, G. (2015). Storage and transformation of organic matter fractions in cryoturbated permafrost soils across the Siberian Arctic. *Biogeosciences*, 12(14), 4525–4542. https://doi.org/10.5194/bg-12-4525-2015.

Grimes, M., Carrivick, J.L., Smith, M.W. and Comber, A.J. (2024). Land cover changes across Greenland dominated by a doubling of vegetation in three decades. *Scientific Reports*, 14(1), p.3120. https://doi.org/10.1038/s41598-024-52124-1.

Hall, K., Thorn, C.E., Matsuoka, N. and Prick, A. (2002). Weathering in cold regions: some thoughts and perspectives. *Progress in Physical Geography: Earth and Environment*, 26(4), 577–603. https://doi.org/10.1191/0309133302pp353ra.

Hassink, J. (1997). The capacity of soils to preserve organic C and N by their association with clay and silt particles. *Plant and Soil*, 191(1), 77–87. https://doi.org/10.1023/a:1004213929699.

Heinemann, G. (1999). The KABEG'97 field experiment: An aircraft-based study of katabatic wind dynamics over the Greenland ice sheet. *Boundary-layer meteorology/Boundary - layer meteorology*, 93(1), 75–116. https://doi.org/10.1023/a:1002009530877.

Herndon, E., Amineh AlBashaireh, Singer, D.J., Taniya Roy Chowdhury, Gu, B. and Graham, D.Y. (2017). Influence of iron redox cycling on organo-mineral associations in Arctic tundra soil. *Geochimica et Cosmochimica Acta*, 207, 210–231. https://doi.org/10.1016/j.gca.2017.02.034.

IUSS Working Group WRB. (2022). World Reference Base for Soil Resources. International classification system for naming soils and creating legends for soil maps. 4th edition. International Union of Soil Sciences (IUSS), Vienna.

Jakobsen, B.H. (1989). Evidence for translocations into the B horizon of a subarctic Podzol in Greenland. *Geoderma*, 45(1), 3–17. https://doi.org/10.1016/0016-7061(89)90053-0.

Jobbágy, E.G. and Jackson, R.B. (2001). The distribution of soil nutrients with depth: Global patterns and the imprint of plants. *Biogeochemistry*, 53(1), 51–77. https://doi.org/10.1023/a:1010760720215.

Kalsbeek, F., Pidgeon, R.T. and Taylor, P.N. (1987). Nagssugtoqidian mobile belt of West Greenland: a cryptic 1850 Ma suture between two Archaean continents—chemical and isotopic evidence. *Earth and Planetary Science Letters*, 85(4), 365–385. https://doi.org/10.1016/0012-821x(87)90134-8.

Knight, P.G., Jennings, C.E., Waller, R.I. and Robinson, Z.P. (2007). Changes in ice-margin processes and sediment routing during ice-sheet advance across a marginal moraine. *Geografiska annaler. Series A, Physical geography/Geografiska annaler. Series A. Physical geography*, 89(3), 203–215. https://doi.org/10.1111/j.1468-0459.2007.00319.x.

Masson-Delmotte, V., Swingedouw, D., Landais, A., Seidenkrantz, M.-S., Gauthier, E., Bichet, V., Massa, C., Perren, B., Jomelli, V., Adalgeirsdottir, G., Hesselbjerg Christensen, J., Arneborg, J., Bhatt, U., Walker, D.A., Elberling, B., Gillet-Chaulet, F., Ritz, C., Gallée, H., van den Broeke, M. and Fettweis, X. (2012). Greenland climate change: from the past to the future. *Wiley Interdisciplinary Reviews: Climate Change*, 3(5), 427–449. https://doi.org/10.1002/wcc.186.

McKeague, J.A. and Day, J.H. (1966). DITHIONITE- AND OXALATE-EXTRACTABLE Fe AND Al AS AIDS IN DIFFERENTIATING VARIOUS CLASSES OF SOILS. *Canadian Journal of Soil Science*, 46(1), 13–22. https://doi.org/10.4141/cjss66-003.

McLennan, S.M. (1993). Weathering and Global Denudation. *The Journal of Geology*, 101(2), 295–303. https://doi.org/10.2307/30081153.

Moskovchenko, D.V. and Romanenko, E.A. (2022). Biogeochemical Features of Landscapes of the Nadym Region of YANAO. *Bulletin of Nizhnevartovsk State University*, (4), 122–136. https://doi.org/10.36906/2311-4444/22-4/12.

Muhs, D.R. (2018). The geochemistry of loess: Asian and North American deposits compared. *Journal of Asian Earth Sciences*, 155, 81–115. https://doi.org/10.1016/j.jseaes.2017.10.032.

Noël, B., van Kampenhout, L., Lenaerts, J.T.M., van de Berg, W.J. and van den Broeke, M.R. (2021). A 21st Century Warming Threshold for Sustained Greenland Ice Sheet Mass Loss. *Geophysical Research Letters*, 48(5). https://doi.org/10.1029/2020gl090471.

Reinhold Jahn (2006). *Guidelines for soil description*. Rome: Fao.

Russell, A.J., Carrivick, J.L., Ingeman-Nielsen, T., Yde, J.C. and Williams, M. (2011). A new cycle of jökulhlaups at Russell Glacier, Kangerlussuaq, West Greenland. *Journal of Glaciology*, 57(202), 238–246. https://doi.org/10.3189/002214311796405997.

Sechi, D., Stevens, T., Hällberg, P., Smittenberg, R.H., Molnár, M., Kertész, G.T., Buylaert, J.P., Schneider, R., Edward, C., Rasmussen, K.R., Knudsen, N.A.T., Andreucci, S. and Pascucci, V. (2024). High resolution luminescence and radiocarbon dating of Holocene Aeolian silt (loess) in west Greenland. *Quaternary Geochronology*, 84, p.101579. https://doi.org/10.1016/j.quageo.2024.101579.

Schwertmann, U., Kodama, H. and Fischer, W.R. (1986). Mutual Interactions Between Organics and Iron Oxides. *SSSA Special Publications*, 223–250. https://doi.org/10.2136/sssaspecpub17.c7.

Schwertmann, U. (1988). Occurrence and Formation of Iron Oxides in Various Pedoenvironments. *Iron in Soils and Clay Minerals*, 267–308. https://doi.org/10.1007/978-94-009-4007-9_11.

Sheinkman, V.S., Sedov, S.N., Ovchinnikov, A.Yu. and Makshanov, A.M. (2025). Role of Cryogenic and Cryopedogenic Processes of the Past in the Formation of Al–Fe-humus Soils in the Nadym–Pur Interfluve, North of Western Siberia. *Eurasian Soil Science*, 58(12). https://doi.org/10.1134/s1064229325602409.

Smeck, N.E. and Wilding, L.P. (1980). Quantitative evaluation of pedon formation in calcareous glacial deposits in Ohio. *Geoderma*, 24(1), 1–16. https://doi.org/10.1016/0016-7061(80)90031-2.

Silva, T., Whitley, B.S., Biersma, E.M., Abermann, J., Raundrup, K., de Vere, N., Høye, T.T., Haring, V. and Schöner, W. (2025). Bio-climatic factors drive spectral vegetation changes in Greenland. *Biogeosciences*, 22(17), 4601–4626. https://doi.org/10.5194/bg-22-4601-2025.

Siqueira, R.G., Ernesto, C., Fernandes, I., Corrêa, G.R., Francelino, M.R., de, L.L. and Pablo (2020). Weathering and pedogenesis of sediments and basaltic rocks on Vega Island, Antarctic Peninsula. *Geoderma*, 382, 114707–114707. https://doi.org/10.1016/j.geoderma.2020.114707.

Storms, J.E.A., de Winter, I.L., Overeem, I., Drijkoningen, G.G. and Lykke-Andersen, H. (2012). The Holocene sedimentary history of the Kangerlussuaq Fjord-valley fill, West Greenland. *Quaternary Science Reviews*, 35, 29–50. https://doi.org/10.1016/j.quascirev.2011.12.014.

Treat, C.C., Natali, S.M., Ernakovich, J.G., Iversen, C.M., Massimo Lupascu, McGuire, A., Norby, R.J., Taniya Roy Chowdhury, Richter, A., Šantrůčková, H., Schädel, C., Edward, Sloan, V.L., Turetsky, M.R. and Waldrop, M.P. (2015). A pan-Arctic synthesis of CH_4 and CO_2 production from anoxic soil incubations. *Global Change Biology*, 21(7), 2787–2803. https://doi.org/10.1111/gcb.12875.

Thomas, M., Monhonval, A., Hirst, C., Bröder, L., Zolkos, S., Vonk, J.E., Tank, S.E., Keskitalo, K.H., Shakil, S., Kokelj, S.V., van and Opfergelt, S. (2023). Evidence for preservation of organic carbon interacting with iron in material displaced from retrogressive thaw slumps: Case study in Peel Plateau, western Canadian Arctic. *Geoderma*, 433, 116443–116443. https://doi.org/10.1016/j.geoderma.2023.116443.

Ten Brink, N.W. and Weidick, A. (1974). Greenland Ice Sheet History Since the Last Glaciation. *Quaternary Research*, 4(4), 429–440. https://doi.org/10.1016/0033-5894(74)90038-6.

Ulery, A.L. and Drees, R. (2008). *Methods of Soil Analysis Part 5—Mineralogical Methods*. *Soil Science Society of America book series*. https://doi.org/10.2136/sssabookser5.5.

van den Broeke, M., Box, J., Fettweis, X., Hanna, E., Noël, B., Tedesco, M., van As, D., van de Berg, W.J. and van Kampenhout, L. (2017). Greenland Ice Sheet Surface Mass Loss: Recent Developments in Observation and Modeling. *Current Climate Change Reports*, 3(4), 345–356. https://doi.org/10.1007/s40641-017-0084-8.

Vodyanitskii, Yu.N., Vasil'ev, A.A., Morgun, E.G. and Rumyantseva, K.A. (2007). Selectivity of reagents used to extract iron from soil. *Eurasian Soil Science*, 40(10), 1076–1086. https://doi.org/10.1134/s1064229307100055.

Vinther, B.M., Buchardt, S.L., Clausen, H.B., Dahl-Jensen, D., Johnsen, S.J., Fisher, D.A., Koerner, R.M., Raynaud, D., Lipenkov, V., Andersen, K.K., Blunier, T., Rasmussen, S.O., Steffensen, J.P. and Svensson, A.M. (2009). Holocene thinning of the Greenland ice sheet. *Nature*, 461(7262), 385–388. https://doi.org/10.1038/nature08355.

Yang, Y., Chen, Z., Song, Y., Yan, M., Xue, C., Ji, J., Ayoko, G.A. and Frost, R.L. (2023). Environmental implication of geochemical record in the Arctic Ny-Ålesund glacial sediment, Svalbard (Norway). *Science of The Total Environment*, 880, p.163255. https://doi.org/10.1016/j.scitotenv.2023.163255.

Yong Rok Lee, Hyoun Soo Lim and Ho Il Yoon (2004). Geochemistry of soils of King George Island, South Shetland Islands, West Antarctica: Implications for pedogenesis in cold polar regions. *Geochimica et Cosmochimica Acta*, 68(21), 4319–4333. https://doi.org/10.1016/j.gca.2004.01.020.

Walker, A.L. (1983). The Effects of Magnetite on Oxalate- and Dithionite-Extractable Iron. *Soil Science Society of America Journal*, 47(5), 1022–1026. https://doi.org/10.2136/sssaj1983.03615995004700050036x.

Wang, Y., Guo, Y., Wang, X., Song, C., Song, Y., Liu, Z., Wang, S., Gao, S. and Ma, G. (2023). Mineral protection controls soil organic carbon stability in permafrost wetlands. *Science of The Total Environment*, 869, p.161864. https://doi.org/10.1016/j.scitotenv.2023.161864.

Wild, B., Schnecker, J., Bárta, J., Čapek, P., Guggenberger, G., Hofhansl, F., Kaiser, C., Lashchinsky, N., Mikutta, R., Mooshammer, M., Šantrůčková, H., Shibistova, O., Urich, T., Zimov, S.A. and Richter, A. (2013). Nitrogen dynamics in Turbic Cryosols from Siberia and Greenland. *Soil Biology and Biochemistry*, 67, 85–93. https://doi.org/10.1016/j.soilbio.2013.08.004.

Willemse, N.W., Koster, E.A., Hoogakker, B. and van Tatenhove, F.G.M. (2003). A continuous record of Holocene eolian activity in West Greenland. *Quaternary Research*, 59(3), 322–334. https://doi.org/10.1016/s0033-5894(03)00037-1.

Wojciech Szymański, Marek Drewnik, Stolarczyk, M., Łukasz Musielok, Gus-Stolarczyk, M. and Skiba, M. (2021). Occurrence and stability of organic intercalation in clay minerals from permafrost-affected soils in the High Arctic – A case study from Spitsbergen

(Svalbard). *Geoderma*, 408, 115591–115591. https://doi.org/10.1016/j.geoderma.2021.115591.

Wojcik, R., Donhauser, J., Frey, B., Holm, S., Holland, A., Anesio, A.M., Pearce, D.A., Malard, L., Wagner, D. and Benning, L.G. (2018). Linkages between geochemistry and microbiology in a proglacial terrain in the High Arctic. *Annals of Glaciology*, 59(77), 95–110. https://doi.org/10.1017/aog.2019.1.

Zhang, Q., Huai, B., Ding, M., Sun, W., Liu, W., Yan, J., Zhao, S., Wang, Y., Wang, Y., Wang, L., Che, J., Dou, J. and Kang, L. (2024). Projections of Greenland climate change from CMIP5 and CMIP6. *Global and Planetary Change*, 232, p.104340. https://doi.org/10.1016/j.gloplacha.2023.104340.

Annexes

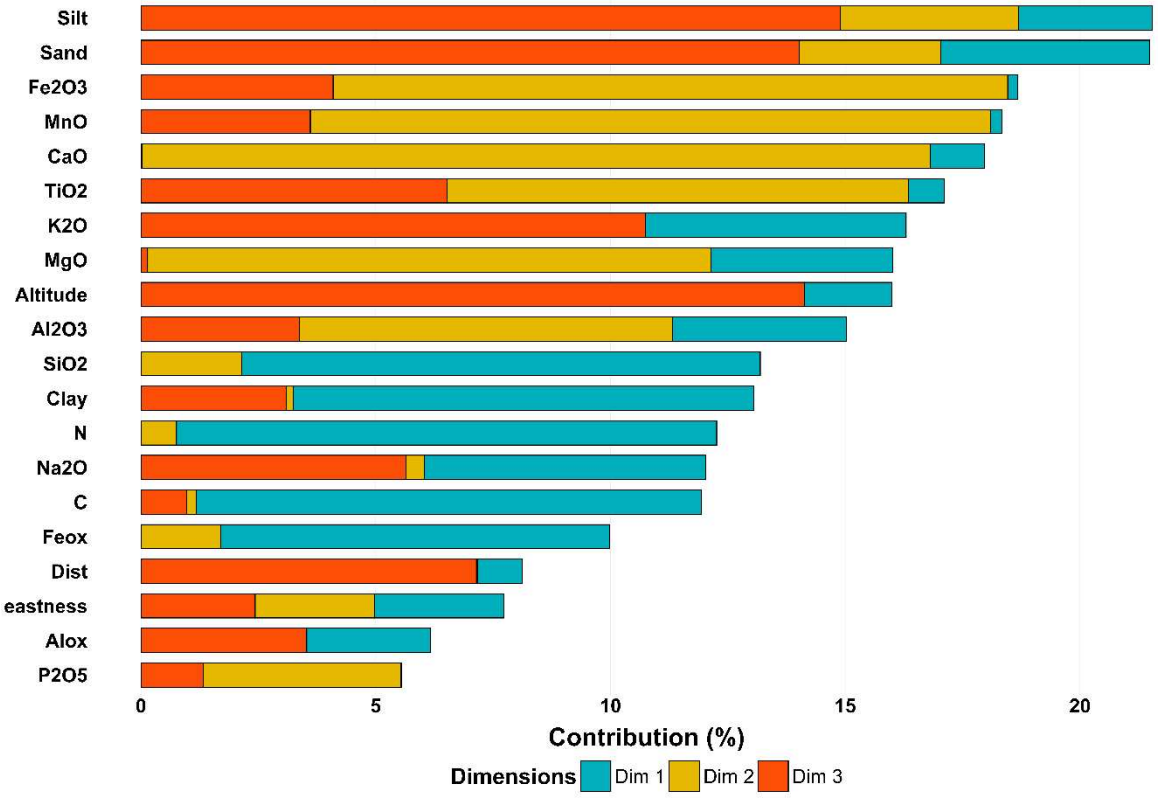

Figure S1: Accumulate contributions of each variable in PCA.

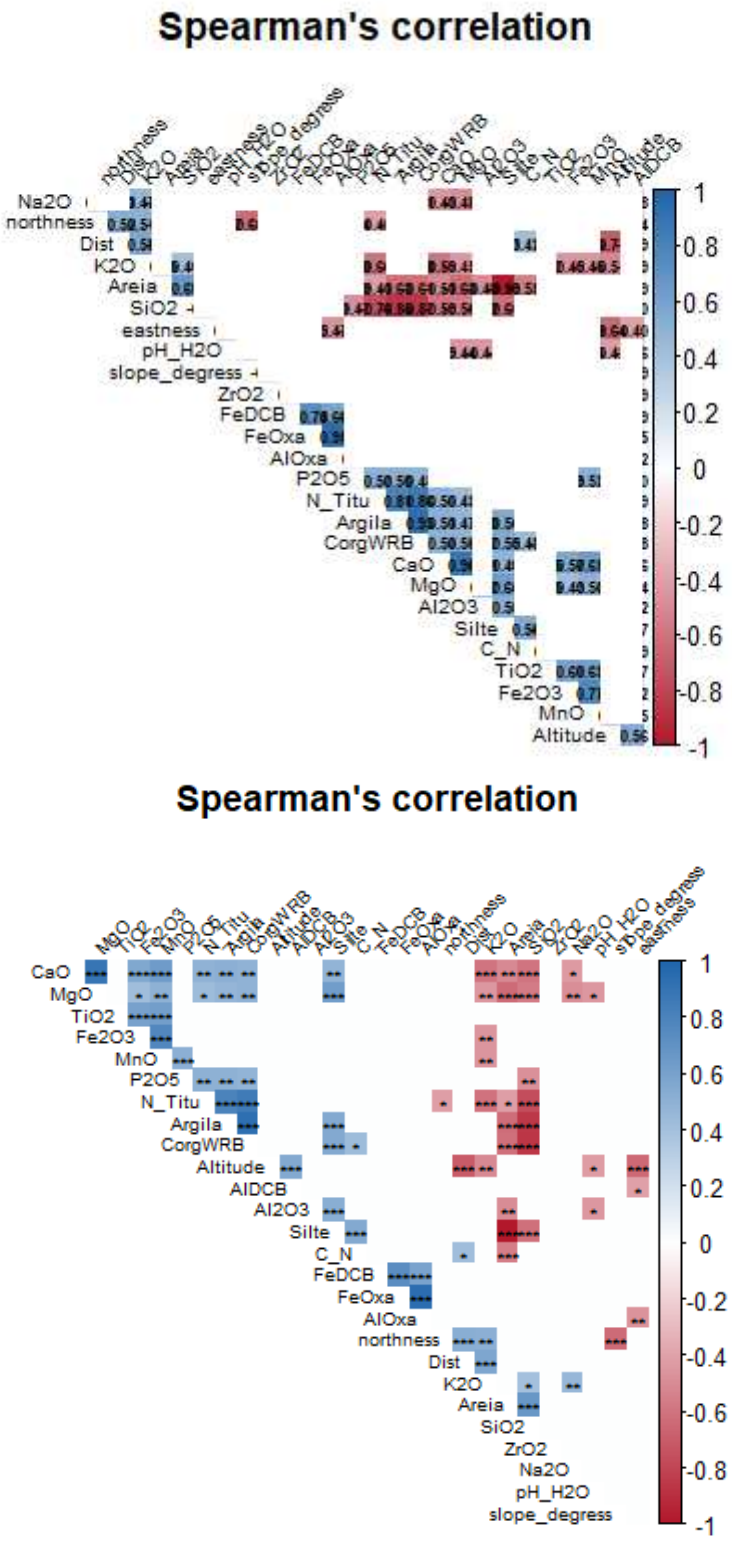

Figure S2: Spearman's correlation.

Profile	Horizons	Depth	Coordinates	Dry Soil (color)	Wet soil (color)	Discontinuity identification	Distance from glacier (km)	Altitude (m)	Aspect	Classification (WRB)
P1	A	0 – 5	66.997°, -50.629°	5Y 6/1	5Y 4/1		29,074	112.68	SE	Hypereutric Leptic Regosol (Siltic, Gelic, Humic, Raptic, Protospodic)
P1	E	5 – 15		5Y 6/1	5Y 2,5/1		29,074	112.69	SE	
P1	Bh	15 – 25		5Y 4/1	10YR 2,5/1	Lithic Discontinuity	29,074	112.70	SE	
P1	2C	25 – 34		5Y 7/1	5Y 4/1		29,074	112.71	SE	
P2	AE	0 – 5	67.146°, -50.048°	5Y 6/1	10YR 2/1		0	523.45	SE	Hypereutric Leptic Regosol (Loamic, Protospodic, Humic, Raptic)
P2	2Bh	5 – 15		5Y 5/1	10YR 2/2	Lithic discontinuity	0	523.46	SE	
P2	2C	15 – 40		5Y 6/2	2,5Y 3/2		0	523.47	SE	
P3	Ah	0 - 10	67.146°, -50.048°	5Y 4/1	2,5Y 2,5/1		0	523.48	SE	Hypereutric Leptic Regosol (Loamic, Protospodic, Humic, Raptic)
P3	C	10 – 30		2,5Y 5/2	10YR 2/1		0	523.49	SE	
P4	A	0 – 20	66.997°, -50.629°	5Y 4/1	10YR 2/1		19,794	270.68	NW	Mollic Reductaquic Turbic Cryosol (Pantoloamic, Hypereutric, Dorsic, Humic)
P4	C@	20 – 40		2,5Y 5/2	10YR 2/2		19,794	270.69	NW	
P5	A1	0 – 5	67.053°, -50.477°	2,5Y 4/1	2,5Y 2,5/1		11,026	124.46	SE	Entic Carbic Podzol (Siltic, Epic, Eutric, Gelic)
P5	A2	5 – 25		2,5Y 5/1	10YR 2/1		11,026	124.47	SE	
P5	Bh1	25 – 35		5Y 6/1	5Y 2,5/1		11,026	124.48	SE	
P5	Bh2	35 – 60		2,5Y 4/1	2,5Y 2,5/1		11,026	124.49	SE	
P5	C1	60 – 70		2,5Y 7/1	2,5 5/2		11,026	124.50	SE	
P5	C2	70 – 85		*	*		11,026	124.51	SE	
P6	A	0 – 5	67.060°, -50.394°	5Y 7/1	5Y 4/1		7,346	125.28	S	Eutric Aeolic Arenosol (Areninovic, Claric) over Dystric Regosol (Siltic, Humic, Panpaic)
P6	C1	5 – 30		5Y 8/1	5Y 5/1	Lithic discontinuity	7,346	125.29	S	
P6	2Ab	30 – 35		5Y 6/1	5Y 2,5/1		7,346	125.30	S	
P6	2C2	35 – 55		2,5Y 7/1	2,5Y 3/2		7,346	125.31	S	
P7	A	0 – 5	67.146°, -50.104°	2,5Y 4/2	2,5Y 3/2	Lithic discontinuity	0,974	350.03	NW	Cambic Someric Phaeozem (Loamic, Humic, Gelic) over Eutric Regosol (Histic, Gelic, Humic)
P7	B	5 – 35		2,5Y 5/2	2,5Y 2,5/1		0,974	350.04	NW	
P7	Hb	35 – 45		10YR 3/2	10YR 2/1		0,974	350.05	NW	
P8	O	0 – 10	67.081°, -50.327°	5Y 6/1	2,5Y 2,5/1		3,813	211.94	N	Histic Turbic Cryosol (Siltic, Folic, Humic, Turbic, Protospodic)
P8	A	10 – 30		5Y 6/1	5Y 3/1		3,813	211.95	N	
P8	E	30 – 50		2,5Y 7/1	10YR 3/2		3,813	211.96	N	
P8	Bh	50 – 60		2,5Y 6/2	10YR 2/2		3,813	211.97	N	
P8	C	60 – 80		5Y 7/2	2,5Y 4/2		3,813	211.98	N	
P9	O	0 – 15	66.995°, -50.983°	*	*		33,379	203.53	N	Protic Histic Turbic Cryosol (Loamic, Hypereutric, Endic, Humic, Limnic, Raptic, Aeolic)
P9	C	15 – 40		2,5Y 4/1	10YR 2/1		33,379	203.54	N	
P9	2C2	40 – 70		5Y 6/2	5Y 4/2		33,379	203.55	N	
P9	2C3	70 – 80		5Y 6/2	5Y 4/2		33,379	203.55	N	

Table S1: Soil Characteristics.

Profile	Depth	pH_H2O	C(%)	N(%)	C:N	Sand	Silt	Clay	FeDCB	Feox	Feox/FeDCB	Aldcb	Alox	Aloc/Aldcb
P1A	0 – 5	6,8	4,102	0,131	31,313	0,25	0,61	0,15	1,582	0,416	0,263	0,152	0,078	0,515
P1E	5 – 15	6,41	6,636	0,168	39,500	0,34	0,56	0,1	0,240	0,292	1,218	0,207	0,350	1,686
P1Bh	15 – 25	7,32	5,241	0,193	27,155	0,32	0,58	0,11	1,992	0,329	0,165	0,294	0,142	0,482
P12C	25 – 34	7,58	0,452	0,018	25,111	0,75	0,2	0,05	0,719	0,220	0,306	0,100	0,431	4,302
P2AE	0 – 5	6,05	3,431	0,129	26,597	0,69	0,22	0,09	1,007	0,287	0,285	0,245	0,117	0,477
P22Bh	5 – 15	5,7	4,268	0,174	24,529	0,49	0,41	0,11	1,736	0,345	0,199	0,470	0,165	0,352
P22C	15 – 40	6,04	0,618	0,024	25,750	0,68	0,28	0,05	0,576	0,330	0,573	0,323	0,695	2,151
P3Ah	0 - 10	6,35	6,628	0,232	28,569	0,63	0,26	0,11	0,325	0,238	0,734	0,349	0,581	1,664
P3C	10 – 30	6,13	6,161	0,242	25,459	0,39	0,48	0,13	0,786	0,620	0,790	1,201	1,455	1,211
P4A	0 – 20	5,14	11,824	0,42	28,152	0,34	0,48	0,18	1,562	1,509	0,966	0,483	0,657	1,360
P4C@	20 – 40	5,7	3,687	0,093	39,645	0,34	0,56	0,09	2,263	0,539	0,238	0,362	0,157	0,432
P5A1	0 – 5	5,1	13,973	0,427	32,724	0,41	0,46	0,13	1,050	0,938	0,893	0,237	0,325	1,373
P5A2	5 – 25	5,52	6,168	0,227	27,172	0,44	0,44	0,13	1,571	0,264	0,168	0,335	0,085	0,255
P5Bh1	25 – 35	5,56	4,826	0,175	27,577	0,36	0,53	0,11	0,459	0,324	0,706	0,386	0,451	1,168
P5Bh2	35 – 60	5,76	12,706	0,378	33,614	0,16	0,65	0,19	1,722	1,777	1,032	0,491	0,567	1,156
P5C1	60 – 70	6,08	1,327	0,039	34,026	0,41	0,53	0,06	0,950	0,315	0,332	0,143	0,371	2,597
P5C2	70 – 85	6,23	0,354	0,026	13,615	0,85	0,11	0,05	0,989	0,372	0,376	0,133	0,429	3,236
P6A	0 – 5	6,55	0,09	0,004	22,500	0,86	0,1	0,03	0,673	0,772	1,148	0,100	0,033	0,332
P6C1	5 – 30	6,77	0,173	0,043	4,023	0,88	0,08	0,04	0,498	0,109	0,219	0,045	0,167	3,735
P62Ab	30 – 35	5,83	3,454	0,058	59,552	0,28	0,63	0,09	2,197	0,461	0,210	0,413	0,159	0,384
P62C2	35 – 55	5,72	1,568	0,043	36,465	0,33	0,59	0,08	1,744	0,352	0,202	0,244	0,117	0,478
P7A	0 – 5	6,02	7,254	0,436	16,638	0,52	0,34	0,14	1,307	1,424	1,090	0,272	0,411	1,512
P7B	5 – 35	5,74	11,462	0,571	20,074	0	0	0	2,163	2,067	0,955	0,513	0,411	0,801
P7Hb	35 – 45	5,74	24,258	0,814	29,801	NA	NA	NA	NA	NA	NA	NA	NA	NA
P8O	0 – 10	5,33	19,907	0,152	130,967	NA	NA	NA	NA	NA	NA	NA	NA	NA
P8A	10 – 30	5,64	1,923	0,08	24,038	0,45	0,47	0,08	0,963	0,294	0,305	0,312	0,433	1,389
P8E	30 – 50	5,94	2,036	0,098	20,776	0,22	0,69	0,08	1,798	0,666	0,370	0,392	0,107	0,273
P8Bh	50 – 60	5,9	3,589	0,112	32,045	0,29	0,61	0,1	0,525	0,598	1,140	0,978	1,036	1,059
P8C	60 – 80	6,41	0,483	0,024	20,125	0,71	0,23	0,06	2,284	0,653	0,286	0,711	0,151	0,212
P9O	0 – 15	4,59	28,843	0,663	43,504	NA	NA	NA	NA	NA	NA	NA	NA	NA
P9C	15 – 40	5,95	0,747	0,02	37,350	0,59	0,32	0,08	0,921	0,394	0,428	0,479	0,906	1,890
P92C2	40 – 70	5,82	0,98	0,028	35,000	0,62	0,32	0,06	2,208	0,834	0,378	0,757	0,239	0,316
P92C3	70 – 80	5,84	0,716	0,021	34,095	0,62	0,29	0,09	NA	NA	NA	NA	NA	NA

Table S2: Physicochemical data of the profiles.

Profile	Depth	SiO2	Al2O3	Fe2O3	CaO	MgO	TiO2	P2O5	Na2O	K2O	MnO	ZrO2	SiO2	Al2O3
P1A	0 – 5	60,9	14,2	4,7	4,43	1,78	0,52	0,15	4,12	1,66	0,08	0,05	60,9	14,2
P1E	5 – 15	62,4	14,4	4,65	4,51	1,91	0,56	0,14	4,1	1,67	0,08	0,05	62,4	14,4
P1Bh	15 – 25	62,9	13,5	4,64	4,98	2,12	0,49	0,12	3,71	1,56	0,08	0,05	62,9	13,5
P12C	25 – 34	67,9	13,4	4,62	4,02	1,58	0,58	0,09	3,78	1,65	0,08	0,04	67,9	13,4
P2AE	0 – 5	64,3	13,3	5,26	4,59	1,89	0,69	0,12	3,64	1,36	0,1	0,07	64,3	13,3
P22Bh	5 – 15	65,5	14,5	4,79	4,69	2,06	0,53	0,13	3,97	1,54	0,09	0,05	65,5	14,5
P22C	15 – 40	66,4	13,9	5,01	4,36	1,87	0,53	0,1	3,76	1,33	0,08	0,04	66,4	13,9
P3Ah	0 - 10	63,4	12,8	4,74	4,57	1,87	0,53	0,11	3,48	1,29	0,08	0,05	63,4	12,8
P3C	10 – 30	60,9	13,3	4,65	4,58	2,03	0,46	0,14	3,43	1,42	0,08	0,04	60,9	13,3
P4A	0 – 20	56,6	11,8	3,8	3,82	1,76	0,47	0,07	3,15	1,44	0,06	0,04	56,6	11,8
P4C@	20 – 40	64,3	13,6	4,51	4,33	2,04	0,49	0,07	3,59	1,66	0,08	0,05	64,3	13,6
P5A1	0 – 5	64,1	13,5	4,45	4,25	1,76	0,47	0,11	3,7	1,74	0,08	0,04	64,1	13,5
P5A2	5 – 25	63,5	13,6	4,55	4,45	1,93	0,46	0,11	3,65	1,6	0,08	0,05	63,5	13,6
P5Bh1	25 – 35	65,2	14	4,76	4,65	2,09	0,47	0,11	3,7	1,63	0,08	0,06	65,2	14
P5Bh2	35 – 60	63,3	13,5	4,3	4,55	2,07	0,43	0,02	3,57	1,52	0,08	0,05	63,3	13,5
P5C1	60 – 70	66,4	13,6	4,88	4,31	1,88	0,51	0,08	3,8	1,73	0,08	0,05	66,4	13,6
P5C2	70 – 85	65,8	13,8	8,05	4,96	2,11	0,9	0,11	3,43	1,65	0,14	0,04	65,8	13,8
P6A	0 – 5	71,6	13,6	4,11	3,77	1,21	0,5	0,09	3,7	1,65	0,07	0,06	71,6	13,6
P6C1	5 – 30	75,9	12,9	2,38	3,08	0,82	0,26	0,04	3,8	1,73	0,04	0,03	75,9	12,9
P62Ab	30 – 35	64,6	14,1	4,87	4,71	2,24	0,52	0,06	3,64	1,62	0,08	0,05	64,6	14,1
P62C2	35 – 55	64,4	14	4,87	4,74	2,4	0,51	0,07	3,63	1,55	0,08	0,05	64,4	14
P7A	0 – 5	60,6	12,9	4,3	4,39	1,93	0,5	0,13	3,56	1,27	0,07	0,04	60,6	12,9
P7B	5 – 35	58,4	12,4	4,36	4,35	2,01	0,45	0,09	3,31	1,39	0,07	0,05	58,4	12,4
P7Hb	35 – 45	59,6	12,8	4,35	4,36	2,02	0,49	0,06	3,5	1,46	0,08	0,05	59,6	12,8
P8O	0 – 10	66,2	13,7	4,8	4,36	1,71	0,58	0,12	3,74	1,63	0,09	0,07	66,2	13,7
P8A	10 – 30	65,25	13,95	5,04	4,56	1,85	0,59	0,16	3,83	1,64	0,09	0,08	65,25	13,95
P8E	30 – 50	65,1	13,8	4,77	4,57	1,95	0,47	0,12	3,81	1,58	0,08	0,05	65,1	13,8
P8Bh	50 – 60	64,2	13,9	4,99	4,77	2,33	0,47	0,09	3,57	1,58	0,08	0,05	64,2	13,9
P8C	60 – 80	69,9	13,5	4,13	3,94	1,44	0,44	0,09	3,9	1,74	0,07	0,05	69,9	13,5
P9O	0 – 15	54,2	11,6	4,07	3,84	1,72	0,42	0,08	3,09	1,31	0,07	0,04	54,2	11,6
P9C	15 – 40	69	13,8	4,54	4,15	1,61	0,52	0,09	3,78	1,66	0,07	0,05	69	13,8
P92C2	40 – 70	68	13,9	4,89	4,31	1,68	0,6	0,12	3,71	1,62	0,08	0,05	68	13,9
P92C3	70 – 80	47,7	10,6	3,62	3,68	1,53	0,37	0,13	2,71	1,15	0,06	0,04	47,7	10,6

Table S3: Total oxides from XRF.

3. CAPÍTULO 2: Mineral protection and thermal regime constrain soil organic matter stabilization in soils of West Greenland.

Abstract: The stability of soil organic matter (SOM) in the Arctic depends on chemical stabilization via mineral associations and thermal regime, yet the relative importance of these mechanisms remains poorly understood. We investigated SOM stabilization alternatives in Kangerlussuaq, West Greenland, a rapidly changing region at the western margin of the Greenland Ice Sheet, using geochemical analysis of Fe and Al oxides of the bulk soil, integrated physical fractionation (POM/MAOM), stable isotope ratios ($\delta^{13}C$, $\delta^{15}N$), and 14-month in situ soil thermal monitoring in three depths (10, 50 and 130 centimeters). We identified a minimally transformed particulate organic matter (POM) with high C:N ratios, on average, and range (13–70) reflecting limited microbial processing, and a mineral-associated organic matter (MAOM) with lower C:N ratios (10–26), reflecting partial microbial transformation. Low concentrations of poorly crystalline Fe and Al minerals, combined with weak correlations with organic matter content in both fractions, indicate limited organo-mineral interaction. However, the presence of exchangeable Ca^{2+} suggests a secondary pathway for organic matter stabilization through cation bridging, potentially acting against carbon loss where amorphous oxides are scarce. Concurrently, soil temperature monitoring revealed episodic freeze–thaw cycles concentrated at the soil surface, with most of the year characterized by sustained freezing or thawing. We conclude that Kangerlussuaq soils face a dual constraint on vulnerable SOM stability based on weak chemical stabilization due to limited availability of reactive phases, combined with physical instability driven by seasonal thermal fluctuations. This dual vulnerability likely reflects the interplay of incipient mineral weathering and intense thermal variability characteristic of greenlandic environments, potentially enhancing the sensitivity of these carbon stocks to losses under increasingly variable or warmer conditions.

Keywords: Soil Organic Matter; Greenland Soils; Arctic Soils; Thermal monitoring; Organo-mineral interaction, POM, MAOM.

6. Introduction

The Arctic region is a fragile and sensitive area highly susceptible to the effects of climate change, and is undergoing rapid environmental changes (Rantanen et al., 2022). The current warming rate in the Arctic is nearly four times higher than the global average, a process known as Arctic amplification (Rantanen et al., 2022). Arctic amplification contributes not only to sea-level rise and glacier retreat but also to permafrost thaw and longer growing seasons (Liu et al., 2023), which stimulate biological activity in soil, boosting the dynamics of the soil organic carbon.

Soils in periglacial environments, such as those in western Greenland, store large quantities of organic carbon that have accumulated under colder conditions and limited biological activity (Schuur et al., 2015). It is estimated that around 1672 Pg of organic carbon is contained in the northern circumpolar soil carbon, of which approximately 88%, 1466 Pg, is preserved in perennially frozen layers and deposits (Tarnocai et al., 2009). Uncertainties remain about the stability of organic matter in those soils (Alekseev & Abakumov, 2021). One effective approach to better understand this stability involves separation into physical fractions known as Particulate Organic Matter (POM) and Mineral-Associated Organic Matter (MAOM). POM consists of light, relatively undecomposed plant residues, whereas MAOM mostly comprises low molecular weight compounds derived from necromass and microbial metabolism that are tightly bound to mineral particles via adsorption, complexation, or occlusion within microaggregates (Cotrufo et al., 2013; Cotrufo et al., 2015). Although both fractions are known for having mixes of fast- and slow-cycling components (Angst, et al., 2021), in temperate systems, POM generally has shorter residence times (years to decades), while MAOM persists longer (decades to centuries) (Yu et al., 2022).

In periglacial environments, MAOM formation may reflect microbial processing without guaranteeing long-term physicochemical protection, since even the most recalcitrant organic compounds are influenced by the polar environments (Mikan et al., 2002). The relative abundance of each fraction depends on environmental factors such as geochemistry, climatic conditions, and soil depth (Galluzi et al., 2024), which can help infer potential responses of soil organic matter (SOM) to environmental change.

Kangerlussuaq, located in western Greenland, at the head of a fjord near the Greenland Ice Sheet, represents the largest ice-free region in Greenland (Anderson & Stedmon, 2007). This region is of significant scientific interest due to its complex climatic history, marked by a 20th-

century cooling followed by accelerated warming in recent years (Anderson et al., 2017). Notable alterations include glacier advance episodes from 1964 to 2002 (Knight et al., 2007), jökulhlaup cycles (Russell et al., 2011), and vegetation increments over the last years (Grimes et al., 2024; Silva et al., 2025). These changes influence soil formation and development, requiring continuous monitoring given the Arctic's status as the fastest-warming region globally (Bruhwiler et al., 2021). The rapid transitions between proglacial and periglacial zones in this region drive abrupt ecological shifts, during which vegetation patterns can change drastically due to energy fluctuations, often resulting in sharp soil horizon discontinuities and permafrost thawing, which triggers the mineralization of previously frozen organic carbon (Miner et al., 2022).

In this context, the present study aims to evaluate the distribution, isotopic composition, and stability of soil organic matter in profiles from the Kangerlussuaq region through (i) physical separation into POM and MAOM, (ii) $\delta^{13}C$ analysis of each fraction, and (iii) characterization of pedogenic Fe and Al oxides, and bioavailable components as Ca^{2+}, Fe^{3+}, K^{+}, Na^{+}, Al^{+} and Mn^{+} to determine their role in SOM stabilization. We hypothesize that (I) incipient mineral weathering limits the availability of reactive Fe–Al phases, constraining organo-mineral stabilization of SOM, and that (II) seasonal thermal variability, including freeze–thaw cycling and episodic summer thawing, imposes additional physical instability on organic matter pools. Together, these mechanisms render Arctic SOM in this region particularly vulnerable to carbon losses under warming conditions. Consequently, this enhances the vulnerability of these carbon stocks, potentially increasing greenhouse gas (GHG) emissions under current climate conditions.

7. Material and methods

7.1. Study area

The Kangerlussuaq region in western Greenland is part of the Nagssugtoqidian orogenic belt, composed mainly of Archean gneisses reworked during the Proterozoic (Kalsbeek et al., 1987). The climate is classified as Polar Tundra (ET), characterized by cold and dry conditions, with mean summer temperatures ranging from 0 to 10°C (Beck et al., 2018). In recent decades, the region has experienced increasing temperature and precipitation (Boberg et al., 2018). The dominant vegetation is tundra, reflecting the region's low temperatures and short growing season. The Postglacial era and glacier retreat have left a legacy of eroded uplands, contributing to the deep fjords, glacial valleys, and uplifted marine terraces which characterize the modern

landscape. Crucially, the large valley system extending from the Ice Sheet margin acts as a conduit for meltwater and a primary source area for fine-grained sediments entrained by katabatic winds.

At the onset of the Holocene, Kangerlussuaq was entirely ice-covered. Gradual deglaciation occurred as early Holocene temperatures in central Greenland were approximately 1°C higher than at present (Vinther et al., 2009). This warming, combined with reduced snow accumulation under arid conditions, facilitated the formation of multiple moraine systems, including the Sarfartôq-Avatdleq (8.8 – 9.7 ka BP) and the Ørkendalen (6.4 – 7.0 ka BP) moraines (Ten Brink & Weidick, 1974). Regional glacier recession culminated around 4 ka BP, followed by a later advance strongly influenced by the Little Ice Age (0.7 – 0.1 ka BP) (Forman et al., 2007). Sedimentological records document repeated geomorphic transitions, including ice-margin retreat, marine transgression-regression cycles, and recent neoglacial advances (Storms et al., 2012). Surficial soil horizons are primarily formed through continuous aeolian deposition, characterized by silty loam and sandy loam textures, particularly in proximity to the ice margin (Muller et al., 2016).

7.2. Sampling and description of soil profiles

Fieldwork was conducted during the summer of 2024 and 2025. Nine representative soil profiles were selected across the region (Figure 1) based on elevation, varying between 112 and 513 meters above sea (Figure 2), distance from the glacier margin, parent material, vegetation cover, and accessibility. Each profile was described following the guidelines of the World Reference Base for Soil Resources (IUSS, 2022) and collected following international soil sampling protocols (Schoeneberger et al., 2012). All horizons were subjected to a fizz test to detect the presence of carbonates. The bulk soil samples were air-dried. After drying, samples were disaggregated and sieved to 2mm to remove coarse fragments, being reserved as air-dried fine earth.

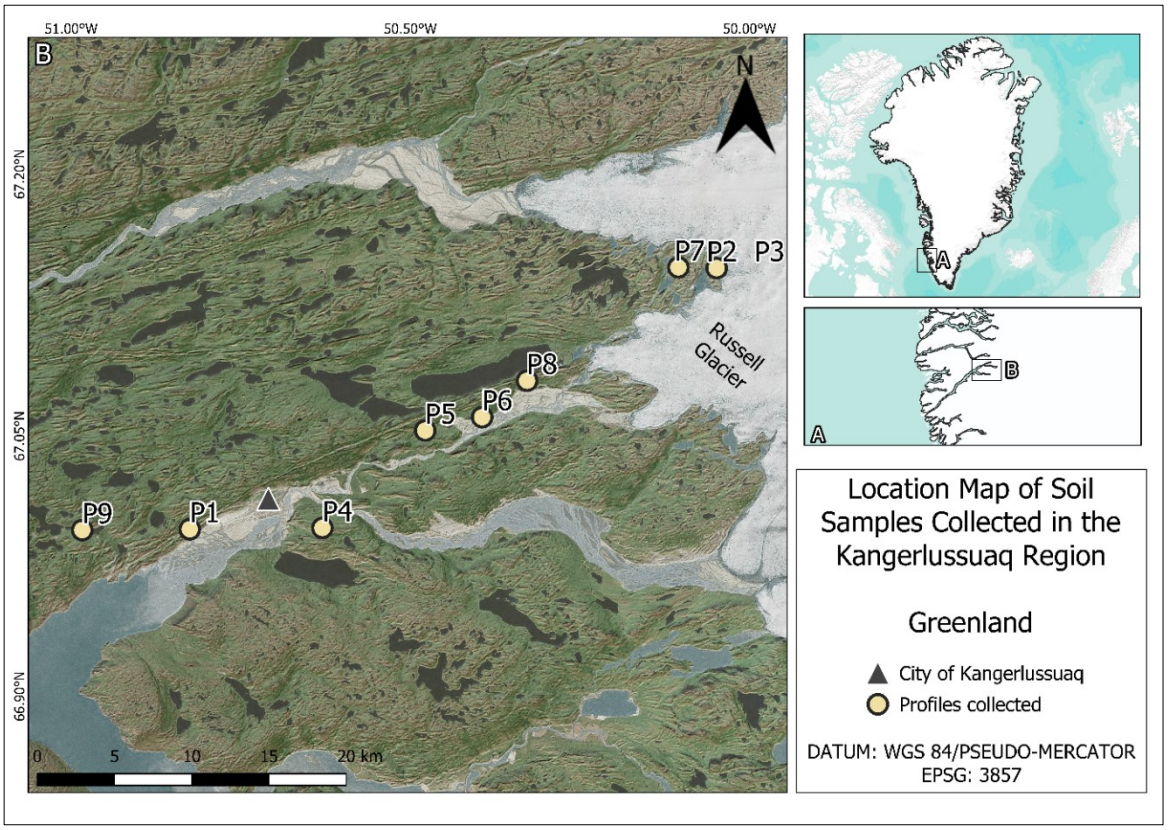

Figure 1: Location Map with representation of profiles collected.

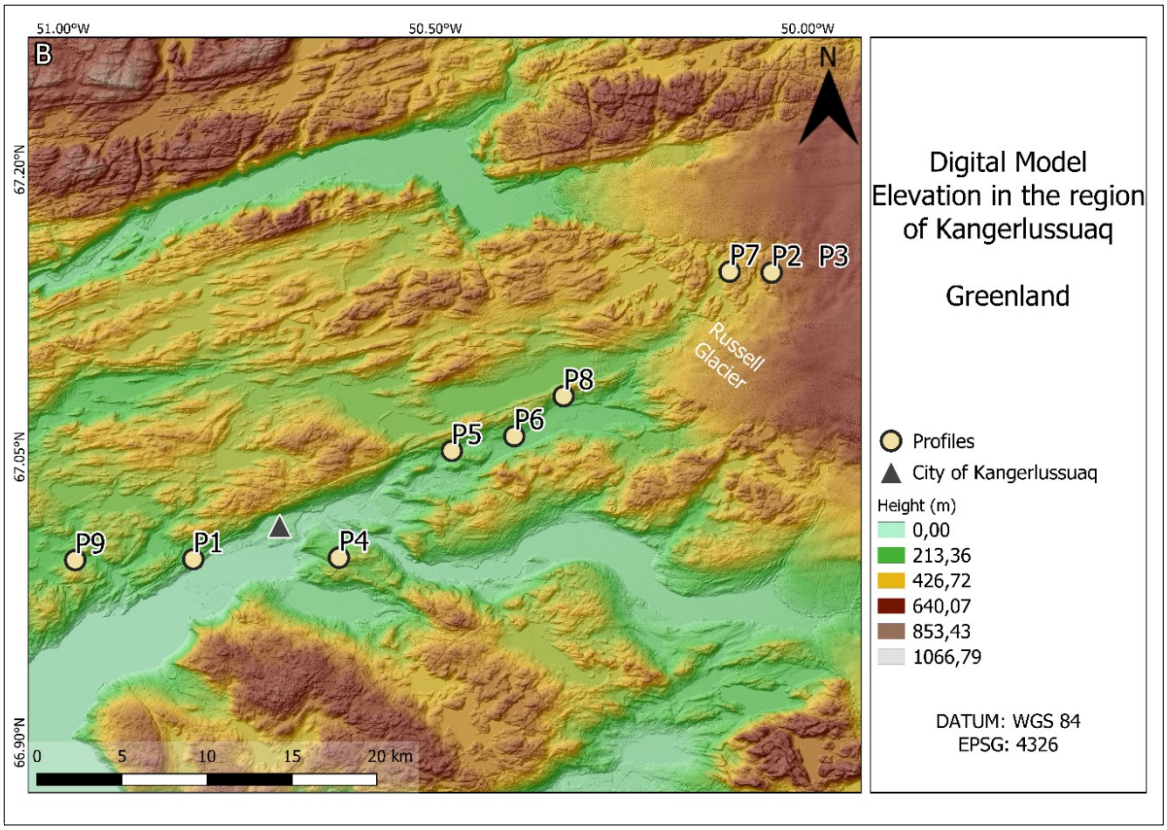

Figure 2: Elevantion map across profiles collected.

7.3. Bulk Soil Analysis

After air-drying, subsamples of each horizon were collected to determine the total carbon in soils using Walkley-Black method (Walkley and Black, 1934) and then multiplied by a correction factor of 1.3 due to the incomplete recovery of total organic carbon (IUSS, 2022) used here primarily for soil characterization and profile classification. Soil pH was measured in a 1:2.5 soil-to-deionized-water suspension and in a 1 mol.L^{-1} KCl solution. Al3+ and Ca2+ was extracted with KCl (1 mol.L-1) and determined volumetrically with a NaOH (0.025 mol.L-1) solution. Bioavailability of Fe, Mn, K and Na were measured through Mehlich – 1 method. Particle-size distribution was analyzed following dispersion with 0.1 mol L-1 $Na_6[(PO_3)_6]$ (sodium hexametaphosphate) under slow agitation (50 rpm) for 16 hours using a Wagner-type shaker. Coarse sand and fine sand fractions were separated by sieving through 0.2 mm and 0.053 mm screens, respectively. Clay content was determined by the pipette method, while silt content was calculated by the difference between the total soil mass and the sum of sand and clay fractions (Teixeira et al., 2017). Iron and aluminum oxides were quantified by two selective extractions: amorphous and poorly crystalline phases (Fe_{ox} and Al_{ox}) were extracted using 0.2 mol L^{-1} acid ammonium oxalate at pH 3.0, and crystalline phases (Fed and Ald) were extracted using the dithionite-citrate-bicarbonate (DCB) method (Mehra & Jackson, 1960). The extracted Fe and Al concentrations were determined by atomic absorption spectrometry.

7.4. POM and MAOM composition and isotopic analysis

Physical organic matter fractions were isolated in all samples using a physical fractionation method (Cambardella and Elliott, 1992). Aliquots of 10 g of 2-mm sieved soil sample were dispersed in 30 mL of 5 g L^{-1} sodium hexametaphosphate [(NaPO3)6] and agitated for 18h. The suspension was wet-sieved through a 0.053 mm mesh to separate particulate organic matter (POM) and mineral-associated organic matter (MAOM) fractions. Both fractions were oven-dried at 60 °C until constant mass, and the relative proportion of each fraction in the bulk soil was determined gravimetrically.

The POM and MAOM fractions from all soil horizons were finely milled (<149 μm) and analyzed for $\delta^{13}C$ and $\delta^{15}N$, while total carbon and nitrogen concentrations were determined using an elemental CN analyzer coupled to an isotope ratio mass spectrometer (IRMS; ANCA GSL 20–20, Sercon Ltd., UK). For each horizon, the proportional mass contribution of the POM and MAOM fractions and their respective C:N ratios were subsequently calculated.

7.5. Relative stability of SOM

The relative stability of soil organic matter was estimated based on the equations (1 - 3) proposed by Conen et al. (2008). This index uses the $\delta^{15}N$ enrichment of MAOM relative to POM as a proxy for the degree of microbial processing of organic matter, under the assumptions of a steady-state nitrogen cycle and a closed system with respect to N inputs and outputs.

The fraction of nitrogen lost during degradation (fN) was calculated as:

$$fN = 1 - e^{\left(\frac{\delta m - \delta p}{\varepsilon}\right)} \quad (1)$$

where δm and δp are the $\delta^{15}N$ values (‰) of MAOM and POM, respectively, and ε [‰] is the isotopic enrichment factor, set to –2.0‰, following standard values reported in the literature (Robinson, 2001; Conen et al., 2008; De Clercq et al., 2015).

The fraction of carbon lost (fc) was determined as:

$$fc = fN + (1 - fN).\left(1 - \left(\frac{rm}{rp}\right)\right) \quad (2)$$

where rm and rp are the C:N ratios of MAOM and POM respectively.

The relative SOM stability index (n) was calculated as:

$$n = \frac{Cm}{Cp.(1-fc)} \quad (3)$$

where Cm and Cp correspond to the carbon contents of MAOM and POM, respectively.

As the validity of this factor in cold, low-activity Arctic soils has not been independently established, the values were compared only among soil horizons and profiles according to depth and local environment.

7.6. Thermal analysis

Three soil temperature monitoring stations were installed near profiles with distinct distance from the glacier, during the 2024 field campaign. Using an earth auger, iButtons temperature loggers (1-Wire model DS1922L) were inserted at depths of 10, 50 and 130 cm below the surface. Each iButton was programmed to record temperature every six hours, totalizing four measurements per day at each depth. Data collected between summer 2024 and summer 2025

were retrieved during the following field campaign, totalizing one complete year of data collection.

For each depth, monthly mean temperature was calculated. In addition, the following thermal indicators were also calculated based on an adaptation, considering the frequency collection limitation, from Guglielmin et al. (2008):

- Thawing Days – days in which all soil temperature measurements are positive and at least one reading is warmer than +0.5ºC;
- Freezing Days – days in which all soil temperature measurements and at least one reading are colder than -0.5ºC;
- Isothermal days – days when the measurements range only between ±0.5ºC;
- Freeze-Thaw Days (FTD) – days in which there are both negative and positive temperatures with at least one value greater than ±0.5ºC;
- Thawing Degree Days (TDD) – cumulative sum of the mean daily temperatures above 0ºC;
- Freezing Degree Days (FDD) – obtained by the cumulative sum of the mean daily temperatures below 0ºC.

These indicators were compared among depths and profiles to evaluate the intensity and frequency of thermal perturbations within the active layer.

7.7. Data analysis and Calculation

All collected data were subjected to statistical analysis using R v4.1.3 (R Studio Team, 2022). Non-parametric statistical tests were applied to evaluate relationships between soil properties, organic matter fractions, and spatial parameters.

Spearman's rank correlation coefficients (ρ_s) were used to assess associations among chemical, isotopic, and physical variables, as these data showed non-linear relationships and non-normal distributions. In addition, a Principal Component Analysis (PCA) was performed to identify the main gradients controlling soil geochemical composition, organic matter fractions, and SOM stability across profiles. PCA loadings and scores were examined to interpret the influence of environmental variables.

8. Results

8.1. Soil classification and properties

The profiles studied were classified among diverse classes with distinct qualifiers (Figure 3). P1 was classified as Hypereutric Leptic Regosol (Siltic, Gelic, Humic, Raptic, Protospodic), P2 and P3 were classified as Hypereutric Leptic Regosol (Loamic, Protospodic, Humic, Raptic), P4 as Mollic Reductaquic Turbic Cryosol (Pantoloamic, Hypereutric, Dorsic, Humic), P5 as Entic Carbic Podzol (Siltic, Epic, Eutric, Gelic), P6 as Eutric Aeolic Arenosol (Areninovic, Claric) over Dystric Regosol (Siltic, Humic, Panpaic), P7 as Cambic Someric Phaeozem (Loamic, Humic, Gelic) over Eutric Regosol (Histic, Gelic, Humic), P8 as Histic Turbic Cryosol (Siltic, Folic, Humic, Turbic, Protospodic), and P9 as Protic Histic Turbic Cryosol (Loamic, Hypereutric, Endic, Humic, Limnic, Raptic).

Profile thickness ranged from 35 to 85 cm. Soil pH varied from 4.59 to 7.58 (average of 5.98). Mineral horizons have predominance of silt or sand, with low clay contents. Textural classes varied between Silty Loam, Loam, Sandy Loam, and Silt. The organic carbon content determined by the Walkley-Black method varied between 0.09% and 28.84%, both extremes occurring in surface horizons. The Na varied between 0.05 to 0.26 (mean of 0.11 $mg.kg^{-1}$), Al varied between 0 to 93.6 (mean of 7.63 $mg.kg^{-1}$), Fe varied between 53.6 to 501.8 (mean of 171.53 $mg.kg^{-1}$), Ca^{2+} varied between 0.31 to 4.12 (average of 1.53 $g.kg^{-1}$), Mn ranged to 0.7 to 62.5 (average of 12.07 $mg.kg^{-1}$), and K varied from 0.07 to 0.82 (average of 0.21 $mg.kg^{-1}$). The Fe_{OX} concentrations ranged from 0.109 to 2.067 $g.kg^{-1}$ (mean 0.612 $g.kg^{-1}$) while Fe_{DCB} ranged from 0.240 to 2.284 $g.kg^{-1}$ (mean 1.262 $g.kg^{-1}$). For aluminum, Al_{OX} varied between 0.033 and 1.455 $g.kg^{-1}$ (mean 0.392 $g.kg^{-1}$) and Al_{DCB} between 0.045 and 1.201 $g.kg^{-1}$ (mean 0.387 $g.kg^{-1}$). Limited downward translocation of Fe-Al complexes were observed, may showing an incipient podzolization process in the soil (Figure 4).

These results highlight the great pedodiversity of Kangerlussuaq region, reflecting contrasting soil development pathways and environmental heterogeneity across the samples. The predominance of silt and sand fractions coupled with low Fe–Al oxide contents, indicates limited chemical weathering, comparable to other Arctic soils (Thomas et al., 2023).

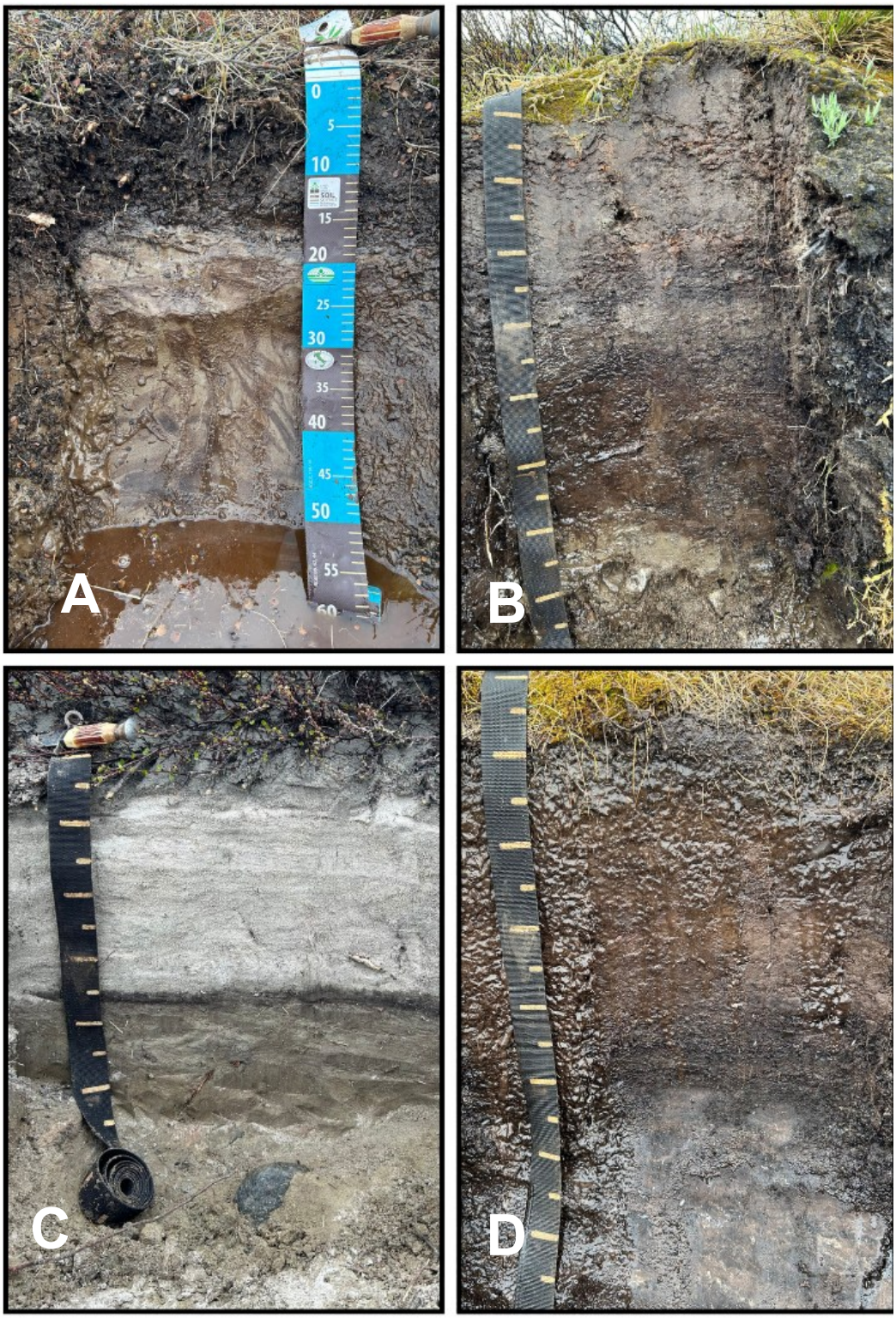

Figure 3: Soil profiles: (A) Cryosol (P4), (B) Podzol (P5), (C) Arenosol over Regosol (P6), and Phaeozem over Regosol (P7)

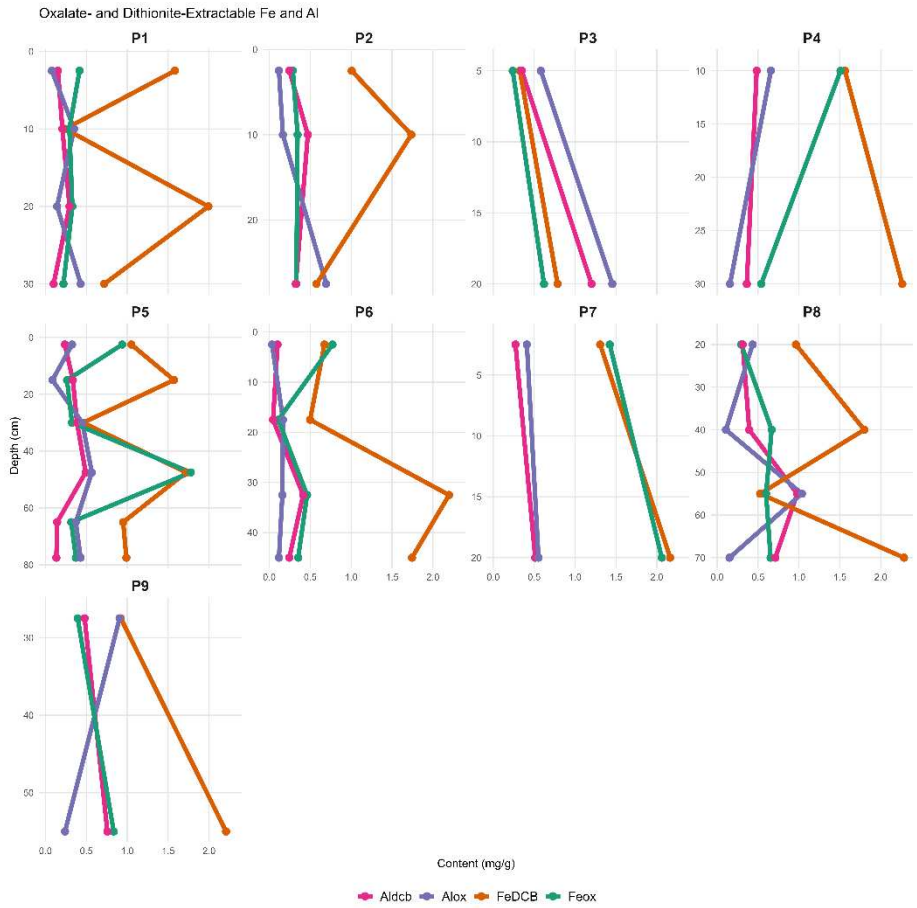

Figure 4: Fe and Al contents in soil depth.

8.2. Organic matter fractions and C and N composition

The relative proportion of POM and MAOM varied widely among soil horizons and profiles collected. The variation of POM in soil horizons ranged from 27.40% - 90.17% of total soil mass, while MAOM fraction varied between 9.83% and 72.59% of the total mass (Table S2).

The C content of the POM fraction varied from 0.593 to 200.206 $mg.g^{-1}$ of soil, with an average 26.893 $mg.g^{-1}$, whereas N content ranged between 0.057 to 9.664 $mg.g^{-1}$ of soil with an average of 1.711 $mg.g^{-1}$. In many subsurface horizons, N contents in the POM fraction were below the detection limit, suggesting minimal N inputs. The C content on the MAOM fraction varied between 1.698 and 45.687 $mg.g^{-1}$ of soil (Figure 5), with a mean of 12.150 $mg.g^{-1}$, and N contents varying between 0.131 and 4.027 $mg.g^{-1}$ of soil (Figure 6), mean of 0,927 $mg.g^{-1}$. Additionally, the results show a wide variation of C:N ratios in POM fraction, from 13.197 to 70.000, with an average of 26.120, and the MAOM fraction, varying from 10.356 to 26.000 (Figure 7), with an average of 15.314. The lower C:N ratios of MAOM compared to POM

indicate a more advanced stage of decomposition and stronger microbial processing, consistent with its mineral association (Soldatova et al., 2024).

The highest concentrations of C and N in both MAOM and POM fractions were generally found in the surface layers, though substantial subsurface peaks occurred in profiles such as P5, P6, P7, and P8. These mid-horizon accumulations suggest the downward transport of organic matter or the burial of older surface layers. The presence of higher C and N contents in these mid-layers coupled with lower MAOM C:N ratios indicate a mixture of microbially processed organic material and physically protected fractions. Furthermore, C:N ratios of both POM and MAOM are slightly higher at surface for some profiles, which is consistent with the input of fresh organic residuals into the topsoil. However, a strong tendency of increasing C:N values for POM fraction can be observed for profiles such as P4, P5 and P9, which can be related to the burial of formerly surface layers. One horizon (P5 2C1) exhibited an exceptionally high POM C:N ratio of approximately 90, substantially above the dataset range. This value may reflect the presence of charcoal-like pyrogenic organic material, highly recalcitrant aeolian organic inputs, or an analytical artifact associated with the very low N content of this horizon approaching instrument detection limits.

$\delta^{13}C$ and $\delta^{15}N$ content and Organic Matter Stabilization

The $\delta^{13}C$ in POM and MAOM showed variation among profiles. $\delta^{13}C$ in POM varied from -27.73‰ to -17.64‰, having an average value of -25.99‰, while MAOM varied within -26.80‰ to -23.76‰, with an average value of -23.76‰, with both fractions varying $\delta^{13}C$ in depth (Figure 8). These signatures are typical of C3 vegetation, which is expected for the tundra vegetation dominating the Kangerlussuaq region, where C4 plants are generally absent. The unusually enriched $\delta^{13}C$ value observed in the surface horizon of profile P9 (−17.64‰) was confirmed in replicate analyses, having values similar to regional macrophyte-derived organic material (Osburn et al., 2019).

The $\delta^{15}N$ in POM and MAOM showed greater variability, with POM varying between -18.88‰ to +4.08‰, and MAOM varying between -6.68‰ to +4.91‰, with an average value of -1.63‰ in POM and 0.19‰ in MAOM fraction, with both fractions' also varying $\delta^{15}N$ in depth (Figure 8). The absence of measurable $\delta^{15}N$ in several deep (C) horizons reflects their limited biological influence and weak connectivity with the surface nitrogen cycle. Similarly, the lack of a $\delta^{15}N$ signal in the A horizon of profile P6 – located in a fluvioglacial and aeolian depositional zone – likely results from recent sediment accumulation with minimal organic

nitrogen incorporation. Weak, non-significant positive correlations were observed between $\delta^{13}C$ and $\delta^{15}N$ in both fractions (POM: $\rho = 0.28$, p-value = 0.17; MAOM: $\rho = 0.25$, p-value = 0.17), indicating limited isotopic covariation.

Relative SOM stability (n) was calculated for selected horizons with sufficient isotopic data, yielding values between 0.05 and 3.583 (mean 1.30). These values are substantially lower than those reported for pasture soils in alpine environments, where *n* commonly ranges from 3 to 100 (Conen et al.,2008), and from agricultural experiments with *n* from 2 up to 1012 in sublayers in temperate and subtropical environments (Samson et al., 2024; De Clercq et al., 2015). Thus, the comparison of our results with those of previous works suggests the Kangerlussuaq soils generally show low relative organic matter stabilization. However, because *n* depends on assumptions about steady-state conditions and closed N cycles that may not fully apply in periglacial soils, these values should be viewed as comparative indicators within our dataset rather than as definitive measures of SOM persistence. The comparatively low *n* values observed in Kangerlussuaq soils indicate dominance of recent organic inputs and/or limited transformation of plant-derived material, consistent with reduced microbial turnover under cold and seasonally saturated conditions, which is also suggested by the high C:N ratios of these soils.

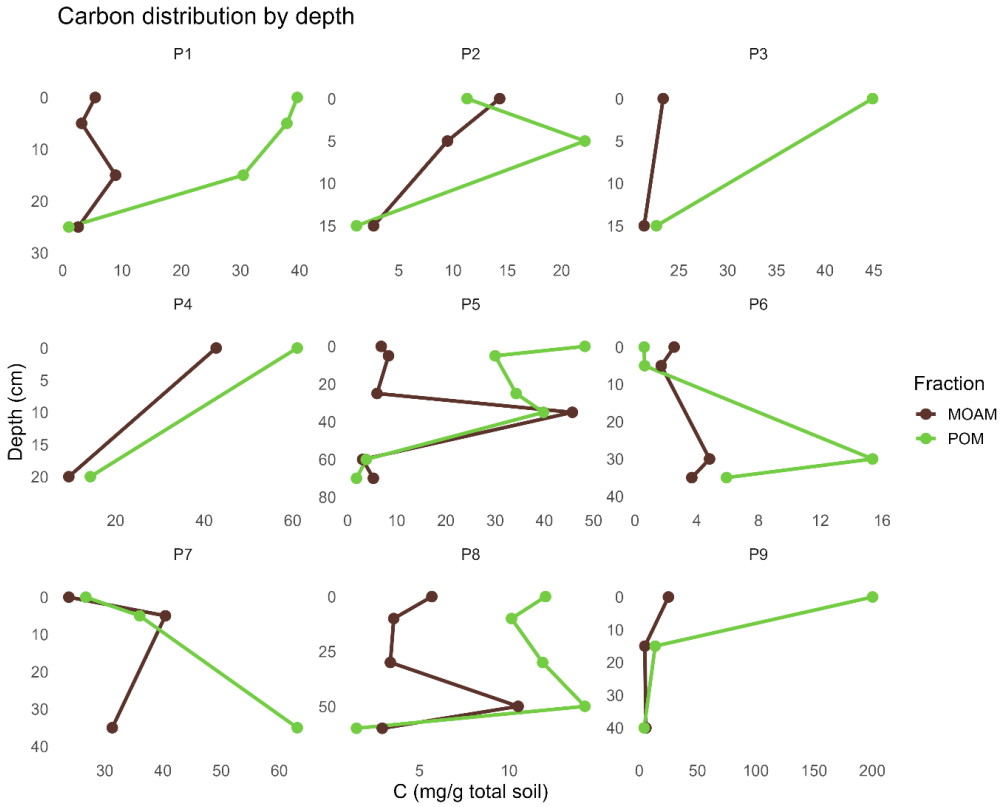

Figure 5: Carbon distribution in profiles at each organic matter physical fraction.

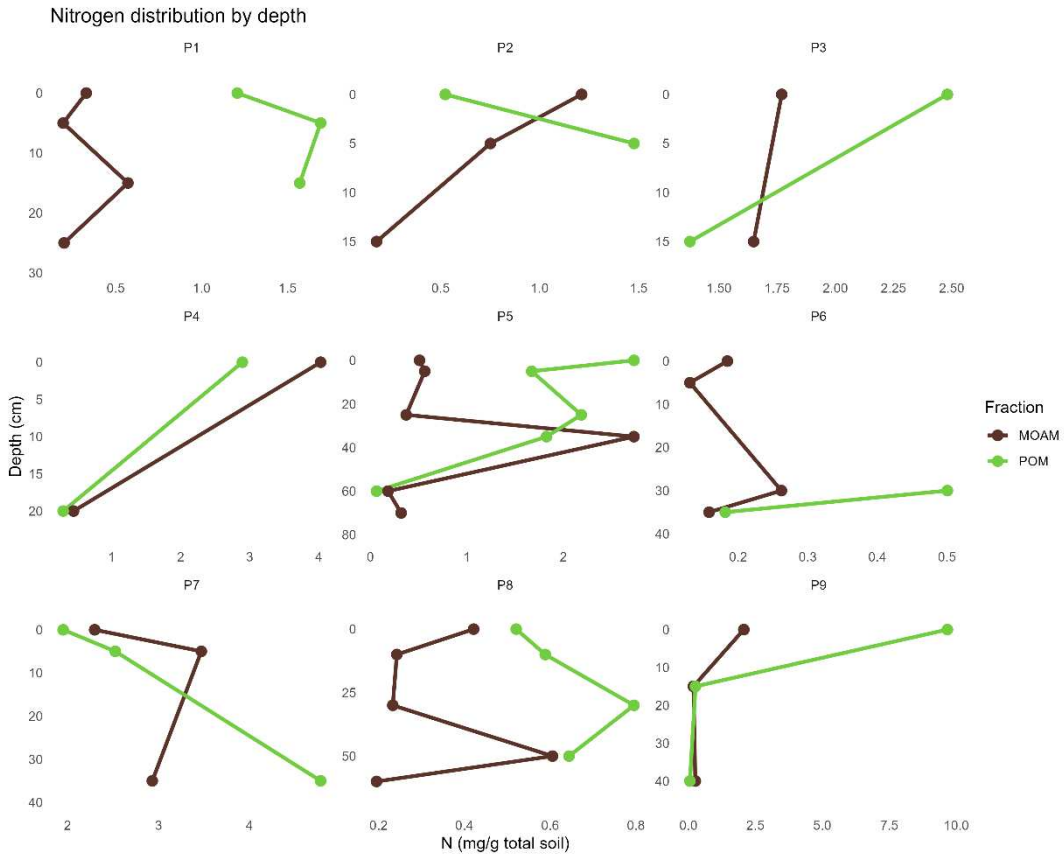

Figure 6: Nitrogen distribution in profiles at each organic matter physical fraction.

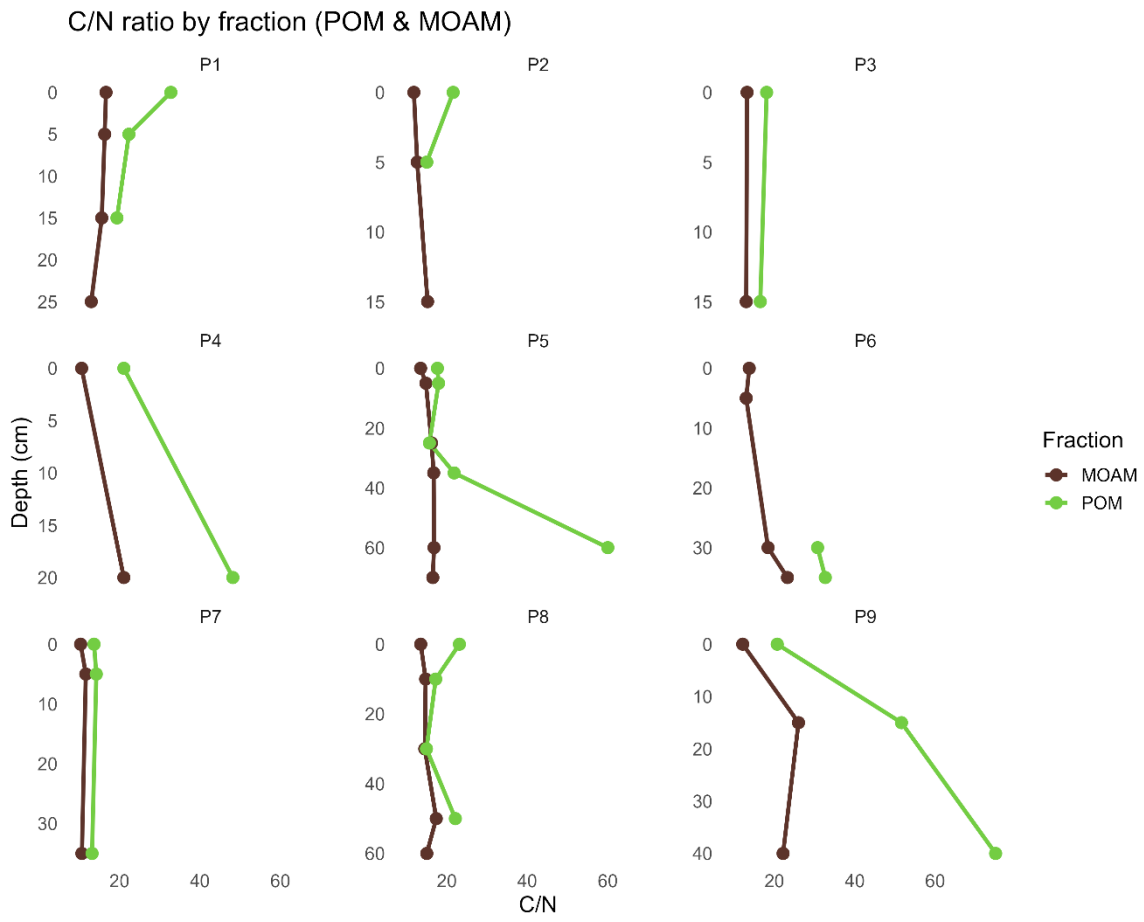

Figure 7: C/N ratio distributed in profiles of each organic matter physical fraction.

8.3. $\delta^{13}C$ and $\delta^{15}N$ content and Organic Matter Stabilization

The $\delta^{13}C$ in POM and MAOM showed variation among profiles. $\delta^{13}C$ in POM varied from -27.73‰ to -17.64‰, having an average value of -25.99‰, while MAOM varied within -26.80‰ to -23.76‰, with an average value of -23.76‰, with both fractions varying $\delta^{13}C$ in depth (Figure 8). These signatures are typical of C3 vegetation, which is expected for the tundra vegetation dominating the Kangerlussuaq region, where C4 plants are generally absent. The unusually enriched $\delta^{13}C$ value observed in the surface horizon of profile P9 (−17.64‰) was confirmed in replicate analyses, having values similar to regional macrophyte-derived organic material (Osburn et al., 2019).

The $\delta^{15}N$ in POM and MAOM showed greater variability, with POM varying between -18.88‰ to +4.08‰, and MAOM varying between -6.68‰ to +4.91‰, with an average value of -1.63‰ in POM and 0.19‰ in MAOM fraction, with both fractions' also varying $\delta^{15}N$ in depth (Figure 8). The absence of measurable $\delta^{15}N$ in several deep (C) horizons reflects their limited biological influence and weak connectivity with the surface nitrogen cycle. Similarly, the lack of a $\delta^{15}N$ signal in the A horizon of profile P6 – located in a fluvioglacial and aeolian depositional zone – likely results from recent sediment accumulation with minimal organic nitrogen incorporation. Weak, non-significant positive correlations were observed between $\delta^{13}C$ and $\delta^{15}N$ in both fractions (POM: $\rho = 0.28$, p-value = 0.17; MAOM: $\rho = 0.25$, p-value = 0.17), indicating limited isotopic covariation.

Relative SOM stability (n) was calculated for selected horizons with sufficient isotopic data, yielding values between 0.05 and 3.583 (mean 1.30). These values are substantially lower than those reported for pasture soils in alpine environments, where *n* commonly ranges from 3 to 100 (Conen et al.,2008), and from agricultural experiments with *n* from 2 up to 1012 in sublayers in temperate and subtropical environments (Samson et al., 2024; De Clercq et al., 2015). Thus, the comparison of our results with those of previous works suggests the Kangerlussuaq soils generally show low relative organic matter stabilization. However, because *n* depends on assumptions about steady-state conditions and closed N cycles that may not fully apply in periglacial soils, these values should be viewed as comparative indicators within our dataset rather than as definitive measures of SOM persistence. The comparatively low *n* values observed in Kangerlussuaq soils indicate dominance of recent organic inputs and/or limited transformation of plant-derived material, consistent with reduced microbial turnover under cold

and seasonally saturated conditions, which is also suggested by the high C:N ratios of these soils.

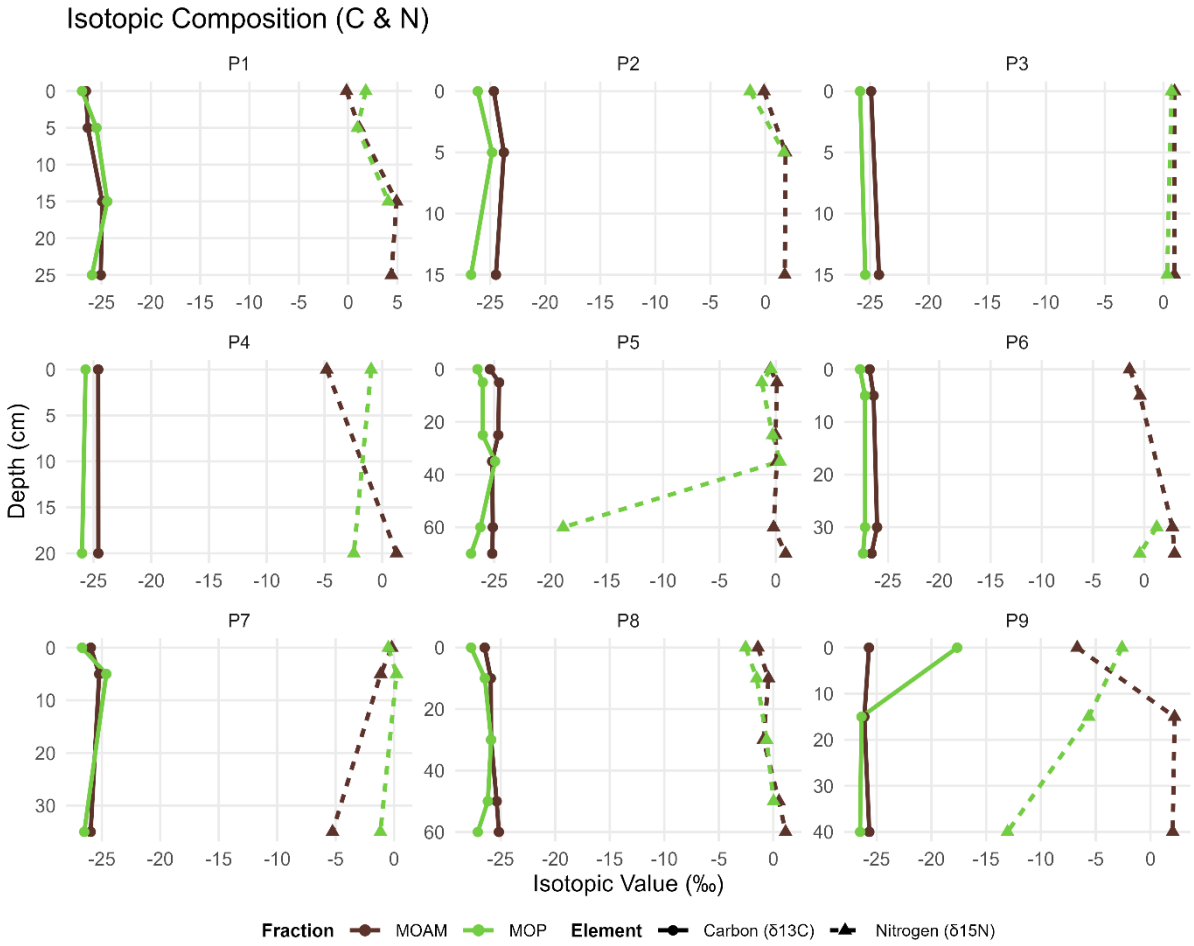

Figure 8: Isotopic composition of $\delta^{15}N$ and $\delta^{13}C$ distributed through depth in each profile.

8.4.Soil Temperature

Soil temperature was monitored continuously for 14 months across three profiles (P4, P5, and P7) at depths of 10, 50, and 130 cm. Mean monthly temperatures over the monitoring period ranged from −10.73 °C to 9.78 °C (Figure 9). The highest monthly mean temperature was recorded at 10 cm depth in profile P4 (9.78 °C), while the lowest was observed at the same depth in profile P7 (−10.73 °C). Over the monitoring period at 10 cm depth, cumulative thawing degree days (TDD) reached 1017.98 degree days in P4, with a maximum monthly value of 293.48 degree days in June 2025. In P7, cumulative TDD totaled 546.90 degree days, with a maximum of 121.96 degree days in June 2025. In P5, cumulative TDD reached 144.35 degree days, with a maximum monthly value of 21.49 degree days in June 2025 (Figure 10). At 50 and 130 cm depths, TDD values decreased markedly, totaling 95.09 and 93.29 degree days in P4;

84.62 and 124.43 degree days in P5; and 99.21 and 122.95 degree days in P7, respectively. Conversely, freezing degree days (FDD) ranged between −1352.40 and −671.11 degree days across the profiles (Figure 10). Profile P7 exhibited the lowest FDD values at all depths (−1352.40, −1212.52, and −1057.80 degree days at 10, 50, and 130 cm, respectively). These were followed by P4 (−1063.29, −708.39, and −599.19 degree days) and P5 (−671.11, −710.00, and −828.56 degree days).

Isothermal days were rare at 10 cm depth in P4 and P7, with only two days recorded in each profile. In contrast, P5 exhibited 84 isothermal days at the surface. At greater depths, the number of isothermal days increased substantially, with the highest values occurring at mid-depths. At 50 and 130 cm, isothermal days totaled 227 and 178 days in P4, 208 and 56 days in P5, and 174 and 85 days in P7, respectively. Freeze–thaw cycle (FTC) frequencies ranged from 0 to 7 days per month (Figure 11). The highest FTC frequencies were recorded at 10 cm depth in profiles P4 and P7. In P5, FTC values across all depths remained consistently low, averaging approximately one day per month. At deeper layers, FTC frequencies decreased, with maximum values of one day per month in P4 sublayers and two and one day per month at 50 and 130 cm in P7, respectively.

These thermal patterns indicate substantial heterogeneity in active-layer thermal regimes across short spatial distances, potentially reflecting differences in vegetation cover, soil moisture, and surface energy balance.

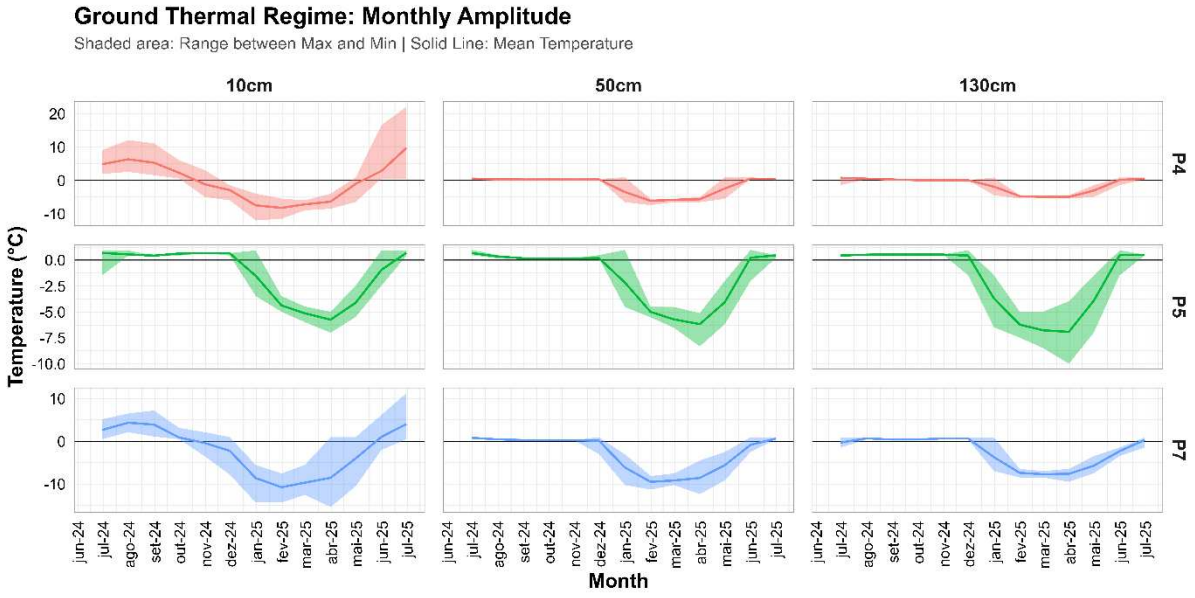

Figure 9: Average soil temperature at each month along July 2024 through July 2025.

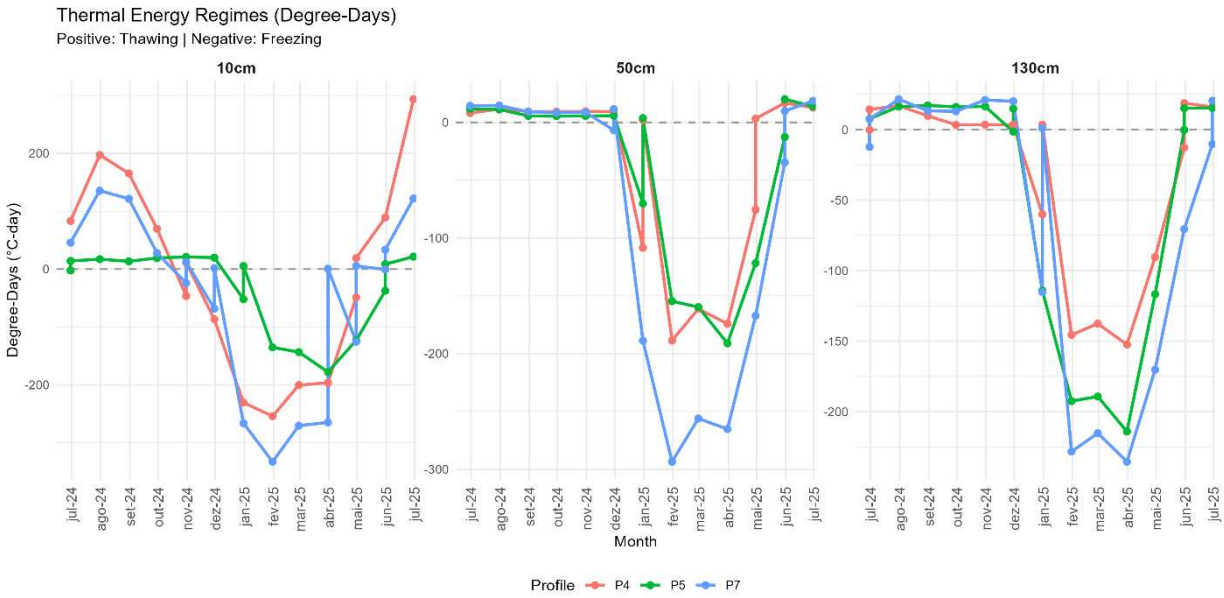

Figure 10: Thaw Degree-Days and Freezing Degree Days along July 2024 through July 2025.

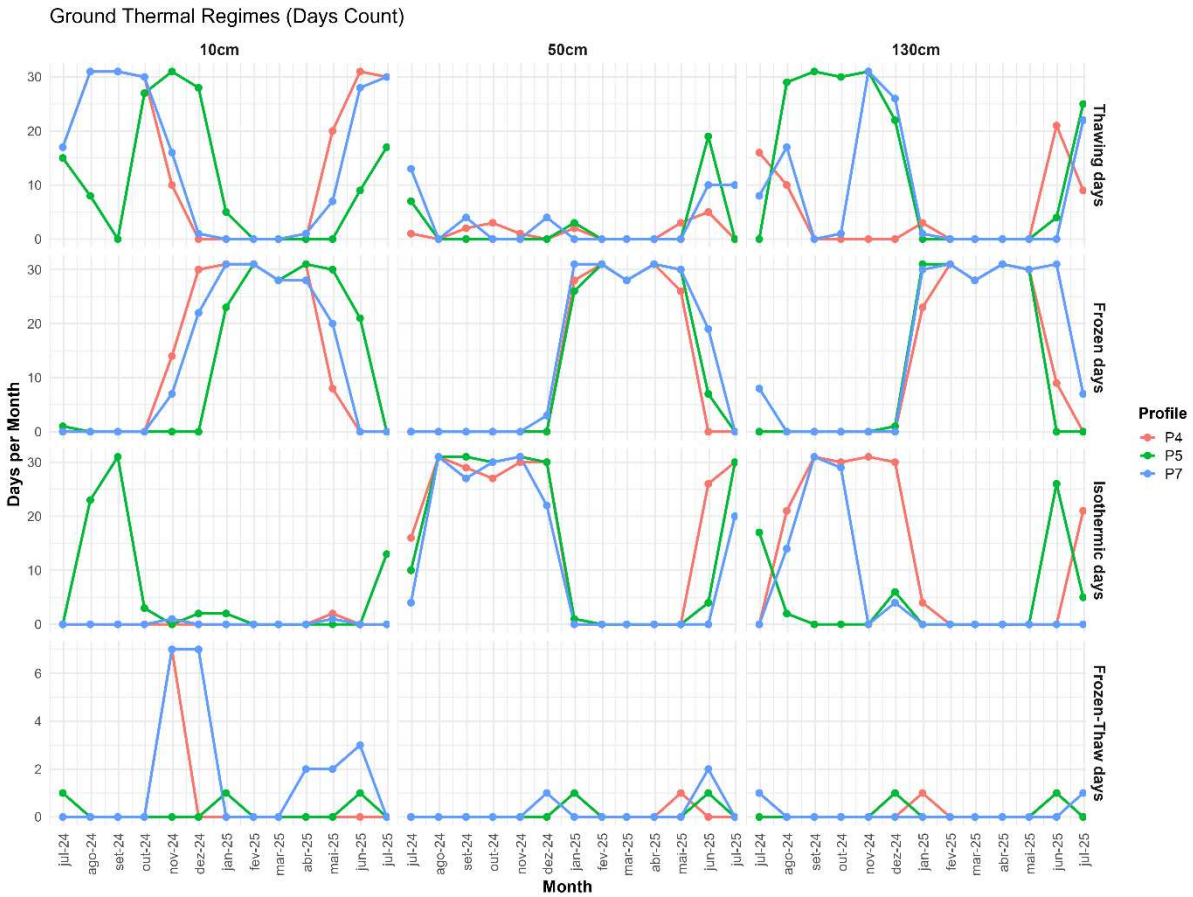

Figure 11: Thawing, Freezing, and Isothermic days, Froozen-Thaw Cycles along July 2024 through July 2025.

8.5. Statistical analysis

The number of principal components retained for interpretation was determined using the broken stick criterion (Jackson, 1993). All five first components exceeded the broken-stick threshold; however, PC1 and PC2 showed larger exceedances, 6.6% and 5.3% above the broken-stick expectation, compared to PC3–PC5 (≤2.4%). PC1 and PC2 accounting together for 44.0% of cumulative variance (Figure 12). These two components were therefore selected for interpretation, as they capture the dominant gradients controlling soil organic matter (SOM) and geochemical variability in the dataset (Figure 13).

The first principal component (PC1) represents a gradient of organic matter content and its intrinsic vulnerability to decomposition. The strongest loadings on this axis were associated with C:N ratios in both fractions, relative stability index on the negative axis and C in both fraction on the positive axis (Figure 12). Clay also contributed substantially to PC1, suggesting that even the modest clay fraction influences the organic matter dynamics. $\delta^{13}C$ variables in both fractions contributed to PC1 but also carried substantial weight in PC2, reflecting their dual sensitivity to organic matter source and decomposition state rather than serving as exclusive markers of either gradient.

In contrast, nitrogen isotopic signatures $\delta^{13}C$ variables, $\delta^{15}N$_POM and $\delta^{15}N$_MAOM loaded primarily on PC2, suggesting that nitrogen dynamics respond to independent processes – such as mineralization intensity or localized microbial fractionation – rather than being strictly coupled with carbon source shifts. The close association between the C:N ratios of both fractions and the relative stability index η indicates that, in these periglacial soils, C:N serves as a proxy for SOM persistence. This relationship suggests that humification is not the primary driver of stabilization; instead, the main stabilization mechanism in these incipient soils appears to be the low lability associated with high C:N ratios, where the most stable compounds are those least altered by biological activity, consistent with findings by Samson et al. (2024).

PC2 (18.8%) represents a geochemical and textural gradient with secondary isotopic influence. On the positive axis, DN15_POM co-varied with Na and Ca, suggesting a coupling between base cation availability and nitrogen isotopic fractionation in the particulate organic matter fraction. In contrast, DN15_mOM was associated with Al_ox and D_Glac on the negative PC2, indicating that mineral-associated nitrogen fractionation responds to proximity to the glacier margin and amorphous Al availability, two spatially structured variables that reflect the pedogenic gradient across the transect. Sand contributed negatively to PC2, opposing

the silt-dominated textural pole represented by Silt and pH. Notably, Ca exhibited substantial contributions to both PC1 and PC2 (Figure 12), making it the only ionic variable with meaningful weight in the organic-matter-dominated axis. This pattern may indicate a secondary role of divalent cation bridging in organo-mineral interactions, even in the absence of abundant reactive Fe-Al phases. Similarly, $\delta^{13}C$ of both fractions and DN15_mOM showed divided contributions across dimensions, suggesting these isotopic variables integrate signals from both the organic and mineral domains simultaneously. Conversely, K, Mn and Al_dcb exhibited low total contributions across both dimensions, indicating that these elements do not constitute structuring gradients in the Kangerlussuaq soil system despite their potential relevance in other Arctic environments.

Together, these two axes reveal a partial decoupling between organic and mineral domains in Kangerlussuaq soils, which is observed in the contribution of each variable in both dimensions (Figure 13). PC1 captures the influence of organic inputs and isotopic differentiation, while PC2 reflects the pedogenic and textural variation associated with Fe–Al oxides and other elements and the limited organo-mineral coupling. The weak association between mineral variables and organic fractions suggests that organo-mineral stabilization mechanisms are limited, reflecting low chemical weathering intensity and a scarcity of reactive mineral surfaces for sorptive SOM protection. Such sorption processes are primarily mediated by poorly crystalline iron oxyhydroxides and hydroxylated mineral surfaces, which tend to be more abundant under conditions of advanced chemical weathering (Kleber et al., 2005; Herndon et al., 2017).

In addition, Spearman's rank correlation analysis (Figure S.1) was conducted to complement the PCA interpretation by quantifying pairwise associations among soil physical, geochemical, and isotopic variables. These mineral phases exhibited weak or negative correlations with organic fractions and isotopic variables, confirming the limited role of organo-mineral interactions in SOM stabilization. Organic carbon contents in both POM and MAOM fractions were positively associated with clay ($\rho = 0.74–0.81$), consistent with the contribution of Clay to PC1 and reinforcing the disproportionate importance of this minor fraction in carbon retention. $\delta^{13}C$ values of POM and MAOM were strongly correlated ($\rho = 0.65$), whereas $\delta^{15}N$ values showed weak associations across fractions, consistent with the independent nitrogen cycling processes identified along PC2.

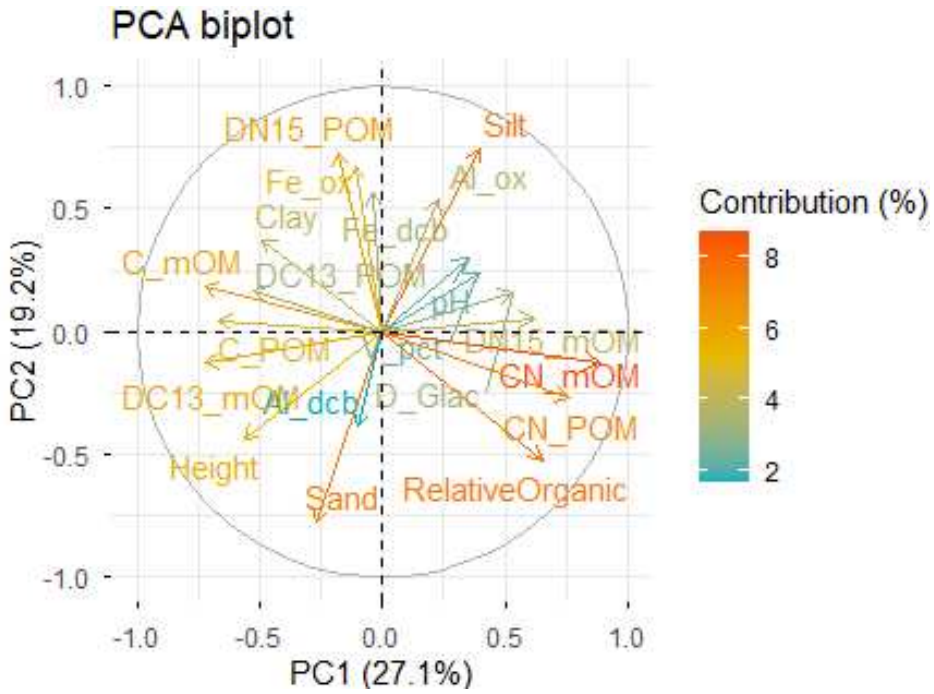

Figure 12: PCA analysis.

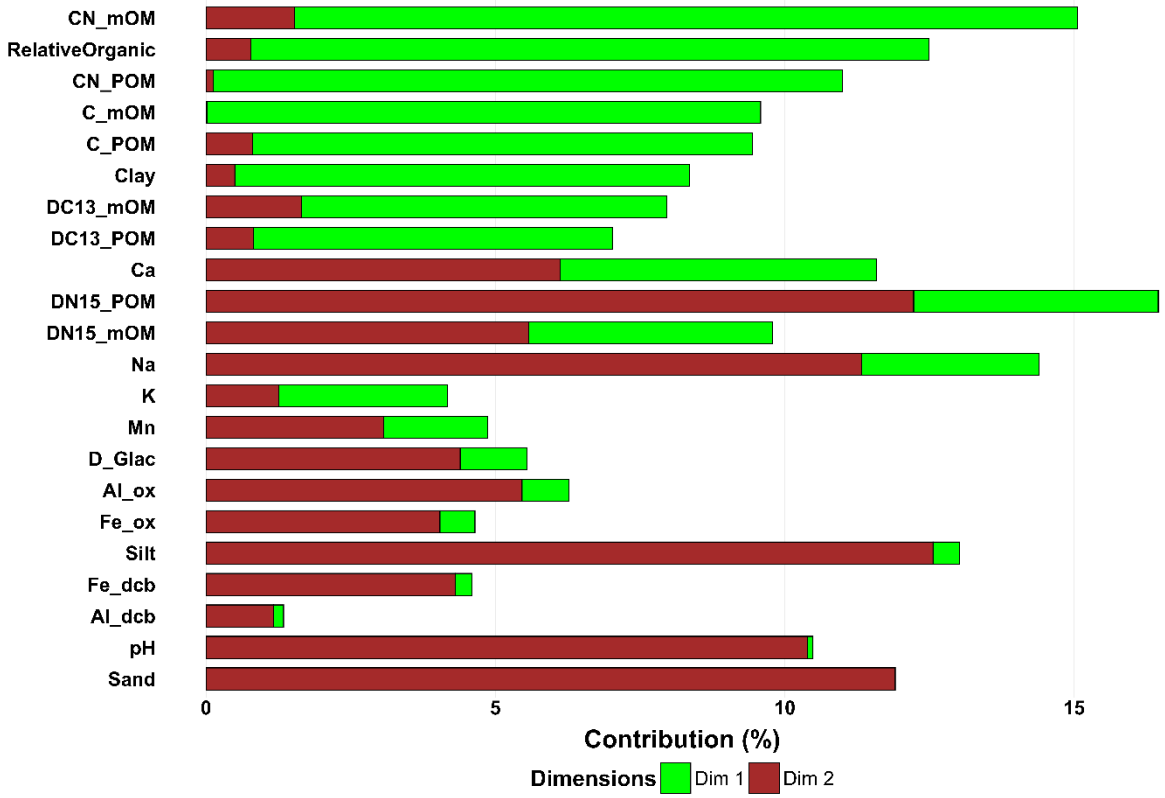

Figure 13: Contribution of each variable in both dimensions.

9. Discussion

9.1. Dynamics of organic C in profiles and their properties

The pedodiversity in the region is reflected in the classification and qualifies found in the profiles. The occurrence of organic surface horizons in P8 and P9 plus an organic buried profile (P7) in 35 centimeters indicate local conditions favorable to organic matter accumulation, where low temperatures, poor drainage, and slow decomposition rates promote the buildup of thick organic layers. This variety of soils reflects spatial heterogeneity in parent material, organic matter content, and depositional history, consistent with the dominance of silt and sand fractions and limited chemical weathering.

The wide variability in total organic carbon (0.2 – 28.84%) among profiles reflects the strong environmental heterogeneity in the Kangerlussuaq region. The aeolian influence has occurred continuously in the region over the last 4 kyr (Willesem et al., 2003) which contributes to depositions and frequent soil particle movement, which may justify the presence of incipient horizons. For this reason, many profiles were observed buried horizons and classified as Regosols, even though some pedogenetic activities were found in sub-layers. This aeolian influence may justify the high level of carbon in the POM fraction in some mid-layers, which may result from the burial and preservation of former surface horizons. In profiles classified as Turbic Cryosols (P4, P8, P9) an additional mechanism must be considered alongside aeolian burial. Cryoturbation, the physical mixing and displacement of soil material driven by differential frost heave and ice segregation during repeated freeze-thaw cycling. Cryoturbation can transport organic-rich surface material into subsurface mineral horizons on timescales of decades to centuries (Kaiser et al., 2007) that can insert organic content in depth horizons. In the present dataset, the mid-profile carbon peaks observed in P8 (Histic Turbic Cryosol) and P9 (Protic Histic Turbic Cryosol) are consistent with cryoturbation-driven incorporation of formerly surface organic horizons into mineral subsoil, a process that is particularly pronounced in waterlogged, organically enriched active layers (Bockheim et al., 1999). Critically, cryoturbation does not merely relocate organic matter, it also physically disrupts organo-mineral associations that have formed at the surface, disaggregating microaggregates and exposing previously protected organic compounds to renewed microbial attack once conditions permit. In this sense, cryoturbation operates as an additional destabilizing mechanism in the Cryosol profiles, compounding the mineral protection limitations and thermal instability described above.

These findings are indicate that climate and landscape evolution exert significant influence over pedogenesis in Arctic environments. In cold, recently deglaciated terrains, organic matter accumulation appears to be driven primarily by the physical preservation of plant residues under conditions of reduced decomposition, rather than through stabilization via organo-mineral associations (García-Palacios et al., 2024).

9.2. Low chemical weathering as a factor for low SOM stabilization component

Organic-rich Arctic soils typically contain large proportions of mineral-associated organic carbon that can be stabilized through interactions with mineral surfaces and spatial occlusion within aggregates (Herndon et al., 2017). Iron has a strong capacity to stabilize organic matter through various binding mechanisms (Herndon et al., 2017). However, the most reactive Fe phases are the poorly crystalline or amorphous forms, rather than well-crystallized oxides, which exhibit lower surface reactivity (Kleber et al., 2005). This pattern also applies to Arctic soils, where amorphous Fe phases predominantly mediate the formation of organo-mineral associations (Thomas et al., 2023). From this perspective, the low Fe_{ox} and FeDCB values observed in our samples indicate that both amorphous and crystalline Fe phases are scarce.

The scarcity of pedogenic Fe–Al oxides is consistent with a dominance of physical weathering processes, specifically cryoclasty and glacial comminution, characteristic of recently deglaciated polar environments in which chemical weathering is limited (Hall et al., 2002). This interpretation is supported by the high FeOX/FeDCB ratios approaching unity, which suggest minimal crystallization of amorphous Fe phases and are indicative of early-stage pedogenesis (Dahms et al., 2012). These low Fe and Al oxide concentrations are consistent with global observations, which show a general decline in the abundance of these elements toward higher latitudes (Jia et al., 2024).

Similarly, the contents of Al in both forms were low, with a mean value of 0.4 g.kg-1, demonstrating a general paucity of reactive Al phases. This scarcity implies that organic–mineral stabilization is unlikely to be governed predominantly by Fe–Al oxides. Although extractions revealed elevated levels of exchangeable and soluble Fe^{2+} and Al^{3+}, these forms primarily contribute to transient ionic interactions rather than stable organo–mineral associations. Free Fe^{2+} and Al^{3+} cations can participate in the formation and stabilization of soil aggregates through cationic bridging between organic and inorganic colloids, particularly within smaller aggregates (<20 μm) (Barberis et al., 1991; Amezketa, 1999). Nonetheless,

amorphous iron and aluminum oxides are more chemically and physically active in SOM stabilization (Lin et al., 2022), and their scarcity suggests limited aggregate stabilization mediated by organo–mineral associations, consistent with field observations of weak structural development. Spearman's rank correlations further support this interpretation: Fe_{ox}, Al_{ox}, and Fedcb were strongly correlated ($\rho = 0.61–0.90$), indicating coordinated pedogenic distribution of Fe–Al oxides. In contrast, these mineral phases showed weak or negative correlations with organic fractions ($\rho = –0.3$ to 0.2; Figure S1), suggesting that Fe–Al oxide–mediated sorptive interactions contribute modestly to SOM stabilization relative to other mechanisms such as physical occlusion or limited clay-associated sorption.

The strong co-variation between Fe_{ox} and Al_{ox} ($\rho = 0.90$) and their association with the silt fraction ($\rho = 0.56–0.61$) indicate that these phases are largely associated with weakly reactive mineral matrices, further limiting the availability of reactive surfaces for stable SOM binding. Despite the generally limited Fe-Al oxide concentrations, some incipient pedogenic processes involving both compounds can be observed in the profiles. This indicates that even minimal weathering and eluviation processes can contribute to SOM redistribution within these soils, despite the overall limited chemical activity in the system (Jakobsen, 1989).

In soils with near-neutral pH, as observed in several horizons in this study, the dissolution of Fe and Al hydroxides is reduced, potentially limiting the formation of ligand-exchange complexes that dominate organo-mineral stabilization in acidic soils (Kleber et al., 2005). Under these conditions, divalent Ca^{2+} ions can form both inner- and outer-sphere complexes with negatively charged organic functional groups, bridging them to mineral surfaces and contributing to SOM stabilization even where Fe–Al oxide availability is limited (Clarholm & Skyllberg, 2013; Rowley et al., 2018). While a direct quantification of Ca^{2+} mediated stabilization was beyond the scope of this study, the co-occurrence of high exchangeable Ca^{2+}, near-neutral pH, and elevated MAOM-C across several profiles is consistent with this mechanism operating alongside or in some horizons substituting for Fe–Al-mediated associations. We suggest that future studies in Arctic soils developed on carbonate-rich glacially derived substrates explicitly partition Ca^{2+}-associated from Fe/Al-associated MAOM fractions, as the relative importance of these stabilization pathways is likely to shift substantially across the pH gradients characteristic of these landscapes.

The PCA incorporating textural and geochemical variables (Figure 11) supports these interpretations. Fe_{ox} and Al_{ox} clustered closely with the silt fraction, indicating that these oxides

are primarily associated with less reactive mineral components rather than actively participating in organic matter stabilization. In contrast, organic carbon in both the POM and MAOM fractions showed weak associations with geochemical variables, reinforcing the limited coupling between SOM and the mineral phase. The soils are dominated by silt-sized particles and are texturally classified as loam to silty loam. Although SOM can be associated with silt-sized particles through limited sorption or physical protection mechanisms (Virto et al., 2008), silt minerals generally exhibit low specific surface area and cation exchange capacity, which constrains their capacity to stabilize organic carbon. Accordingly, the silt fraction was positioned distantly from organic carbon variables in the PCA, showing little influence on SOM contents and instead clustering with Fe_{ox}, Fe_{DCB}, and Al_{DCB}. Although clay represents only a minor proportion of the soil texture, it showed a positive association with organic carbon in both POM and MAOM fractions. This suggests that even small amounts of clay contribute disproportionately to SOM stabilization due to their higher specific surface area and greater reactivity compared to other soil fractions. These findings indicate that, despite its low abundance, the clay fraction plays a key role in organic carbon retention in Kangerlussuaq soils, as also related in other study in Arctic (Herndon et al., 2017).

9.3. Relative organic stability and isotopic composition ($\delta^{13}C$ and $\delta^{15}N$)

The $\delta^{13}C$ values in both MAOM and POM fractions exhibited limited variability, indicating relatively homogeneous organic matter sources across the study area. This isotopic uniformity suggests stable plant-derived carbon inputs along the soil profiles, reflecting limited spatial variation in vegetation composition and environmental conditions. The average $\delta^{13}C$ signatures are characteristic of C_3 plant dominance, which is typical of high-latitude Arctic ecosystems, as also reported for Svalbard soils and sediments (Kim et al., 2023). An exception was observed in the O horizon of profile P9, which exhibited a markedly enriched $\delta^{13}C$ value (–17.64‰) in the POM fraction. P9 is located adjacent to a lake, and this enrichment is consistent with the incorporation of macrophyte-derived organic matter, which commonly exhibits higher $\delta^{13}C$ values in lacustrine systems in the Kangerlussuaq region (Osburn et al., 2019). Comparable isotopic enrichment has been documented in lake sediments from the Kangerlussuaq fjord system (Leng & Anderson, 2003; Auqué et al., 2019), where it has been attributed to a combination of aquatic primary production and contributions from inorganic carbon during organic matter mineralization. In this same horizon, the highest POM-associated organic carbon content and the lowest pH (H_2O = 4.72) were recorded, indicating distinct pedogenic conditions relative to the other profiles. Together, these characteristics suggest

localized depositional and biogeochemical processes associated with lacustrine influence, resulting in organic matter inputs and soil conditions that differ from the surrounding terrestrial system.

The $\delta^{15}N$ values in POM and MAOM span both negative and positive ranges, reflecting variability in nitrogen cycling and degrees of microbial processing across horizons. MAOM $\delta^{15}N$ values, mostly between -2‰ and +4‰, are consistent with microbial transformation and partial recycling of organic nitrogen. In contrast, strongly depleted $\delta^{15}N$ values observed in some deep POM horizons, particularly in profiles P5 and P9, coincide with elevated C:N ratios and low SOM stability indices (n), indicating limited microbial alteration and preservation of relatively undecomposed organic material. The most extreme depletions – $\delta^{15}N$ POM of -18.88‰ in P5 2C1 and -13.05‰ in P9 C1, are, however, difficult to attribute solely to low decomposition rates. Values in this range suggest the influence of isotopically light N sources operating independently of decomposition dynamics. Profile P5 is located approximately 11 km from the glacier margin, within a zone of documented proglacial outwash influence, where glacially-derived meltwater nitrogen, known to carry depleted $\delta^{15}N$ signatures, may contribute to subsurface N pools. Profile P9, located adjacent to a lake and classified as a Protic Histic Turbic Cryosol, may additionally receive nitrogen inputs from aquatic or semi-aquatic N-fixing communities, consistent with its anomalous $\delta^{13}C$ signature in the O horizon noted above. Regardless of mechanism, the reliability of the n index for these specific horizons is reduced, as the Conen et al. (2008) model assumes that $\delta^{15}N$ differentiation between fractions reflects microbial processing rather than source heterogeneity.

The low n values (median 1.01) compared with temperate and subtropical systems indicate that, relative to POM, the MAOM pool in these soils has undergone only limited isotopic enrichment and C:N narrowing. This pattern is consistent with incomplete microbial transformation of plant-derived inputs (Conen et al., 2008). This pattern aligns with Arctic conditions, since low temperatures and continuous freezing reduces microbial transformation of SOM and may restrict enzymatic depolymerization, resulting in a slow decomposition (Pengerud et al., 2017; Conant et al., 2011). Without independent age constraints or decomposition measurements, these results cannot be directly translated into turnover times or projected mineralization rates under warmer conditions. Nonetheless, they suggest that a substantial fraction of SOM resides in a comparatively weakly transformed state that could become more available to microbial decomposition if environmental constraints on microbial activity and substrate accessibility (e.g., through permafrost melting) were favorable.

The predominance of incomplete residue transformation also aligns with the incipient degree of soil development observed in the Kangerlussuaq region. Most profiles are dominated by sand and silt fractions, which provide limited surface area for organo–mineral interactions. This pattern was confirmed by the low correlations between these fractions and the soil organic carbon (Figure 11). Conversely, even the modest clay content exhibited a stronger association with organic matter stabilization, underscoring the importance of mineral surface chemistry in these weakly weathered environments. Although MAOM is typically a stable fraction, our isotopic and C:N data shows that in the profile analyzed, the MAOM has similar biochemical features to POM, with the values of n furtherly corroborating the low relative stability of the SOM in the studied soils.

Overall, these findings demonstrate that climate exerts a dominant control over both pedogenic and mineralization processes in Kangerlussuaq soils. We also note the limitations of the Conen et al. (2008) stability model, which assumes steady-state conditions and may not capture rapid changes associated with climate warming or cryoturbation. Validation by independent age measurements (14C) or targeted studies under non-equilibrium conditions is needed.

9.4. Soil temperature dynamics

Temperature plays a central role in regulating the biochemical processes that control carbon pools and the exchange of carbon and nitrogen between terrestrial and atmospheric systems (Qu et al., 2023). Additionally, in the Arctic environment, warming can significantly influence CH_4 production (de Jong et al., 2018). Year-long soil temperature monitoring revealed that all profiles experienced extended periods of both frozen and thawed conditions, with clear differentiation among the monitored sites. Each profile exhibited at least one full month with thawing conditions above 0.5 °C, whereas all soil layers experienced at least one full month of completely frozen conditions below 0.5 °C. Furthermore, the data highlights a strong contrast between high surface thermal amplitudes, reflected by large differences between thawing degree days (TDD) and freezing degree days (FDD), and colder subsurface layers characterized by abundant isothermal days, particularly at 30 cm depth. These patterns indicate a two-way thermal control on organic matter decomposition along the soil profile.

At the surface, higher TDD and sustained thawing-day values during summer indicate that thawing under low to moderate temperatures (approximately 2–6 °C) can promote increased carbon losses, as observed in incubation experiments (Hartley et al., 2008).

Additionally, under temperatures ranging from +0.5 °C to +14 °C, microbial respiration in Arctic tundra soils has been shown to be comparable to or even exceed that of temperate and tropical soils (Mikan et al., 2002). This enhanced respiration influences the decomposition of both labile and more recalcitrant SOM fractions, which remain sensitive to temperature in Arctic environments and thus represent a potential source of CO_2 emissions (Mikan et al., 2002). Recent studies further indicate that under Arctic warming, soil bacterial communities and overall microbial diversity tend to expand, which may contribute to increased losses of soil carbon stocks over time (Rijkers et al., 2022; Ji et al., 2022). Conversely, extended periods with low FDD values and prolonged frozen conditions indicate that temperature also indirectly constrains respiration through physical controls, such as water availability and substrate diffusion, thereby reducing SOM decomposition (Mikan et al., 2002). Continuous freezing limits microbial activity and slows SOM transformation (Schuur et al., 2008). Moreover, freeze–thaw cycles (FTCs), even when occurring at relatively low frequency, impose physiological stress on microbial communities and can induce substantial microbial mortality and nutrient release during colder periods (Han et al., 2018).

Subsurface layers exhibit distinct thermal regimes between 50 cm and 130 cm depths. At 50 cm depth, a high proportion of isothermal days was observed, whereas at 130 cm depth, profiles showed site-specific patterns, including a combination of isothermal and frozen days in P4 and a relative increase in thawing days in P5 and P7. These differences reflect contrasting subsurface thermal dynamics among profiles. Previous studies have shown that deeper Arctic soil layers can exhibit enhanced mineralization rates due to the combined effects of reduced microbial activity and the downward transport and accumulation of relatively fast-cycling organic carbon (Moni et al., 2015; Waldrop et al., 2010). The increased proportion of isothermal days in mid-layers relative to surface horizons likely indicates higher water contents (Guglielmin et al., 2008), which may favor the development of low-oxygen or anoxic conditions. In such environments, frozen water may persist for extended periods, limiting oxygen diffusion and promoting anaerobic decomposition pathways, as water availability strongly regulates microbial processes controlling SOM turnover (Herndon et al., 2015). Anaerobic conditions in water-saturated soils favor fermentation processes that produce acetate, which can subsequently fuel acetoclastic methanogenesis, the dominant CH_4-producing pathway under these conditions (Herndon et al., 2015). These anaerobic processes complement decomposition occurring during thawing periods in mid-layers, which, although less pronounced than at the surface, remain significant-particularly where more labile SOM is

concentrated at depth. In deeper layers, sensor data indicates a reduction in isothermal days and an increase in thawing days across all profiles, most notably in P5 and P7. Increased thawing frequency in subsurface layers (both 50 cm and 130 cm) can promote redox-driven phase transformations of iron minerals, destabilizing Fe-bound organic carbon and enhancing its mobilization and loss during freeze–thaw cycles (Tian et al., 2025). These processes collectively create favorable conditions for SOM mineralization and the production of both CO_2 and CH_4. Although freeze–thaw days (FTDs) occurred at relatively low frequency, such events may temporarily stimulate microbial activity following thawing, further contributing to SOM decomposition. This effect is particularly relevant in subsurface horizons where organic carbon may be enriched through burial or downward transport.

Overall, surface and subsurface organic matter experience distinct thermal environments, with surface horizons exhibiting larger annual temperature amplitudes and more frequent freeze–thaw events than deeper layers. In Turbic Cryosol profiles specifically, this thermal variability operates in concert with cryoturbation, which continuously repositions organic material across thermal gradients within the active layer, exposing it sequentially to the high-amplitude surface thermal regime and the more buffered but persistently frozen subsurface environment. This coupling between physical mixing and thermal cycling creates conditions harder to organic matter stabilize in any single thermal niche long enough to develop substantial mineral associations or biochemical recalcitrance, a process-level interaction that is absent from non-turbic profiles and that may explain the particularly low n values observed in P4, P8, and P9 relative to the dataset mean. These contrasts imply that the timing and duration of conditions permissive for microbial activity differ with depth, but the net consequences for SOM mineralization cannot be quantified from temperature alone. Laboratory and field studies indicate that both substrate availability and microbial resilience strongly modulate decomposition responses to thermal perturbation. Higher SOM availability can facilitate microbial recovery and renewed activity following freeze–thaw stress (Han et al., 2018), while thaw events can rapidly stimulate enzymatic depolymerization and CO_2 production especially at low temperatures (Conant et al., 2011). In our study, such processes are likely to operate, but they remain inferred rather than directly demonstrated because microbial biomass and gas fluxes were not measured. Throughout the monitoring period, all profiles exhibited positive mean temperatures during summer, indicating seasonal thawing of the active layer, whereas winter conditions were characterized by prolonged freezing and, at depth, frequent isothermal periods. Similar depth-dependent thermal sensitivities of soil processes have been reported

across the pan-Arctic (Guo et al., 2025; Petersen, 2021; Patoine et al., 2022), highlighting the potential for changing temperature regimes to alter SOM dynamics. However, our single-year record does not resolve long-term trends. Multi-year monitoring combined with direct measurements of CO_2 and CH_4 fluxes will therefore be essential to determine how the observed thermal regimes translate into actual carbon losses in the Kangerlussuaq region.

10. Conclusions

Soils studied at Kangerlussuaq, substantial organic carbon is stored in both MAOM and POM fractions, with a clear predominance of different particulate carbon forms. Carbon isotopic signatures ($\delta^{13}C$) and C:N ratios in different fractions suggest relatively homogeneous plant-derived inputs and limited long-term biochemical transformation of much of SOM. The relative stability index n is generally low compared with values reported for alpine, temperate, and agricultural systems (Samson et al., 2024; De Clercq et al., 2015), pointing to a comparatively weak degree of SOM stabilization in the Kangerlussuaq profiles. On the other hand, it is important to consider that the interpretation of these values were driven primarily as comparative indicators of SOM transformation state in selected Arctic soils rather than as direct quantitative measure of decomposition rate or mean residence time, considering the distance from the ideal conditions stated for comparison.

The low concentrations of Fe_{ox} and Al_{ox} indicate a scarcity of amorphous Fe-Al phases, implying a limited capacity for stable organo-mineral association formation. This weak mineral protection is corroborated by multivariate analyses, as PCA results show separation between organic matter pools and mineralogical or textural components. Spearman's correlation analysis further confirms this decoupling, revealing strong internal coherence among Fe–Al oxides but weak relationships with SOM fractions. While the good correlation of Ca^{2+} points to a secondary stabilization mechanism. This suggests that in Greenlandic periglacial landscapes, Ca-mediated cation bridging may be a critical factor in carbon persistence that partially offsets the lack of reactive pedogenic oxides. Together, these findings indicate that SOM stabilization in the Kangerlussuaq region is not primarily governed by mineral sorption mechanisms, resulting in relatively high vulnerability to decomposition.

Thermal monitoring revealed pronounced seasonal and vertical variability in soil temperature regimes. The depth-dependent patterns indicate that both surface and subsurface SOM periodically experiences temperatures that allow microbial activity, although the

magnitude and duration of decomposition under these conditions remain unconstrained in the absence of direct flux measurements.

Sustained summer thawing in surface soils is likely to enhance microbial respiration and carbon losses, whereas episodic thawing and freeze-thaw transitions at depth may affect SOM via microbial stress, transient nutrient release, and redox-sensitive changes in organo-mineral interactions. Although freeze-thaw days occurred at relatively low frequency in our one-year record, their occurrence at multiple depths points to a potential role in regulating short–term SOM dynamics that warrants further investigation. The combination of weak mineral protection, depth-dependent thermal buffering, and intermittent thawing suggests that subsurface horizons in the Kangerlussuaq region may participate more actively in carbon cycling.

Overall, our findings indicate that SOM in the Kangerlussuaq region may be highly vulnerable to degradation due to the combined effects of weak mineral stabilization and thermal disturbance. Continued multi-year investigations that integrate thermal monitoring with geochemical and isotopic analyses, SOM fractionation, and direct measurements of greenhouse gas fluxes will be essential to constrain the mechanisms governing SOM persistence and to refine projections of carbon-cycle feedbacks under future Arctic climate scenarios.

References

Alekseev, I., Abakumov, E., 2022. Soil organic carbon stocks and stability of organic matter in permafrost-affected soils of Yamal region, Russian Arctic. Geoderma Regional 26, e00454. https://doi.org/10.1016/j.geodrs.2021.e00454.

Amézketa, E., 1999. Soil aggregate stability: a review. J. Sustain. Agric. 14, 83-151. https://doi.org/10.1300/j064v14n02_08.

Anderson, N.J., Stedmon, C.A., 2007. The effect of evapoconcentration on dissolved organic carbon concentration and quality in lakes of SW Greenland. Freshw. Biol. 52, 280-289. https://doi.org/10.1111/j.1365-2427.2006.01688.x.

Anderson, N.J., Saros, J.E., Bullard, J.E., Cahoon, S.M.P., McGowan, S., Bagshaw, E.A., Barry, C.D., Bindler, R., Burpee, B.T., Carrivick, J.L., Fowler, R.A., Fox, A.D., Fritz, S.C., Giles, M.E., Hamerlik, L., Ingeman-Nielsen, T., Law, A.C., Mernild, S.H., Northington, R.M.,

Osburn, C.L., 2017. The Arctic in the twenty-first century: changing biogeochemical linkages across a paraglacial landscape of Greenland. BioScience 67, 118-133. https://doi.org/10.1093/biosci/biw158.

Angst, G., Mueller, K.E., Nierop, K.G.J., Simpson, M.J., 2021. Plant- or microbial-derived? A review on the molecular composition of stabilized soil organic matter. Soil Biol. Biochem. 156, 108189. https://doi.org/10.1016/j.soilbio.2021.108189.

Barberis, E., Marsan, F.A., Boero, V., Arduino, E., 1991. Aggregation of soil particles by iron oxides in various size fractions of soil B horizons. J. Soil Sci. 42, 535-542. https://doi.org/10.1111/j.1365-2389.1991.tb00100.x.

Beck, H.E., Zimmermann, N.E., McVicar, T.R., Vergopolan, N., Berg, A., Wood, E.F., 2018. Present and future Köppen-Geiger climate classification maps at 1-km resolution. Sci. Data 5, 180214. https://doi.org/10.1038/sdata.2018.214.

Boberg, F., Langen, P.L., Mottram, R.H., Christensen, J.H., Olesen, M., 2018. 21st-century climate change around Kangerlussuaq, west Greenland: from the ice sheet to the shores of Davis Strait. Arct. Antarct. Alp. Res. 50, S100006. https://doi.org/10.1080/15230430.2017.1420862.

Bockheim, J.G., Tarnocai, C., 1998. Recognition of cryoturbation for classifying permafrost-affected soils. Geoderma 81, 281-293. https://doi.org/10.1016/S0016-7061(97)00115-8.

Bruhwiler, L., Parmentier, F.-J.W., Crill, P., Leonard, M., Palmer, P.I., 2021. The Arctic carbon cycle and its response to changing climate. Curr. Clim. Change Rep. 7, 14-34. https://doi.org/10.1007/s40641-020-00169-5.

Cambardella, C.A., Elliott, E.T., 1992. Particulate soil organic-matter changes across a grassland cultivation sequence. Soil Sci. Soc. Am. J. 56, 777-783. https://doi.org/10.2136/sssaj1992.03615995005600030017x.

Clarholm, M., Skyllberg, U., 2013. Translocation of metals by trees and fungi regulates pH, soil organic matter turnover and nitrogen availability in acidic forest soils. Soil Biol. Biochem. 63, 142-153. https://doi.org/10.1016/j.soilbio.2013.03.019.

Conant, R.T., Ryan, M.G., Ågren, G.I., Birge, H.E., Davidson, E.A., Eliasson, P.E., Evans, S.E., Frey, S.D., Giardina, C.P., Hopkins, F.M., Hyvönen, R., Kirschbaum, M.U.F., Lavallee, J.M., Leifeld, J., Parton, W.J., Steinweg, J.M., Wallenstein, M.D., Wetterstedt, J.Å.M., Bradford, M.A., 2011. Temperature and soil organic matter decomposition rates - synthesis of current knowledge and a way forward. Glob. Change Biol. 17, 3392-3404. https://doi.org/10.1111/j.1365-2486.2011.02496.x.

Cotrufo, M.F., Wallenstein, M.D., Boot, C.M., Denef, K., Paul, E., 2013. The Microbial Efficiency-Matrix Stabilization (MEMS) framework integrates plant litter decomposition with soil organic matter stabilization: do labile plant inputs form stable soil organic matter? Glob. Change Biol. 19, 988-995. https://doi.org/10.1111/gcb.12113.

Cotrufo, M.F., Soong, J.L., Horton, A.J., Campbell, E.E., Haddix, M.L., Wall, D.H., Parton, W.J., 2015. Formation of soil organic matter via biochemical and physical pathways of litter mass loss. Nat. Geosci. 8, 776-779. https://doi.org/10.1038/ngeo2520.

Dahms, D., Favilli, F., Krebs, R., Egli, M., 2012. Soil weathering and accumulation rates of oxalate-extractable phases derived from alpine chronosequences of up to 1 Ma in age. Geomorphology 151-152, 99-113. https://doi.org/10.1016/j.geomorph.2012.01.021.

De Clercq, T., Heiling, M., Dercon, G., Resch, C., Aigner, M., Mayer, L., Mao, Y., Elsen, A., Steier, P., Leifeld, J., Merckx, R., 2015. Predicting soil organic matter stability in agricultural fields through carbon and nitrogen stable isotopes. Soil Biol. Biochem. 88, 29-38. https://doi.org/10.1016/j.soilbio.2015.05.011.

de Jong, A.E., Meisel, O.H., Dean, J.F., Rasigraf, O., Welte, C.U., 2018. Increases in temperature and nutrient availability positively affect methane-cycling microorganisms in Arctic thermokarst lake sediments. Environ. Microbiol. 20, 4314-4327. https://doi.org/10.1111/1462-2920.14345.

Forman, S.L., Marín, L., Van Der Veen, C., Tremper, C., Csatho, B., 2007. Little Ice Age and neoglacial landforms at the Inland Ice margin, Isunguata Sermia, Kangerlussuaq, west Greenland. Boreas 36, 341-351. https://doi.org/10.1080/00173130601173301.

Galluzzi, G., Plaza, C., Priori, S., Giannetta, B., Zaccone, C., 2024. Soil organic matter dynamics and stability: climate vs. time. Sci. Total Environ. 929, 172441. https://doi.org/10.1016/j.scitotenv.2024.172441.

García-Palacios, P., Bradford, M.A., Benavente-Ferraces, I., Celis, M., Delgado-Baquerizo, M., García-Gil, J.C., Gaitán, J.J., Goñi-Urtiaga, A., Mueller, C.W., Panettieri, M., Rey, A., Sáez-Sandino, T., Sokol, N.W., Tedersoo, L., Plaza, C., 2024. Dominance of particulate organic carbon in top mineral soils in cold regions. Nat. Geosci. 17, 145-150. https://doi.org/10.1038/s41561-023-01354-5.

Grimes, M., Carrivick, J.L., Smith, M.W., Comber, A.J., 2024. Land cover changes across Greenland dominated by a doubling of vegetation in three decades. Sci. Rep. 14, 3120. https://doi.org/10.1038/s41598-024-52124-1.

Guglielmin, M., Ellis Evans, C.J., Cannone, N., 2008. Active layer thermal regime under different vegetation conditions in permafrost areas. A case study at Signy Island (Maritime Antarctica). Geoderma 144, 73-85. https://doi.org/10.1016/j.geoderma.2007.10.010.

Guo, H.-X., Zhu, W.-Q., Xiao, C.-D., Zhao, C.-L., Chen, L.-Y., 2025. The freezing-thawing index and permafrost extent in pan-Arctic experienced rapid changes following the global warming hiatus. Adv. Clim. Change Res. https://doi.org/10.1016/j.accre.2025.02.010.

Hall, K., Thorn, C.E., Matsuoka, N., Prick, A., 2002. Weathering in cold regions: some thoughts and perspectives. Prog. Phys. Geogr. 26, 577-603. https://doi.org/10.1191/0309133302pp353ra.

Han, Y., Chen, X., Choi, B., 2019. Effect of freeze-thaw cycles on phosphorus fractions and their availability in biochar-amended Mollisols of Northeast China. Sustainability 11, 1006. https://doi.org/10.3390/su11041006.

Hartley, I.P., Hopkins, D.W., Garnett, M.H., Sommerkorn, M., Wookey, P.A., 2008. Soil microbial respiration in arctic soil does not acclimate to temperature. Ecol. Lett. 11, 1092-1100. https://doi.org/10.1111/j.1461-0248.2008.01223.x.

Herndon, E., Yang, Z., Bargar, J.R., Janot, N., Regier, T., Graham, D.Y., Wullschleger, S.D., Gu, B., Liang, L., 2015. Geochemical drivers of organic matter decomposition in arctic tundra soils. Biogeochemistry 126, 397-414. https://doi.org/10.1007/s10533-015-0165-5.

Herndon, E., AlBashaireh, A., Singer, D.J., Roy Chowdhury, T., Gu, B., Graham, D.Y., 2017. Influence of iron redox cycling on organo-mineral associations in Arctic tundra soil. Geochim. Cosmochim. Acta 207, 210-231. https://doi.org/10.1016/j.gca.2017.02.034.

IUSS Working Group WRB, 2022. World Reference Base for Soil Resources. International Soil Classification System for Naming Soils and Creating Legends for Soil Maps, 4th ed. International Union of Soil Sciences, Vienna.

Jackson, D.A., 1993. Stopping rules in principal components analysis: a comparison of heuristical and statistical approaches. Ecology 74, 2204-2214. https://doi.org/10.2307/1939574.

Jakobsen, B.H., 1989. Evidence for translocations into the B horizon of a subarctic Podzol in Greenland. Geoderma 45, 3-17. https://doi.org/10.1016/0016-7061(89)90053-0.

Ji, M., Kong, W., Jia, H., Delgado-Baquerizo, M., Zhou, T., Liu, X., Ferrari, B.C., Malard, L., Liang, C., Xue, K., Makhalanyane, T.P., Zhu, Y.-G., Wang, Y., Pearce, D.A., Cowan, D., 2022. Polar soils exhibit distinct patterns in microbial diversity and dominant phylotypes. Soil Biol. Biochem. 166, 108550. https://doi.org/10.1016/j.soilbio.2022.108550.

Jia, N., Li, L., Guo, H., Xie, M., 2024. Important role of Fe oxides in global soil carbon stabilization and stocks. Nat. Commun. 15, 10416. https://doi.org/10.1038/s41467-024-54832-8.

Kaiser, C., Meyer, H., Biasi, C., Rusalimova, O., Barsukov, P., Richter, A., 2007. Conservation of soil organic matter through cryoturbation in arctic soils in Siberia. J. Geophys. Res. 112, G02017. https://doi.org/10.1029/2006jg000258.

Kalsbeek, F., Pidgeon, R.T., Taylor, P.N., 1987. Nagssugtoqidian mobile belt of West Greenland: a cryptic 1850 Ma suture between two Archaean continents - chemical and isotopic evidence. Earth Planet. Sci. Lett. 85, 365-385. https://doi.org/10.1016/0012-821x(87)90134-8.

Kim, D., Kim, J.-H., Ahn, Y., Jang, K., Jung, J.Y., Bae, M., Nam, S.-I., 2023. Large contributions of petrogenic and aged soil-derived organic carbon to Arctic fjord sediments in Svalbard. Sci. Rep. 13, 17935. https://doi.org/10.1038/s41598-023-45141-z.

Kleber, M., Mikutta, R., Torn, M.S., Jahn, R., 2005. Poorly crystalline mineral phases protect organic matter in acid subsoil horizons. Eur. J. Soil Sci. 56, 717-725. https://doi.org/10.1111/j.1365-2389.2005.00706.x.

Knight, P.G., Jennings, C.E., Waller, R.I., Robinson, Z.P., 2007. Changes in ice-margin processes and sediment routing during ice-sheet advance across a marginal moraine. Geogr. Ann. Ser. A 89, 203-215. https://doi.org/10.1111/j.1468-0459.2007.00319.x.

Lin, Z., Huang, Z., Liao, D., Huang, W., Huang, J., Deng, Y., 2022. Effects of soil organic matter components and iron aluminum oxides on aggregate stability during vegetation succession in granite red soil eroded areas. J. Mt. Sci. 19, 2634-2650. https://doi.org/10.1007/s11629-021-7185-5.

Liu, Y., Wang, P., Elberling, B., Westergaard-Nielsen, A., 2023. Drivers of contemporary and future changes in Arctic seasonal transition dates for a tundra site in coastal Greenland. Glob. Change Biol. 30, e17118. https://doi.org/10.1111/gcb.17118.

Mehra, O.P., Jackson, M.L., 1960. Iron oxide removal from soils and clays by a dithionite-citrate system buffered with sodium bicarbonate. Clays Clay Miner. 7, 317-327.

Mikan, C.J., Schimel, J.P., Doyle, A.P., 2002. Temperature controls of microbial respiration in arctic tundra soils above and below freezing. Soil Biol. Biochem. 34, 1785-1795. https://doi.org/10.1016/s0038-0717(02)00168-2.

Miner, K.R., Turetsky, M.R., Malina, E., Bartsch, A., Tamminen, J., McGuire, A.D., Fix, A., Sweeney, C., Elder, C.D., Miller, C.E., 2022. Permafrost carbon emissions in a changing Arctic. Nat. Rev. Earth Environ. 3, 55-67. https://doi.org/10.1038/s43017-021-00230-3.

Moni, C., Lerch, T.Z., Knoth de Zarruk, K., Strand, L.T., Forte, C., Certini, G., Rasse, D.P., 2015. Temperature response of soil organic matter mineralisation in arctic soil profiles. Soil Biol. Biochem. 88, 236-246. https://doi.org/10.1016/j.soilbio.2015.05.024.

Müller, M., Thiel, C., Kühn, P., 2016. Holocene palaeosols and aeolian activities in the Umimmalissuaq valley, West Greenland. Holocene 26, 1149-1161. https://doi.org/10.1177/0959683616632885.

Osburn, C.L., Anderson, N.J., Leng, M.J., Barry, C.D., Whiteford, E.J., 2019. Stable isotopes reveal independent carbon pools across an Arctic hydro-climatic gradient: implications for the fate of carbon in warmer and drier conditions. Limnol. Oceanogr. Lett. 4, 205-213. https://doi.org/10.1002/lol2.10119.

Patoine, G., Eisenhauer, N., Cesarz, S., Phillips, H., Xu, X., Zhang, L., Koellner, T., 2022. Drivers and trends of global soil microbial carbon over two decades. Nat. Commun. 13, 4195. https://doi.org/10.1038/s41467-022-31833-z.

Pengerud, A., Dignac, M.F., Certini, G., Strand, L.T., Forte, C., Rasse, D.P., 2017. Soil organic matter molecular composition and state of decomposition in three locations of the European Arctic. Biogeochemistry 135, 277-292. https://doi.org/10.1007/s10533-017-0373-2.

Petersen, G.N., 2021. Trends in soil temperature in the Icelandic highlands from 1977 to 2019. Int. J. Climatol. 42, 2299-2310. https://doi.org/10.1002/joc.7366.

Qu, Q., Xu, H., Ai, Z., Wang, M., Wang, G., Liu, G., Geissen, V., Ritsema, C.J., Xue, S., 2023. Impacts of extreme weather events on terrestrial carbon and nitrogen cycling: a global meta-analysis. Environ. Pollut. 319, 120996. https://doi.org/10.1016/j.envpol.2022.120996.

R Core Team, 2022. R: A Language and Environment for Statistical Computing. R Foundation for Statistical Computing, Vienna. https://www.R-project.org.

Rantanen, M., Karpechko, A.Y., Lipponen, A., Nordling, K., Hyvärinen, O., Ruosteenoja, K., Vihma, T., Laaksonen, A., 2022. The Arctic has warmed nearly four times faster than the globe since 1979. Commun. Earth Environ., 3(1), 1–10. https://doi.org/10.1038/s43247-022-00498-3.

Rijkers, R., Rousk, J., Aerts, R., Sigurdsson, B.D., Weedon, J.T., 2022. Optimal growth temperature of Arctic soil bacterial communities increases under experimental warming. Glob. Change Biol. 28, 6050-6064. https://doi.org/10.1111/gcb.16342.

Robinson, D., 2001. $\delta^{15}N$ as an integrator of the nitrogen cycle. Trends Ecol. Evol. 16, 153-162. https://doi.org/10.1016/s0169-5347(00)02098-x.

Rowley, M.C., Grand, S., Verrecchia, É.P., 2018. Calcium-mediated stabilisation of soil organic carbon. Biogeochemistry 137, 27-49. https://doi.org/10.1007/s10533-017-0410-1.

Russell, A.J., Carrivick, J.L., Ingeman-Nielsen, T., Yde, J.C., Williams, M., 2011. A new cycle of jökulhlaups at Russell Glacier, Kangerlussuaq, West Greenland. J. Glaciol. 57, 238-246. https://doi.org/10.3189/002214311796405997.

Samson, V.M., Wei, Y., Guo, L., Liu, D., Heiling, M., Dercon, G., Guo, Y., Mao, Y., 2024. Evaluation of long-term organic carbon dynamics and organic matter stability in a cultivated paddy soil using a carbon and nitrogen stable isotopes-based model. Soil Tillage Res. 239, 106040. https://doi.org/10.1016/j.still.2024.106040.

Schoeneberger, P.J., Wysocki, D.A., Benham, E.C., Soil Survey Staff, 2012. Field Book for Describing and Sampling Soils, ver. 3.0. USDA Natural Resources Conservation Service, National Soil Survey Center, Lincoln.

Schuur, E.A.G., Bockheim, J., Canadell, J.G., Euskirchen, E., Field, C.B., Goryachkin, S.V., Hagemann, S., Kuhry, P., Lafleur, P.M., Lee, H., Mazhitova, G., Nelson, F.E., Rinke, A., Romanovsky, V.E., Shiklomanov, N., Tarnocai, C., Venevsky, S., Vogel, J.G., Zimov, S.A., 2008. Vulnerability of permafrost carbon to climate change: implications for the global carbon cycle. BioScience 58, 701-714. https://doi.org/10.1641/b580807.

Schuur, E.A.G., McGuire, A.D., Schädel, C., Grosse, G., Harden, J.W., Hayes, D.J., Hugelius, G., Koven, C.D., Kuhry, P., Lawrence, D.M., Natali, S.M., Olefeldt, D., Romanovsky, V.E., Schaefer, K., Turetsky, M.R., Treat, C.C., Vonk, J.E., 2015. Climate change and the permafrost carbon feedback. Nature 520, 171-179. https://doi.org/10.1038/nature14338.

Silva, T., Whitley, B.S., Biersma, E.M., Abermann, J., Raundrup, K., de Vere, N., Høye, T.T., Schöner, W., 2025. Bio-climatic factors drive spectral vegetation changes in Greenland. EGUsphere. https://doi.org/10.5194/egusphere-2024-2571.

Soldatova, E., Krasilnikov, S., Kuzyakov, Y., 2024. Soil organic matter turnover: global implications from $\delta^{13}C$ and $\delta^{15}N$ signatures. Sci. Total Environ. 912, 169423. https://doi.org/10.1016/j.scitotenv.2023.169423.

Storms, J.E.A., de Winter, I.L., Overeem, I., Drijkoningen, G.G., Lykke-Andersen, H., 2012. The Holocene sedimentary history of the Kangerlussuaq Fjord-valley fill, West Greenland. Quat. Sci. Rev. 35, 29-50. https://doi.org/10.1016/j.quascirev.2011.12.014.

Tarnocai, C., Canadell, J.G., Schuur, E.A.G., Kuhry, P., Mazhitova, G., Zimov, S., 2009. Soil organic carbon pools in the northern circumpolar permafrost region. Global Biogeochem. Cycles 23, GB2023. https://doi.org/10.1029/2008gb003327.

Teixeira, P.C., Donagemma, G.K., Fontana, A., Teixeira, W.G. (Eds.), 2017. Manual de Métodos de Análise de Solo, 3rd ed. Embrapa, Brasília.

Ten Brink, N.W., Weidick, A., 1974. Greenland ice sheet history since the last glaciation. Quat. Res. 4, 429-440. https://doi.org/10.1016/0033-5894(74)90038-6.

Thomas, M., Monhonval, A., Hirst, C., Bröder, L., Zolkos, S., Vonk, J.E., Tank, S.E., Keskitalo, K.H., Shakil, S., Kokelj, S.V., van Opfergelt, S., 2023. Evidence for preservation of organic carbon interacting with iron in material displaced from retrogressive thaw slumps: case study in Peel Plateau, western Canadian Arctic. Geoderma 433, 116443. https://doi.org/10.1016/j.geoderma.2023.116443.

Tian, Y., Abulaizi, M., Yang, Z., Kou, T., Jia, Y., Hu, Y., Chen, M., Jia, H., 2025. Iron-oxidizing microorganisms affect the iron-bound organic carbon in the subsoil of alpine grassland during the thawing of seasonal frozen soil. Front. Microbiol. 15, 1523084. https://doi.org/10.3389/fmicb.2024.1523084.

Vinther, B.M., Buchardt, S.L., Clausen, H.B., Dahl-Jensen, D., Johnsen, S.J., Fisher, D.A., Koerner, R.M., Raynaud, D., Lipenkov, V., Andersen, K.K., Blunier, T., Rasmussen, S.O., Steffensen, J.P., Svensson, A.M., 2009. Holocene thinning of the Greenland ice sheet. Nature 461, 385-388. https://doi.org/10.1038/nature08355.

Virto, I., Barré, P., Chenu, C., 2008. Microaggregation and organic matter storage at the silt-size scale. Geoderma 146, 326-335. https://doi.org/10.1016/j.geoderma.2008.05.021.

Waldrop, M.P., Wickland, K.P., White III, R., Berhe, A.A., Harden, J.W., Romanovsky, V.E., 2010. Molecular investigations into a globally important carbon pool: permafrost-protected carbon in Alaskan soils. Glob. Change Biol. 16, 2543-2554. https://doi.org/10.1111/j.1365-2486.2009.02141.x.

Walkley, A., Black, I.A., 1934. An examination of the Degtjareff method for determining soil organic matter, and a proposed modification of the chromic acid titration method. Soil Sci. 37, 29-38.

Willemse, N.W., Koster, E.A., Hoogakker, B., van Tatenhove, F.G.M., 2003. A continuous record of Holocene eolian activity in West Greenland. Quat. Res. 59, 322-334. https://doi.org/10.1016/s0033-5894(03)00037-1.

Yu, W., Huang, W., Weintraub-Leff, S.R., Hall, S.J., 2022. Where and why do particulate organic matter (POM) and mineral-associated organic matter (MAOM) differ among diverse soils? Soil Biol. Biochem. 172, 108756. https://doi.org/10.1016/j.soilbio.2022.108756.

Annexes

Profile	Horizons	Depth	Coordinates	Elevation (m)	pH.H2O	Fe_{ox} (g/Kg)	Fe_{dcb} (g/Kg)	Al_{Ox} (g/Kg)	Al_{DCB} (g/Kg)	V (%)	Sand (Kg/Kg)	Silt (Kg/Kg)	Clay (Kg/Kg)	Distance from glacier (m)
P1	A	0 – 5	66.997°, -50.629°	112.68	6.80	0,416	1,582	0,078	0,152	89.5	0.25	0.61	0.15	29074.03
P1	E	5 – 15		112.69	6.41	0,292	0,240	0,350	0,207	86.7	0.34	0.56	0.1	29074.03
P1	Bh	15 – 25		112.70	7.32	0,329	1,992	0,142	0,294	96.1	0.32	0.58	0.11	29074.03
P1	2C	25 – 34		112.71	7.58	0,220	0,719	0,431	0,100	98	0.75	0.2	0.05	29074.03
P2	AE	0 – 5	67.146°, -50.048°	523.45	6.05	0,287	1,007	0,117	0,245	72.5	0.69	0.22	0.09	0
P2	2Bh	5 – 15		523.46	5.70	0,345	1,736	0,165	0,470	63.8	0.49	0.41	0.11	0
P2	2C	15 – 40		523.47	6.04	0,330	0,576	0,695	0,323	97.3	0.68	0.28	0.05	0
P3	Ah	0 - 10	67.146°, -50.048°	523.48	6.35	0,238	0,325	0,581	0,349	82.9	0.63	0.26	0.11	0
P3	C	10 – 30		523.49	6.13	0,620	0,786	1,455	1,201	76	0.39	0.48	0.13	0
P4	O	0 – 20	66.997°, -50.629°	270.68	5.14	1,509	1,562	0,657	0,483	49.9	0.34	0.48	0.18	19794.08
P4	C@	20 – 40		270.69	5.70	0,539	2,263	0,157	0,362	56.3	0.34	0.56	0.09	19794.08
P5	A1	0 – 5	67.053°, -50.477°	124.46	5.10	0,938	1,050	0,325	0,237	54.6	0.41	0.46	0.13	11026.2
P5	A2	5 – 25		124.47	5.52	0,264	1,571	0,085	0,335	65.8	0.44	0.44	0.13	11026.2
P5	Bh1	25 – 35		124.48	5.56	0,324	0,459	0,451	0,386	67.1	0.36	0.53	0.11	11026.2
P5	Bh2	35 – 60		124.49	5.76	1,777	1,722	0,567	0,491	70.6	0.16	0.65	0.19	11026.2
P5	C1	60 – 70		124.50	6.08	0,315	0,950	0,371	0,143	78.8	0.41	0.53	0.06	11026.2
P5	C2	70 – 85		124.51	6.23	0,372	0,989	0,429	0,133	79.5	0.85	0.11	0.05	11026.2
P6	A	0 – 5	67.060°, -50.394°	125.28	6.55	0,772	0,673	0,033	0,100	89.5	0.86	0.1	0.03	7346.15
P6	C1	5 – 30		125.29	6.77	0,109	0,498	0,167	0,045	83.1	0.88	0.08	0.04	7346.15
P6	2Ab	30 – 35		125.30	5.83	0,461	2,197	0,159	0,413	69.3	0.28	0.63	0.09	7346.15
P6	2C2	35 – 55		125.31	5.72	0,352	1,744	0,117	0,244	67.4	0.33	0.59	0.08	7346.15
P7	A	0 – 5	67.146°, -50.104°	350.03	6.02	1,424	1,307	0,411	0,272	79.3	0.52	0.34	0.14	974.75
P7	B	5 – 35		350.04	5.74	2,067	2,163	0,411	0,513	62.4	0	NA	NA	974.75
P7	Hb	35 – 45		350.05	5.74	NA	NA	NA	NA	70.3	NA	NA	NA	974.75
P8	O	0 – 10	67.081°, -50.327°	211.94	5.33	NA	NA	NA	NA	62.9	NA	NA	NA	3813.87
P8	A	10 – 30		211.95	5.64	0,294	0,963	0,433	0,312	64.5	0.45	0.47	0.08	3813.87
P8	E	30 – 50		211.96	5.94	0,666	1,798	0,107	0,392	72.1	0.22	0.69	0.08	3813.87
P8	Bh	50 – 60		211.97	5.90	0,598	0,525	1,036	0,978	65.1	0.29	0.61	0.1	3813.87
P8	C	60 – 80		211.98	6.41	0,653	2,284	0,151	0,711	77.8	0.71	0.23	0.06	3813.87
P9	O	0 – 15	66.995°, -50.983°	203.53	4.59	NA	NA	NA	NA	34.9	NA	NA	NA	33379.38
P9	C	15 – 40		203.54	5.95	0,394	0,921	0,906	0,479	73.5	0.59	0.32	0.08	33379.38
P9	2C2	40 – 70		203.55	5.82	0,834	2,208	0,239	0,757	63.9	0.62	0.32	0.06	33379.38

Table S1: Main physicochemical properties and classification of soil profiles from Kangerlussuaq, West Greenland.

Profile	Horizons	Depth	POM Composition (%)	MAOM Composition (%)	N POM (%)	C POM (%)	N MAOM (%)	C MAOM (%)	C:N POM	C:N MAOM	δ^{15}N POM	δ^{15}N MAOM	δ^{13}C POM	δ^{13}C MAOM
P1	A	0 – 5	45.713	54.287	0.186	6.226	0.090	1.498	33.484	16.631	1.79	-0.16	-26.98	-26.59
P1	E	5 – 15	35.160	64.840	0.245	5.591	0.060	0.980	22.786	16.329	0.95	1.13	-25.52	-26.39
P1	Bh	15 – 25	37.825	62.175	0.234	4.456	0.176	2.807	19.057	15.929	4.08	4.91	-24.42	-24.94
P1	2C	25 – 34	75.343	24.657	n.d	0.201	0.044	0.518	DL	11.835	n.d	4.39	-25.97	-25.08
P2	AE	0 – 5	72.169	27.831	0.093	1.941	0.286	3.417	20.911	11.935	-1.39	-0.13	-26.13	-24.67
P2	2Bh	5 – 15	52.150	47.850	0.231	3.453	0.207	2.651	14.922	12.795	1.68	1.83	-24.83	-23.76
P2	2C	15 – 40	65.230	34.770	n.d	0.172	0.054	0.756	n.d	14.094	n.d	1.76	-26.74	-24.48
P3	Ah	0 - 10	68.345	31.655	0.376	6.866	0.512	6.736	18.256	13.145	0.68	0.94	-25.84	-24.90
P3	C	10 – 30	43.761	56.239	0.220	3.635	0.439	5.716	16.498	13.029	0.31	0.92	-25.40	-24.23
P4	O	0 – 20	45.424	54.576	0.784	16.461	0.637	6.788	21.003	10.649	-0.96	-4.80	-25.68	-24.59
P4	C@	20 – 40	31.263	68.737	0.047	2.406	0.109	2.325	51.615	21.335	-2.46	1.24	-25.99	-24.58
P5	A1	0 – 5	48.902	51.098	0.337	6.000	0.263	3.502	17.820	13.302	-0.44	-0.49	-26.48	-25.37
P5	A2	5 – 25	48.479	51.521	0.284	5.020	0.138	2.074	17.651	15.017	-1.25	0.10	-26.01	-24.56
P5	Bh1	25 – 35	45.447	54.553	0.329	5.167	0.113	1.782	15.695	15.842	-0.29	-0.02	-26.01	-24.63
P5	Bh2	35 – 60	46.391	53.609	0.449	9.815	0.458	7.688	21.851	16.788	0.37	0.08	-24.92	-25.18
P5	C1	60 – 70	44.087	55.913	0.007	0.595	0.051	0.841	90.861	16.627	-18.88	-0.20	-26.22	-25.12
P5	C2	70 – 85	84.263	15.737	n.d	0.391	0.063	0.993	n.d	15.838	n.d	0.86	-27.05	-25.17
P6	A	0 – 5	85.190	14.810	n.d	0.110	0.040	0.548	n.d	13.652	n.d	-1.43	-27.73	-26.80
P6	C1	5 – 30	90.168	9.832	n.d	0.114	0.030	0.387	n.d	12.771	n.d	-0.41	-27.25	-26.41
P6	2Ab	30 – 35	39.139	60.861	0.078	2.457	0.069	1.287	31.688	18.700	1.22	2.75	-27.24	-26.07
P6	2C2	35 – 55	35.050	64.950	0.029	0.982	0.040	0.934	33.812	23.091	-0.45	2.96	-27.44	-26.61
P7	A	0 – 5	64.825	35.175	0.321	4.378	0.588	6.108	13.622	10.386	-0.48	-0.19	-26.70	-25.95
P7	B	5 – 35	49.362	50.638	0.790	11.261	0.514	5.938	14.263	11.558	0.22	-1.14	-24.62	-25.23
P7	Hb	35 – 45	57.255	42.745	0.759	10.026	0.791	8.434	13.203	10.662	-1.16	-5.26	-26.51	-25.96
P8	O	0 – 10	50.461	49.539	0.089	2.075	0.103	1.348	23.282	13.052	-2.54	-1.41	-27.72	-26.47
P8	A	10 – 30	45.387	54.613	0.089	1.553	0.070	1.034	17.542	14.677	-1.52	-0.44	-26.45	-25.91
P8	E	30 – 50	27.401	72.599	0.127	1.936	0.061	0.871	15.284	14.185	-0.62	-0.91	-25.88	-25.88
P8	Bh	50 – 60	37.488	62.512	0.104	2.207	0.174	2.950	21.129	16.926	0.02	0.52	-26.18	-25.37
P8	C	60 – 80	59.350	40.650	n.d	0.286	0.044	0.600	n.d	13.661	n.d	1.12	-27.10	-25.17
P9	O	0 – 15	56.314	43.686	1.376	28.591	0.686	8.374	20.775	12.214	-2.59	-6.68	-17.64	-25.70

P9	C	15 – 40	61.398	38.602	0.046	2.580	0.041	1.039	56.275	25.635	-5.63	2.21	-26.38	-26.12
P9	2C2	40 – 70	64.339	35.661	0.008	0.748	0.064	1.333	89.869	20.703	-13.05	2.04	-26.51	-25.67

Table S2: Isotopic composition ($\delta^{13}C$ and $\delta^{15}N$). C:N ratios. and calculated relative organic stability (n) for selected horizons of POM and MAOM fractions from Kangerlussuaq soils.

Profile	Date	Average Temperature (ºC)			Profile	Date	Average Temperature (ºC)			Profile	Date	Average Temperature (ºC)		
		10cm	50cm	130cm			10cm	50cm	130cm			10cm	50cm	130cm
P4	jun/24	4.9	0.5	0.8	P5	jun/24	0.7	0.7	0.4	P7	jun/24	2.7	0.8	-0.3
	jul/24	6.4	0.4	0.5		jul/24	0.6	0.4	0.5		jul/24	4.4	0.5	0.7
	ago/24	5.3	0.3	0.3		ago/24	0.4	0.2	0.6		ago/24	3.9	0.3	0.4
	set/24	2.3	0.3	0.1		set/24	0.6	0.2	0.5		set/24	0.9	0.3	0.4
	out/24	-1.1	0.3	0.1		out/24	0.7	0.2	0.5		out/24	-0.4	0.3	0.7
	nov/24	-2.9	0.3	0.1		nov/24	0.7	0.2	0.4		nov/24	-2.2	0.2	0.7
	dez/24	-7.4	-3.4	-1.8		dez/24	-1.5	-2.1	-3.7		dez/24	-8.6	-6.1	-3.7
	jan/25	-8.2	-6.1	-4.7		jan/25	-4.4	-5.0	-6.2		jan/25	-10.7	-9.5	-7.4
	fev/25	-7.2	-5.8	-4.9		fev/25	-5.1	-5.7	-6.8		fev/25	-9.7	-9.1	-7.7
	mar/25	-6.3	-5.6	-4.9		mar/25	-5.7	-6.2	-6.9		mar/25	-8.5	-8.6	-7.6
	abr/25	-1.0	-2.4	-3.0		abr/25	-4.1	-4.1	-3.9		abr/25	-4.0	-5.6	-5.7
	mai/25	2.9	0.5	0.2		mai/25	-0.9	0.2	0.5		mai/25	1.1	-0.8	-2.3
	jun/25	9.8	0.4	0.5		jun/25	0.7	0.5	0.5		jun/25	4.1	0.6	0.3
	jul/25	9.0	0.3	0.4		jul/25	0.4	0.2	0.5		jul/25	4.5	0.5	0.5

Table S3.1: Average Temperature of profiles.

Profile	Date	Frozen days			Profile	Date	Frozen days			Profile	Date	Frozen days		
		10cm	50cm	130cm			10cm	50cm	130cm			10cm	50cm	130cm
P4	jun/24	0	0	0	P5	jun/24	1	0	0	P7	jun/24	0	0	8
	jul/24	0	0	0		jul/24	0	0	0		jul/24	0	0	0
	ago/24	0	0	0		ago/24	0	0	0		ago/24	0	0	0
	set/24	0	0	0		set/24	0	0	0		set/24	0	0	0
	out/24	14	0	0		out/24	0	0	0		out/24	7	0	0
	nov/24	30	0	0		nov/24	0	0	1		nov/24	22	3	0
	dez/24	31	28	23		dez/24	23	26	31		dez/24	31	31	30
	jan/25	31	31	31		jan/25	31	31	31		jan/25	31	31	31
	fev/25	28	28	28		fev/25	28	28	28		fev/25	28	28	28
	mar/25	31	31	31		mar/25	31	31	31		mar/25	28	31	31
	abr/25	8	26	30		abr/25	30	30	30		abr/25	20	30	30
	mai/25	0	0	9		mai/25	21	7	0		mai/25	0	19	31
	jun/25	0	0	0		jun/25	0	0	0		jun/25	0	0	7
	jul/25	0	0	0		jul/25	0	0	0		jul/25	0	0	0

Table S3.2: Frozen days of profiles.

Profile	Date	Thawing degree days (TDD)			Profile	Date	Thawing degree days (TDD)			Profile	Date	Thawing degree days (TDD)		
		10cm	50cm	130cm			10cm	50cm	130cm			10cm	50cm	130cm
P4	jun/24	83.2	8.1	14.3	P5	jun/24	14.1	11.6	7.6	P7	jun/24	45.7	14.3	7.4
	jul/24	197.2	11.5	17.0		jul/24	17.1	11.2	16.3		jul/24	135.4	14.6	21.6
	aug/24	165.4	9.4	9.7		aug/24	13.5	5.6	17.1		aug/24	121.5	9.1	13.3
	sep/24	69.7	9.3	3.4		sep/24	19.1	5.4	16.1		sep/24	27.7	8.4	12.9
	oct/24	11.5	9.5	3.5		oct/24	21.1	5.6	16.5		oct/24	12.4	8.7	21.0
	nov/24	0.0	9.3	3.4		nov/24	19.8	5.8	14.9		nov/24	1.7	11.4	20.1
	dez/24	0.0	1.8	3.4		dez/24	5.3	3.7	0.0		dez/24	0.0	0.0	0.9
	jan/25	0.0	0.0	0.0		jan/25	0.0	0.0	0.0		jan/25	0.0	0.0	0.0
	fev/25	0.0	0.0	0.0		fev/25	0.0	0.0	0.0		fev/25	0.0	0.0	0.0
	mar/25	0.0	0.0	0.0		mar/25	0.0	0.0	0.0		mar/25	0.7	0.0	0.0
	abr/25	18.8	3.3	0.0		abr/25	0.0	0.0	0.0		abr/25	5.5	0.0	0.0
	mai/25	89.1	16.8	18.7		mai/25	8.5	20.1	15.2		mai/25	33.5	9.8	0.0
	jun/25	293.5	12.8	16.1		jun/25	21.5	13.9	15.4		jun/25	122.0	18.6	20.5
	jul/25	89.7	3.3	3.9		jul/25	4.4	1.8	5.5		jul/25	40.8	4.3	4.9

Table S3.3: Thawing degree days of profiles.

Profile	Date	Freezing degree days (FDD)			Profile	Date	Freezing degree days (FDD)			Profile	Date	Freezing degree days (FDD)		
		10cm	50cm	130cm			10cm	50cm	130cm			10cm	50cm	130cm
P4	jun/24	0.00	0.00	-0.25	P5	jun/24	-2.29	0.00	0.00	P7	jun/24	0.00	0.00	-12.29
	jul/24	0.00	0.00	0.00		jul/24	0.00	0.00	0.00		jul/24	0.00	0.00	0.00
	aug/24	0.00	0.00	0.00		aug/24	0.00	0.00	0.00		aug/24	0.00	0.00	0.00
	sep/24	0.00	0.00	0.00		sep/24	0.00	0.00	0.00		sep/24	0.00	0.00	0.00
	oct/24	-46.45	0.00	0.00		oct/24	0.00	0.00	0.00		oct/24	-24.21	0.00	0.00
	nov/24	-86.64	0.00	0.00		nov/24	0.00	0.00	-1.45		nov/24	-68.33	-6.82	0.00
	dez/24	-230.54	-108.53	-60.11		dez/24	-52.09	-70.28	-114.17		dez/24	-266.04	-188.86	-115.25
	jan/25	-254.04	-188.75	-145.58		jan/25	-135.23	-154.71	-192.53		jan/25	-332.64	-293.53	-228.36
	fev/25	-200.40	-161.30	-137.62		fev/25	-143.39	-159.81	-189.31		fev/25	-270.40	-256.18	-215.30
	mar/25	-196.34	-174.24	-152.45		mar/25	-177.73	-191.14	-214.11		mar/25	-264.82	-265.30	-235.51
	abr/25	-48.87	-75.58	-90.37		abr/25	-123.07	-121.75	-116.74		abr/25	-125.34	-167.25	-170.27
	mai/25	0.00	0.00	-12.81		mai/25	-37.32	-12.69	-0.25		mai/25	-0.63	-34.58	-70.56
	jun/25	0.00	0.00	0.00		jun/25	0.00	0.00	0.00		jun/25	0.00	0.00	-10.27
	jul/25	0	0	0		jul/25	0	0	0		jul/25	0	0	0

Table S3.4: Freezing degree days of profiles.

Profile	Date	Isothermal days			Profile	Date	Isothermal days			Profile	Date	Isothermal days		
		10cm	50cm	130cm			10cm	50cm	130cm			10cm	50cm	130cm
P4	jun/24	0	16	0	P5	jun/24	0	10	17	P7	jun/24	0	4	0
	jul/24	0	31	21		jul/24	23	31	2		jul/24	0	31	14
	aug/24	0	29	31		aug/24	31	31	0		aug/24	0	27	31
	sep/24	0	27	30		sep/24	3	30	0		sep/24	0	30	29
	oct/24	0	30	31		oct/24	0	31	0		oct/24	1	31	0
	nov/24	0	30	30		nov/24	2	30	6		nov/24	0	22	4
	dez/24	0	0	4		dez/24	2	1	0		dez/24	0	0	0
	jan/25	0	0	0		jan/25	0	0	0		jan/25	0	0	0
	fev/25	0	0	0		fev/25	0	0	0		fev/25	0	0	0
	mar/25	0	0	0		mar/25	0	0	0		mar/25	0	0	0
	abr/25	2	0	0		abr/25	0	0	0		abr/25	1	0	0
	mai/25	0	26	0		mai/25	0	4	26		mai/25	0	0	0
	jun/25	0	30	21		jun/25	13	30	5		jun/25	0	20	0
	jul/25	0	8	10		jul/25	10	10	0		jul/25	0	9	7

Table S3.5: Isothermal days of profiles.

Profile	Date	Freeze –Thaw days			Profile	Date	Freeze – Thaw days			Profile	Date	Freeze – Thaw days		
		10cm	50cm	130cm			10cm	50cm	130cm			10cm	50cm	130cm
P4	jun/24	0	0	1	P5	jun/24	1	0	0	P7	jun/24	0	0	1
	jul/24	0	0	0		jul/24	0	0	0		jul/24	0	0	0
	aug/24	0	0	0		aug/24	0	0	0		aug/24	0	0	0
	sep/24	0	0	0		sep/24	0	0	0		sep/24	0	0	0
	oct/24	7	0	0		oct/24	0	0	0		oct/24	7	0	0
	nov/24	0	0	0		nov/24	0	0	1		nov/24	7	1	0
	dez/24	0	1	1		dez/24	1	1	0		dez/24	0	0	0
	jan/25	0	0	0		jan/25	0	0	0		jan/25	0	0	0
	fev/25	0	0	0		fev/25	0	0	0		fev/25	0	0	0
	mar/25	0	0	0		mar/25	0	0	0		mar/25	2	0	0
	abr/25	0	1	0		abr/25	0	0	0		abr/25	2	0	0
	mai/25	0	0	1		mai/25	1	1	1		mai/25	3	2	0
	jun/25	0	0	0		jun/25	0	0	0		jun/25	0	0	1
	jul/25	0	0	0		jul/25	0	0	0		jul/25	0	0	0

Table S3.6: Freeze-Thaw days of profiles.

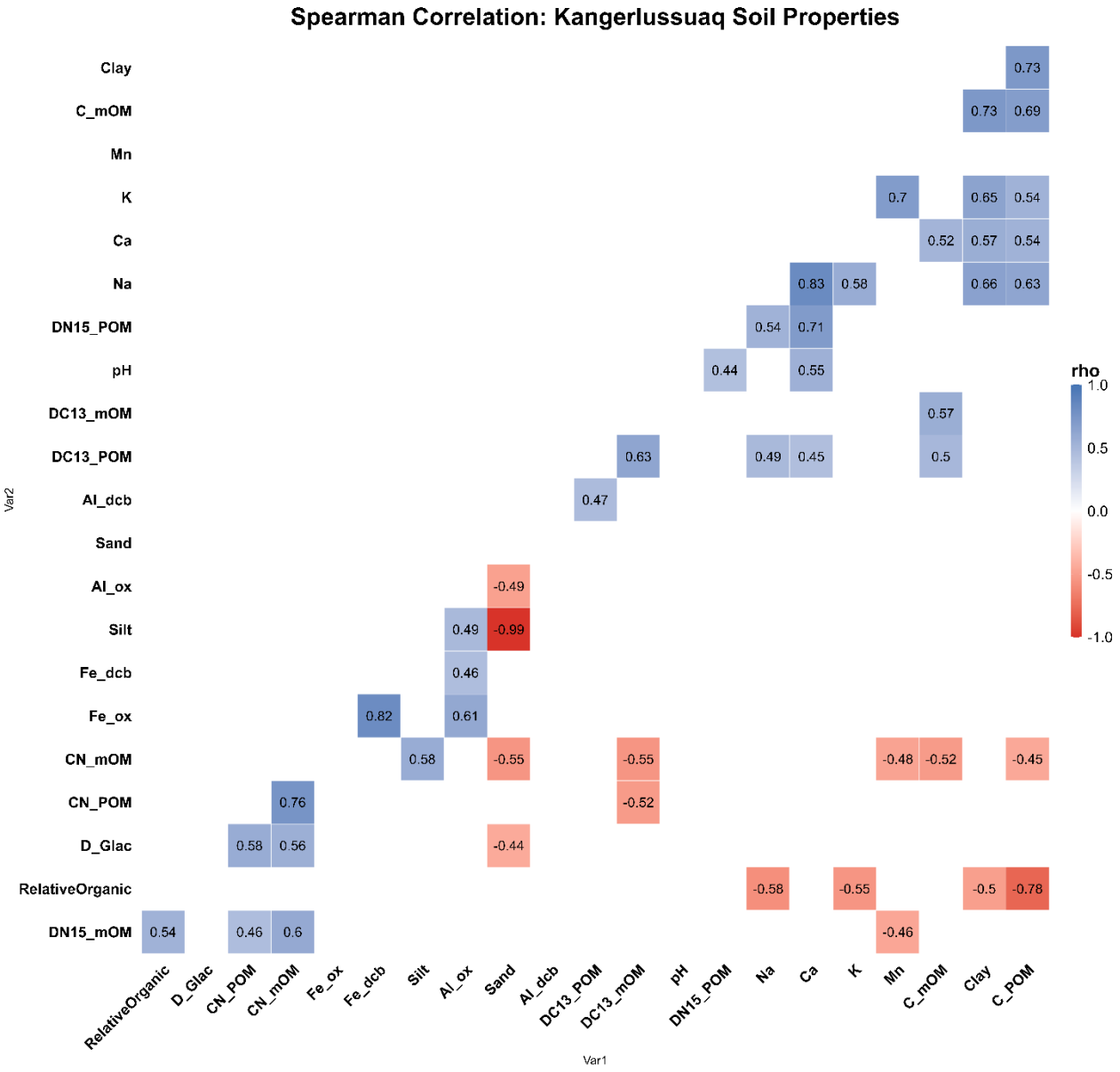

Figure S.2: Spearman correlation.

4. CONCLUSÃO GERAL

Os solos periglaciais de Kangerlussuaq desenvolvem-se sob um regime pedogenético caracterizado pela interação entre processos físicos herdados de períodos glaciais e processos deposicionais contemporâneos. Esta dissertação demonstrou, através de abordagens mineralógicas, geoquímicas, isotópicas e térmicas, que a trajetória evolutiva desses solos e a vulnerabilidade de seus estoques de carbono orgânico são governadas por dois mecanismos: o legado do intemperismo físico glacial e o rejuvenescimento superficial contínuo por deposição eólica.

A dupla gênese proposta nesta dissertação demonstrou no primeiro capítulo a imaturidade geoquímica observada nos solos e os gradientes invertidos de intemperismo identificados próximos às descontinuidades de deposição eólica. Três achados principais sustentam esse modelo. Primeiro, a composição mineralógica uniforme de todas as frações granulométricas, dominadas por minerais primários, indica que mesmo a fração argila consiste predominantemente de rochas trituradas por moagem mecânica, e através de intemperismo químico originando argilominerais secundários. Segundo, os baixos valores de CIA (média 49,64) e altos valores de ICV (média 1,24) confirmam que o intemperismo químico permanece em estágio inicial, com ausência de gradientes de alteração progressiva com a profundidade. Terceiro, as descontinuidades líticas identificadas em quatro dos nove perfis estudados, somadas a gradientes invertidos de intemperismo com valores de CIA mais elevados abaixo dos contatos de enterramento, fornecem evidência estratigráfica de eventos recorrentes de deposição eólica que interrompem a continuidade vertical dos gradientes pedogenéticos. Esse regime atua como retardante pedogenético ao introduzir material minimamente intemperizado que se sobrepõe aos processos de alteração química in situ e reconfigura as condições superficiais de desenvolvimento do solo.

Adicionalmente, os perfis analisados exibem evidências de podzolização incipiente, acúmulo subsuperficial de Fe, Al e carbono orgânico em horizontes eluviais e iluviais, que, embora não atinja os limiares diagnósticos determinados pela WRB para horizontes espódicos, satisfaz os critérios do qualificador *Protospodic*. A extensão desse qualificador como subqualificador de *Regosols* é proposta como contribuição taxonômica necessária para capturar o desenvolvimento pedogenético sutil que ocorre nos intervalos entre eventos deposicionais, e que tende a ser cada vez mais relevante à medida que o aquecimento ártico intensifica os processos de lixiviação e translocação em ambientes periglaciais.

As razões C:N elevadas observadas em horizontes soterrados indicam que o soterramento rápido preserva matéria orgânica relativamente fresca, criando um registro estratigráfico de fases alternadas de deposição e pedogênese incipiente. Dessa forma, os perfis de solo preservam uma sequência de eventos deposicionais e pedogenéticos descontínuos, ao invés de uma evolução unidirecional. Cada evento eólico atua como reinício pedogenético, gerando uma arquitetura vertical cumulativa de matéria orgânica na qual o carbono recentemente fixado ocupa a superfície enquanto reservatórios progressivamente mais antigos são fisicamente protegidos em profundidade por soterramento e preservação criogênica.

As consequências desse regime de gênese para a estabilidade da MOS foram elucidadas no segundo capítulo através da integração de fracionamento físico, análises isotópicas e monitoramento térmico. A fração POM apresentou razões C:N elevadas (13 – 91) e composição isotópica consistente com material vegetal pouco transformado, enquanto a fração MAOM exibiu razões C:N mais baixas (10 – 26), indicando processamento microbiano parcial. Contudo, os valores baixos do índice de estabilidade relativa n (mediana 1,01) em comparação com sistemas temperados e alpinos sugerem que mesmo a fração MAOM nesses solos permanece em estado de transformação incompleta, refletindo as limitações ambientais à atividade microbiana impostas pelo frio e pela sazonalidade do descongelamento.

Complementarmente, as baixas concentrações de óxidos de Fe e Al amorfos indicam escassez de fases minerais reativas capazes de estabilizar a MOS através de interações sortivas. Essa limitação é consequência direta do baixo grau de intemperismo químico documentado no primeiro capítulo. Contudo, a ocorrência de pH próximo à neutralidade e elevados teores de Ca^{2+} trocável em vários perfis sugere que a formação de pontes catiônicas mediadas por Ca^{2+} pode representar uma via secundária de estabilização da MOS onde os óxidos de Fe e Al são escassos. Dessa forma, a estabilização da MOS nesses solos não é primariamente governada por mecanismos de proteção mineral mediados por Fe e Al, mas sim pela preservação física através do soterramento, pelas restrições ambientais à decomposição e, potencialmente, por associações catiônicas mediadas por Ca^{2+} em horizontes de pH mais elevado.

O monitoramento térmico contínuo ao longo de 14 meses estabeleceu as condições de base do regime térmico e revelou heterogeneidade vertical e temporal pronunciada. As camadas superficiais a 10 cm exibiram amplas variações sazonais de temperatura, com verões caracterizados por temperaturas médias positivas (até 9,8°C) e acúmulo substancial de graus-dia de descongelamento (TDD acumulado de até 1.017 *degree-days*), alternados com invernos de congelamento prolongado (FDD de até -1.352 *degree*-days). Em contraste, as camadas subsuperficiais a 50 e 130 cm apresentaram amplitudes térmicas reduzidas e elevada frequência

de dias isotérmicos, particularmente a 50 cm de profundidade. Essa diferenciação vertical implica que a MOS em diferentes horizontes está sujeita a regimes térmicos distintos, com a MOS superficial experimentando janelas sazonais de atividade microbiana potencialmente intensa e a MOS subsuperficial permanecendo sob condições de menor amplitude térmica, porém com períodos isotérmicos que podem favorecer condições anaeróbicas e processos redox cíclicos. Embora os ciclos de congelamento e descongelamento tenham ocorrido em frequência relativamente baixa, máximo de sete dias por mês nas camadas superficiais, sua ocorrência em múltiplas profundidades aponta para um papel potencial na regulação da dinâmica da MOS que merece investigação direta.

A integração dos resultados dos dois capítulos revela uma vulnerabilidade dupla da MOS nos solos de Kangerlussuaq. Por um lado, o regime de gênese caracterizado por intemperismo químico limitado resulta em escassez de fases minerais reativas capazes de estabilizar quimicamente a matéria orgânica. Por outro, o regime térmico heterogêneo, embora atualmente restrinja a decomposição através do congelamento prolongado, pode favorecer perdas rápidas de carbono caso as janelas de descongelamento se tornem mais extensas sob aquecimento contínuo. Diferentemente de solos temperados, onde a proteção mineral pode conferir estabilidade de longo prazo à fração MAOM, nos solos de Kangerlussuaq essa fração permanece potencialmente vulnerável devido à limitada sorção em superfícies minerais e ao estágio incipiente de desenvolvimento pedogenético.

Essas constatações têm três implicações centrais para a compreensão da dinâmica do carbono no Ártico. Primeiro, solos em regiões de deglaciação acelerada podem não desenvolver mecanismos robustos de estabilização mineral da MOS dentro de escalas de tempo relevantes para as mudanças climáticas atuais, permanecendo dependentes de proteção física e térmica que é intrinsecamente sensível ao aquecimento. Segundo, o soterramento episódico por deposição eólica, embora atue como retardante pedogenético, pode funcionar simultaneamente como mecanismo de sequestro de carbono ao enterrar horizontes orgânicos para profundidades onde as amplitudes térmicas são menores e a conectividade com processos superficiais é reduzida, afirmação que somente pode ser quantificada com datação absoluta dos horizontes soterrados. Terceiro, a heterogeneidade vertical nos regimes térmicos indica que modelos de resposta da MOS ao aquecimento devem considerar não apenas mudanças nas temperaturas médias, mas também alterações na frequência e magnitude dos ciclos de congelamento-descongelamento e na profundidade das camadas ativas.

As perspectivas futuras para pesquisa incluem a integração de técnicas de datação absoluta, luminescência opticamente estimulada (LOE) e radiocarbono (^{14}C), para compreender

as frequências de soterramento e as taxas de acumulação de carbono, alinhando os eventos deposicionais identificados estratigraficamente com os pulsos eólicos documentados na literatura regional. Adicionalmente, faz-se necessário estudo aprofundado da biogeoquímica do material orgânico presente nesses perfis, avaliando se os compostos orgânicos identificados apresentam qualidade recalcitrante ou resistência média a elevada à decomposição microbiana. Medições diretas de fluxos de CO_2 e CH_4 ao longo de ciclos sazonais completos são essenciais para traduzir os regimes térmicos caracterizados nesta dissertação em taxas reais de mineralização e para identificar quais horizontes contribuem mais significativamente para as emissões de gases de efeito estufa. Por fim, estudos microbiológicos integrando sequenciamento metagenômico e análises funcionais contribuiriam para compreender como as comunidades microbianas respondem aos regimes térmicos heterogêneos e como sua diversidade e atividade modulam a vulnerabilidade da MOS à decomposição.

Em síntese, os solos de Kangerlussuaq representam sistemas pedologicamente imaturos onde a matéria orgânica é mantida em estado de vulnerabilidade elevada devido à combinação de proteção mineral limitada e instabilidade térmica sazonal. À medida que o aquecimento ártico prossegue, esses solos podem transicionar de sumidouros para fontes de carbono atmosférico, com implicações para o clima global. A compreensão integrada dos processos de gênese e dos mecanismos de estabilização da MOS fornecida por esta dissertação contribui para as projeções sobre a resposta dos estoques de carbono ártico às mudanças climáticas e para nortear estratégias de monitoramento em regiões de deglaciação acelerada.